UNIVERSITY OF OKLAHOMA

GRADUATE COLLEGE

COMPARATIVE EVALUATION OF DELAMINATION IN CARBON FIBER REINFORCED COMPOSITES (CFRPs) UTILIZING VARIOUS COMMON NON-DESTRUCTIVE INSPECTION TECHNIQUES

A THESIS

SUBMITTED TO GRADUATE FACULTY

In partial fulfillment of the requirements for the degree of

MASTER OF SCIENCE

By

IAIN DOUGLAS KENNEDY

Norman, OK

2022

COMPARATIVE EVALUATION OF DELAMINATION IN CARBON FIBER REINFORCED COMPOSITES (CFRPs) UTILIZING VARIOUS COMMON NON-DESTRUCTIVE INSPECTION TECHNIQUES

A THESIS APPROVED FOR THE
SCHOOL OF AEROSPACE AND MECHANICAL ENGINEERING

BY THE COMMITTEE CONSISTING OF

Dr. Mrinal C Saha, Chair

Dr. M. Cengiz Altan

Dr. Yingtao Liu

Acknowledgments

I would like to express my gratitude for my committee members: Dr. Mrinal C. Saha, Dr. M. Cengiz Altan. Their guidance in my studies and support throughout my master's program has been invaluable. Dr. Saha, who I have worked for as an undergraduate researcher as well as a current graduate, has always been supportive in letting me pursue my passions and ideas. Under his guidance I have gained invaluable experience which I will always cherish. Dr. Altan, who's vast knowledge of composites manufacturing, and material properties have been instrumental in the development of my thesis and his advice and support throughout have enabled me to refine my skills as a researcher. I would also like to thank Dr. Liu, for joining my committee and assisting in guiding me through the master's process, his kindness and willingness to aid is unparalleled.

I count myself fortunate to have had great friends and colleagues throughout my tenure at the University of Oklahoma, whether for advice or a shoulder to lean on, their continued comradery and support have helped to push me to succeed when I thought I could not.

Finally, I would like to thank my family. Their love and adamant support for me to pursue my degree have always been the rock I can count on. My father Douglas Kennedy and mother Victoria Kennedy, their undying encouragement has always helped me in dark times, and I am lucky to have them as parents. It is impossible to thank everyone, but to all who have been with me on this journey- you have my undying respect and gratitude.

Table of Contents

List of Tables

List of Figures

Abstract

Non-destructive Inspection (NDI) is routinely used to diagnose and monitor defects in composite parts, which could impact composite lifespan and performance. There are a variety of methods to conduct NDT in composites, the most popular being ultrasonic c-scan, shearography (thermal and vacuum excitation), and pulsed thermography testing. This study evaluates these NDT methods by testing on a set of CFRP laminates fabricated through a vacuum infusion process with artificially programmed defects. Firstly, these methods are evaluated based upon their detection capability- i.e., can each find the programmed defect in a standard inspection procedure. Secondly, how well do the scans predict the defect area? This is done utilizing a computed tomography scanning (CT-Scan) of the same laminates to create a benchmark to reference for the other three NDT methods. Finally, these methods are compared and contrasted. This study finds that ultrasonic c-scans and pulsed thermography share near-identical detection capabilities in the range of depths analyzed. Shearography, utilizing thermal excitation, could not detect any of the programmed delaminations, while partial vacuum shearography was only able to detect a limited selection of the largest sized defects. Under CT scans, the programmed defects were found to have inconsistencies, error correction was performed and relationships for ultrasonic scanning and thermography were able to be ascertained. Ultrasonic scans show consistent levels of error past near surface defects and thermography sees increased error in area detection as defect depth increases.

Chapter 1: Background

1.1 Composites in the Aerospace Industry

Composite materials are presently in the fastest expansionary period of this technology's adoption within aerospace. As engineered structures aim to become stronger, lighter, and environmentally resilient, carbon fiber reinforced plastic (CFRPs) in aircraft skins, and support structures have grown ever more prevalent. More and more industries are becoming reliant on these highly advanced materials; for example, the Airbus A300 aircraft, when introduced to service in 1972, was slightly less than 5% composite materials by weight [1,2]. In contrast, the Airbus A350-900, when put into service in 2015, was 53% composite materials by weight [1]. As seen in Figure 1, the adoption of composites by Airbus in their mainline commercial aircraft increased over 10-fold in just over four decades at an increasing rate with new generations of aircraft platforms. Other commercial aircraft manufacturers have begun

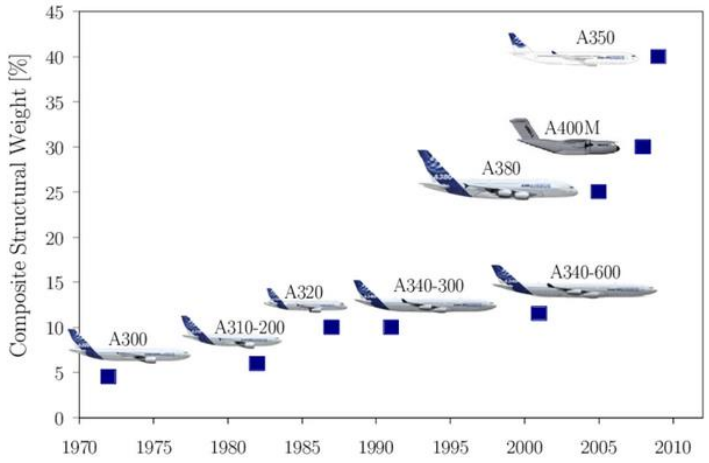

Figure 1: Airbus Composites Use (Kesarwani, S, 2017)

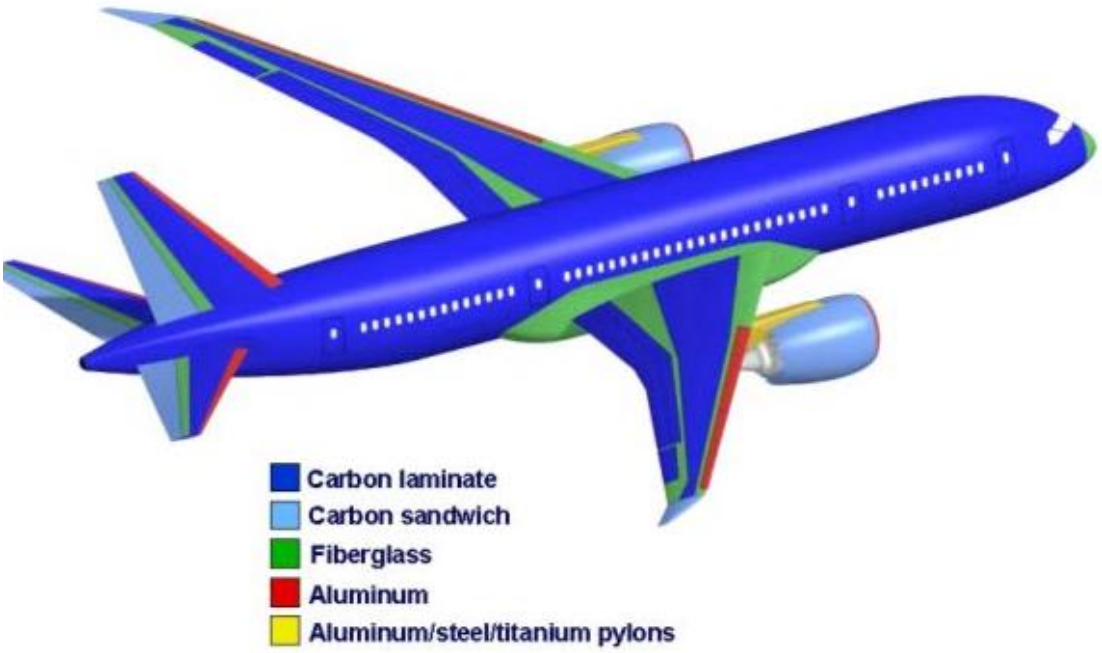

Figure 2: Boeing 787 Structure Summary (Paria N, 2011)

producing aircraft made with an almost entire composite structure, such as the Boeing 787 seen in Figure 2. The market for composite materials is expected to grow by 7.3% annually and reach $30 billion by 2026 [1]. That being said, this increased reliance on composites in aircraft structures comes at a cost. Composite materials have notoriously complex manufacturing processes, involving high tech machinery such as autoclaves, and advanced materials like prepreg fiber weaves. These are combined in order to reach the end goal of fiber volume fractions between 45 and 65 percent to be considered aerospace-grade [47]. There is potential to introduce defects into the composite as a result of poor manufacturing processes, or lack of quality control for the materials being used. Defects can also occur as a result of in service use, which result from severe loading on the composite during flight. Damage resulting from physical shocks like impacts or aerofoil lift can be examples of these loadings. When seeking to repair these composite damage, most methods involve removing the damaged area of a composite structure, and then patching the spot with a

limited variety of filler materials which depend on application [48]. The repair difficulty makes for a tricky balancing act for those who use and manufacture these aircraft structures- given that patch repairing the composite pieces may be impossible given the extent of the damage and could require the fabrication of a completely new piece of composite structure [48]. Users of composite aircraft structures aim to stretch as much life out of the material for as long as is feasibly possible before failure. However, understanding when a composite structure will fail is very difficult as defects such as composite delamination occur beneath the surface of the material. This makes it hard for inspectors of composites to identify them with just their eyes. Delamination can occur in a number of ways: as a product of resin starved regions in manufacturing, poorly bonded joints, edge fraying, as a result drilling out a composite, or impact damage and many more [49]. While composite defects are by no means limited to delmaniation- delamination is serious as it creates high stress zones in the composite material and occurs beneath the surface and can result in material separation, dramatically reducing the strength of the composite [49]. As seen in Figure 3, a CFRP laminate is put under loading which initiates delamination from an initial layer separation (commonly simply referred to as delamination itself) which results in the propagation and eventual total failure of the laminate. This particular case could represent a load resulting from unpredicted impact in flight operation. Understanding

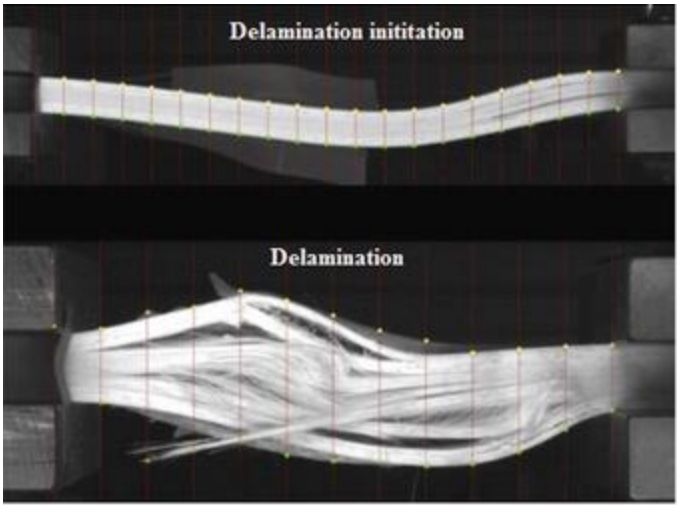

Figure 3: Extreme Example of Delamination in Fiber Reinforced Composite (Sheedev A. 2018)

the extent at which a composite defect has occurred is essential to its lifespan. Seemingly small defects in a composite can have dire consequences, for instance a study done at the University of Utah found that microcracking defects in a carbon fiber composite at an area density of $2mm^2$ would result in a 60% drop off in its effective shear strength [4] in that particular area. Other defects such as impact damage, fluid ingress and delamination etc. [6] all impact composite integrity. A small failure in a composite laminate has compounding effects, as one area of a composite fails- other areas are put under higher stress concentration which could result in catastrophic failure. Thus, diagnosis of these defects early and monitoring them is critical. It is critical to identify these defects before they have the chance to impact the composite structure. One way in which this problem is being combated is through the use of non-destructive inspection (NDI) techniques to understand potential defects found inside of a composite laminate. By diagnosing these defects, it can better inform inspectors as to the method of repair.

1.2 Non Destructive Inspection of Composite Aircraft Structures

Non-destructive inspection (NDI) is a non-invassive method and can provide useful insights into the state of damage in the composite parts. This can be done using a wide variety of techniques, the most widely used NDI methods which are most applicable for composites include: Visual Inspection, Interferometry (Optical Shearography), Radiography, Thermography and Ultrasonic Testing [5]. These technologies, referred to as NDI methods offer the ability to inspect a composite and allow for judgement on whether a composite is in jeopardy of failure or is still within safety factor. However, NDI

techniques are not made equal and accel in different areas. For instance, visual inspection, strictly speaking, is using handheld tools like a flashlight and the human eye to judge for defects in a composite. This is extremely cheap to do and quick, however it is limited to detecting macroscopic surface visible defects. While this method would be good for detecting something like surface damage such as impact damage which leaves a visible dent, it would be a poor way to detect if there had been any delamination as that is not clearly visible on the surface. Then there are methods such as Radiography, which utilize X-Ray technology, similar to those found in the medical field [25,26], to scan the internal microstructure of a composite laminate. This in contrast to Visual Inspection is much better suited for detecting defects delamination, which is the separation the composite lamina, resulting in a detectable discontinuity in the material. In this study we will be reviewing and investigating the capabilities of Shearography, Thermography, Radiography (2D X-Ray and Computed Tomography) and Ultrasonic Testing NDTs.

1.3 Types of NDI Method usind in Composite Materials

1.3.1 Shearography

Shearography NDT goes back to the early 1990s in its testing of glass fiber composites [7]. Shearography detects displacement derivatives on the surface of a material by applying a load to it the test specimen. This load is usually internal pressure, vacuum pressure, or thermal loading [8]. What makes Shearography a powerful tool is that it allows for the detection of subsurface defects in a composite very rapidly through the use of a camera measuring the shear strain, or surface warping of the material when loading is introduced. The defects which are most easily detected by this method are delamination, core debonding and microcracking [8]. Delamination is a very common defect. It can be the result of a variety of factors induced into composites due to the highly complex manufacturing process involved in their creation [9]. Shearography NDT can be a quick and efficient method for identifying these defects. It does not detect defect depth however, as there is not visual indication of the actual depth nor rigid dimensions of the defect, rather that it exists somewhere within the thickness of the laminate and the defects general form. As seen in Figure 3, this NDT is capable of detecting defects as small as microcracks on a

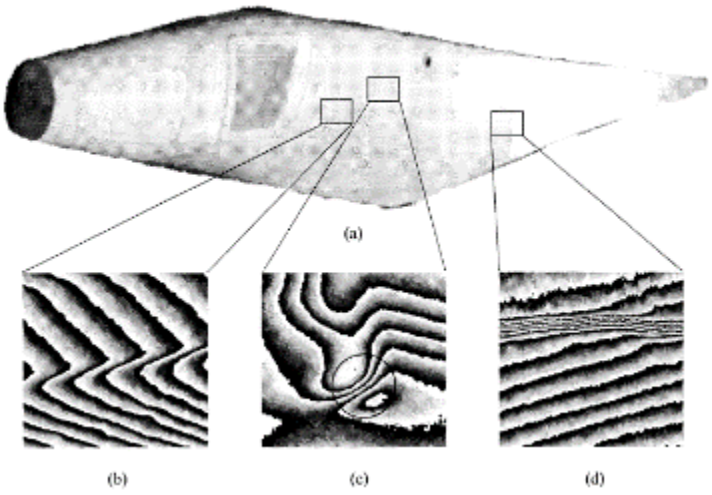

Figure 4: (a) GFRP Rotor Vane with Shearographic Detection of (b) Laminate Pattern (c) Disbonding and (d) Microcracking (Steinchen W., et. al., 1998)

5m long GFRP rotor blade [8]. The rotor blade in Figure 3 underwent an internal pressure loading of 0.1 MPa.

This method itself is also very quick, if done efficiently a piece such as the 5m blade seen in Figure 3 can be inspected on both its front and back surface in 15 minutes [8]. Shearography, though capable of detecting subsurface defects sees a drop-off in accuracy the depth of the defect, smaller sizes and at lower excitation amounts. For instance, in the first studies into Shearography in composites- a 1x1" delamination in fiber glass composites undergoing Shearographic testing with internal pressure was found to detect at a depth of 3.196mm in a 6 ply GFRP laminate at 13.8kPa [7]. That same defect at 6.9 kPa was undetected. This is because the defect must allow for shearing of the surface, if the defect is unable to be propagated to the surface, then it will not be detected. Shearography can also create non-intuitive results. Since the resulting images from Shearography are fringe patterns, it can be hard to see these fringes depending on lighting conditions of the space or the amount in which the defect has been excited and general resolution limitations. Recent efforts into Shearography have sought to make the method easier for users to interpret by digitizing the process. Utilizing computing technology allows for the post-processing of Shearographic image results and creating higher contrast images. As seen in Figure 4, through the use of Phase Measurement (TPS-DS) technique, a digital processing method, creates a much clearer image with 10x higher resolution [9].

The current trajectory of Shearography is refining systems using digitization methods such as TPS-DS.

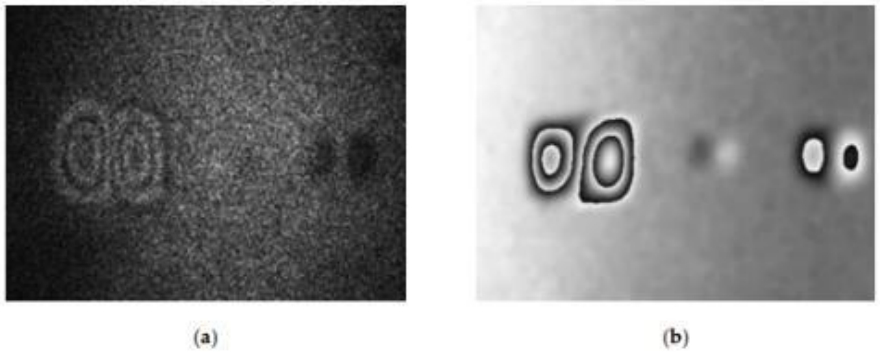

Figure 5: (a) Standard Real-Time Subtraction Shearography Image (b)Temporal Phase-Shift Digital Shearography Image (Zhao Q., et al.

1.3.2 Optical Thermography

Optical Thermography is another NDI method, similar to Shearography in the sense that a load is applied to a material and the physical interaction with the energy and the material is monitored. However, instead of detecting the shearing on a material surface Thermography utilizes an infrared radiation (IR) sensor to see variations in heat diffusivity through a material. This is done with an excitation source which provides heat energy to a material surface. There are multiple varieties of Optical Thermography utilized for composite materials including: Pulsed Thermography (PT), Stepped Thermography (ST), Lock-In Thermography (LT), Pulsed Phase Thermography (PPT) and Frequency Modulated Thermography (FMT) [10]. Thermography has been found to be widely applicable across composites, however it has been shown to be exceptionally useful for detecting defects such as delamination and debonding since a larger lateral defect area is most easily detected by IR technology [10]. In a study performed at the University of

Singapore in 2001 [11] it was found that utilizing the LT technique on a CFRP laminate those defects with a lateral diameter of 6 mm could be detected at up to 2.1 mm depth, yet a defect with a diameter of 1 mm could barely be detected at a depth of 0.84 mm. Similar to Shearography, this optical NDI method is much better suited for close to surface defects since it relies on the propagation of heat through the material to detect defects. More modern studies in thermography have refined the technology through the understanding of material thermal frequency. The deeper a defect is in a composite laminate, the lower its thermal frequency captured by the IR camera will be. Thus, cameras capable of accurately capturing low thermal frequencies are capable of analyzing defects very deep inside of composite laminates [11]. For instance, a study performed in December of 2019 was able to defects as 10 mm when scanning at a 0.002 Hz frequency [12]. Additionally, refinement of imaging technology through the incorporation of predictive algorithms into image processing, as can be seen in Figure 5 which utilizes a technique called Sparse Ensemble Matrix Factorization (SEMF) which filters out unremarkable thermal signatures to better isolate defects in a composite laminate [13]. Innovations such as these are making Thermographic analysis for composite materials with non-uniform

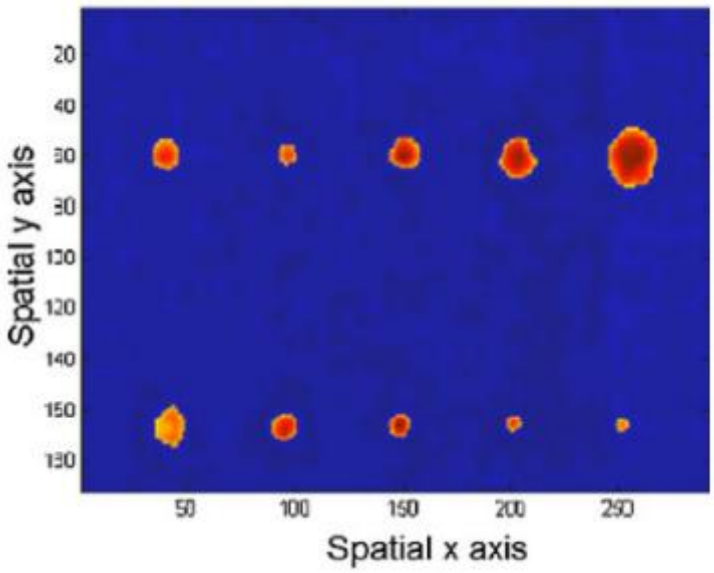

Figure 6: SEMF Processed PT Image (Ahmed J., et al. 2018)

thermal characteristics in the matrix and fiber thermal diffusivity substantially more reliable and increasingly useful in determining defect depth.

1.3.3 Ultrasonic Testing

Ultrasonic Testing (UT) utilizes guided ultrasonic waves being emitted through a medium [16]. This method of NDI has been well documented as a highly reliable and trusted method for composite materials defect inspection, particularly for its ease of implementation in the manufacturing process as well as post manufacturing inspection [17]. If any defects are present inside of a composite material, these ultrasonic waves will be reflected back to the interrogating probe sooner than when hitting the back wall of the test piece, this is measured and stored by the UT device. There are a variety of forms UT scanning methods, those being A-Scan, being the analog data received by the UT probe. B-Scan creates a mapping of defect thickness based off of the ultrasonic echoes detected throughout the material piece, being able to measure the area behind a defect [18]. The major limitation in B-Scanning is that the defect area is often times imprecisely measured due to the nature of the scanning method and generally requires geometric correction [19,20]. The

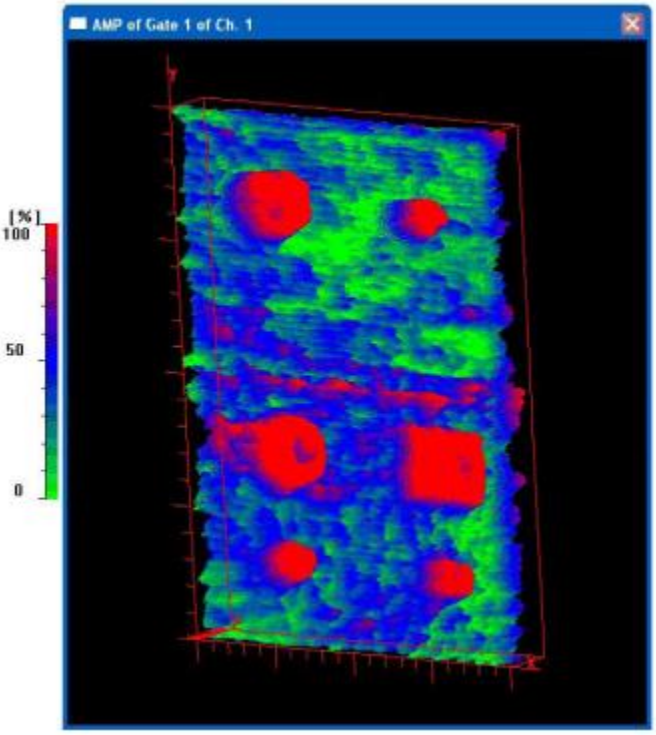

Figure 7: Ultrasonic C-Scan Between Layers 3 and 5 of a CFRP Laminate (Hasiotis T., et al. 2011)

most popular scanning method for inspection composites is ultrasonic C-Scan. This method maps the times of flight of the ultrasonic waves in x-y space. This method creates much more accurate areas than B-Scanning, however defect thickness is often difficult to accurately determine and can require correction as well [21]. Seen in Figure 6 is a map of a CFRP sample with different size and shape delamination's throughout the laminate [17]. The images clearly depict both depth of defect as well as shape, but the accuracy of the defect edges can vary. Advancements in the field of UT scanning, much like other methods, are creating digitization algorithms based on physical phenomena of the NDT method as well as references to other more accurate NDT methods like CT scans such as in study [21].

1.3.4 Radiography: Computed Tomography

X-Ray Imaging technology falls under the umbrella of radiography. Many are likely familiar with the application of radiography technology in the medical field, particularly in dentistry [25]; however, there has been application in composites NDI over the past few decades. What makes radiography appealing is that it can give highly detailed images down to the micron level, even as small as 1 μm depending on the field of view (FOV) of the inspected area [22]. This allows for the detection of very small defects such as composite voids, microcracks and porosity. Other methods such as UT struggle to detect such small defects. Conventional CT Scanning requires a finite space to control the resolution of the images of the object, this geometrical limitation can become problematic in aerospace NDI as typically the part being interrogated is attached to a massive aircraft structure [23]. This does not mean that the method itself is not applicable, however. Even when using individual 2D scans, which instead of creating an x-y-z axis reconstruction

would only have an x-y reconstruction, these can still detect contrast in the absorbed radiation traveling through a material- even in cases where the changes are as small as individual fibers, as seen in Figure 7, those fibers being glass and carbon fiber [24]. This is due to materials having different radiopacity values, meaning that they absorb x-ray radiation differently. This additionally makes radiography a powerful tool for finding foreign object debris (FOD) inside of a composite structure. It is clear that this method of NDT allows for distinction of different materials quite well, which helps for further understanding of a composite defects. That being shared, it is a costly and energy intensive process, so it is typically used in compliment to some of the previous methods mentioned such as UT in order to gain greater insight to a suspected defect. Higher quality images with fine resolution require more scanning time. Additionally, operators of these tools must be careful around x-ray radiation as it poses a much more significant health hazard than of the other method mentioned. Often x-ray imaging systems require large x-ray chambers to be constructed to scan large parts because of the hazard posed by said radiation. As aforementioned, Computed Tomography (CT) scanning is a 3-Dimensional image constructed by a 360-degree rotational scan of a test subject. CT scanning is most commonly found used in the medical field to study the human body [25,26]. The application of CT scanning in the aerospace industry is quite small, given the geometric constrains a CT scanning device does not allow for the testing of often quite large composite laminates. This is the least popular of the NDT methods being evaluated in this study, as the equipment is highly specialized and rather novel in its application to composites testing. However, there is always demand for high resolution full context imagery of composite components in aerospace. A CT scan of a part is effectively a “holy

grail" as it not only delivers the micron level detail of a 2D X-Ray, but additional depth information can be ascertained from the scan. 3D image reconstruction of a scanned object allows for unparalleled defect understanding compared to any of the other methods cited [27, 28]. The limitation of CT scans are their geometric constraints inside the testing chamber as well as the scanning field of view limitations. To achieve more detailed scans the area viewed must be reduced, this dramatically drives up inspection times. In academia this is not an issue however in modern industry where speed is critical the larger and faster CT times and lowest resolution, still micron level, are utilized.

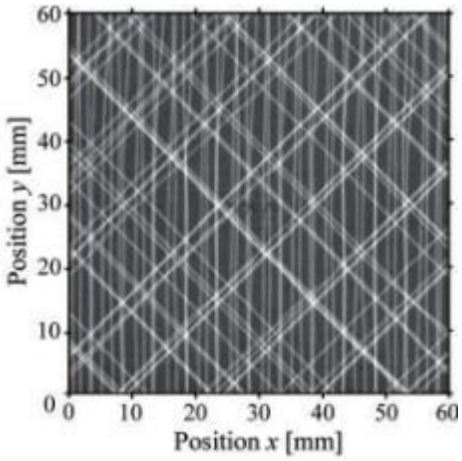

Figure 8: X-Ray Contrast Between Carbon and Glass Fiber (Glass in White) (Rus J., et al. 2020)

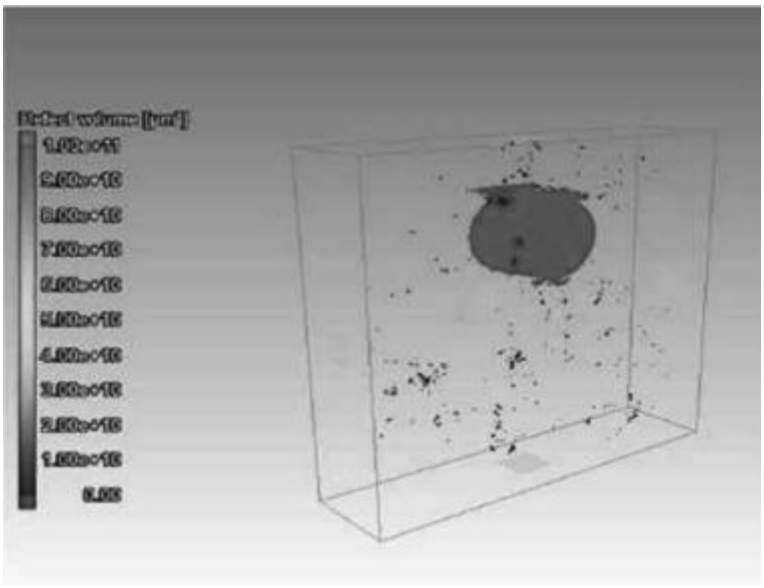

Figure 9: CT Scan of CFRP Delamination and Porosity (Liu X., F Chen. 2016)

1.4 Scope of Work

To summarize composites NDI takes a number of forms. The most popular methods being Shearography, Optical Thermography, 2D X-Ray Imaging, and Ultrasonic C-Scanning. Ultrasonic C-Scans measure the time of flight of pulsated ultrasonic sound waves through a medium while mapping x-y positioning over a surface, composite defects are identified by more rapid time of flight readings. Shearography, which detects shearing, or strain, in a materials surface when a load is applied to the material, those loadings vary depending on application- the most popular being thermal and partial vacuum. Optical Thermography, which uses infrared sensing equipment to measure the heat diffusivity of a material to find points where there are large variations in thermal diffusivity by applying a thermal load to the material. Lastly Computed Tomography, which utilized a series of 2-dimensional x-ray images 360° around the test specimen, these utilize the same x-ray shadow phenomena however utilizes algorithms to construct 3-D images from the scans.

1.5 Research Objective

The goal of this study is to evaluate the effectiveness of Non-Destructive Testing methods Shearography, Thermographic, Ultrasonic and Radiographic in finding delamination defects in aerospace CFRP use cases. Understanding effectiveness of different NDT methods ability to identify nearly identical defects through thickness in materials commonly used aerospace skin panels is key. The study will attempt to find understanding of the relationship between delamination sizes and depth detection within CFRP laminates for these different methods. This study also aims to create the groundwork for future studies, including potential algorithms to predict defect depth and size for composite NDT systems. Another goal is to then understand how accurately these methods can capture these defects utilizing X-Ray CT Scanning to get exact dimensions of the defects and quantifying the accuracy of the NDT methods being examined.

Chapter 2: Creating Multi-Thickness NDT Test Specimen

2.1 Introduction

2.1.1 Test Specimen Purpose

The goal of this study was to analyze the effectiveness of a variety of NDT methods in detecting delamination through a variety of laminate thicknesses. The strategy was to utilize a range of laminate thicknesses since certain NDT methods may be ideal for detecting defects closer to surface defects or detecting or a particular range of defect sizes, as not all methods of NDT are made equal. The aim of this study is to have quantified and demonstrated which NDT methods are ideal for differing composite NDI scenarios and deliver an informed recommendation meeting various differing scenario's needs. The defect which will be analyzed for this study is interlaminar delamination. The delamination was simulated utilizing a thin (0.28mm) DuPont Teflon^{TM} sheet between laminae. This is a common method for simulating composite delamination [30, 31, 32]. The multiple thicknesses of laminates allow for the consideration of a variety of aerospace NDI scenarios which occur at different depths.

2.1.2 Basis for Specimen

The design of this test specimen was inspired by a Thermographic NDT study [29] in which a multi-tiered structure with different sized defects were artificially introduced into the test piece. Additionally, for defect edge characterization by CT, study [21] in which the researchers used UT B-Scan and C-Scan NDT methods and utilized X-Ray CT to propose an algorithm which could be used to refine and predict over/undershoots in defect dimension identification. However, in this study characterized the accuracy of a variety of

methods as it comes to simulated delaminate defect detection areas using square Teflon™ tape samples at four different laminate depths. This study did not propose an algorithm, but rather demonstrated the general shortcomings and strengths of each individual NDT method when used to detect delamination defects.

2.2 Specimen Design, Materials and Fabrication

2.2.1 Artificially Induced Defect Methodology

To achieve the study's goal a range of methodologies were employed. The design choices made for the test specimen's design, material selection and laminate construction is discussed in this Section. The test specimen being created laminate nature can be seen in the edge schematic in Figure 10. With the test specimen seen in Figure 11, a variety of identical defects are introduced in each of the laminates in a patterned arrangement. The methodology employed was to create similar defect samples but with the simulated delamination at a similar depth from the Inner Test Surface but with a range of laminas in the laminate. These defects are positioned at a depth just one layer beneath the Top Layup Surface (n^{th} + 1 lamina) in the vacuum-assisted resin transfer molding (VARTM layup such that they will be uniformly near the Bottom Test Surface of the laminate in each thickness while testing. The Top Layup Surface, given the particular infusion process protocol detailed later in this section, will have a rough, porous finish. Conversely, the Bottom Layup Surface, in contact with the base mold tooling will have a much smoother surface with less porosity. This bottom surface will be the face from which scanning will be conducted as that will allow for the variable laminate depth to be observed as well. The

configuration can be seen depicted in Figure 10 below. In each laminate the position of the Teflon™ defects can be seen in Figure 11.

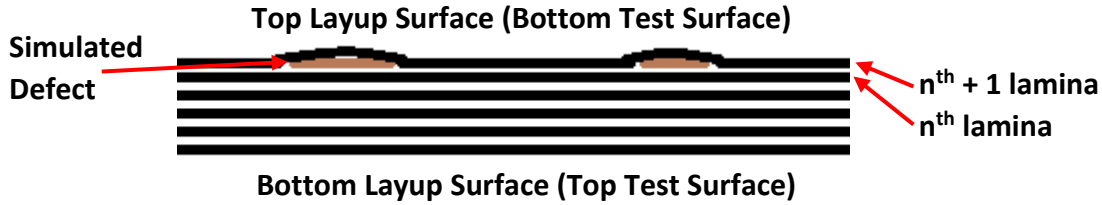

Figure 10: Schematic of Programmed Defect Sample Cross Section

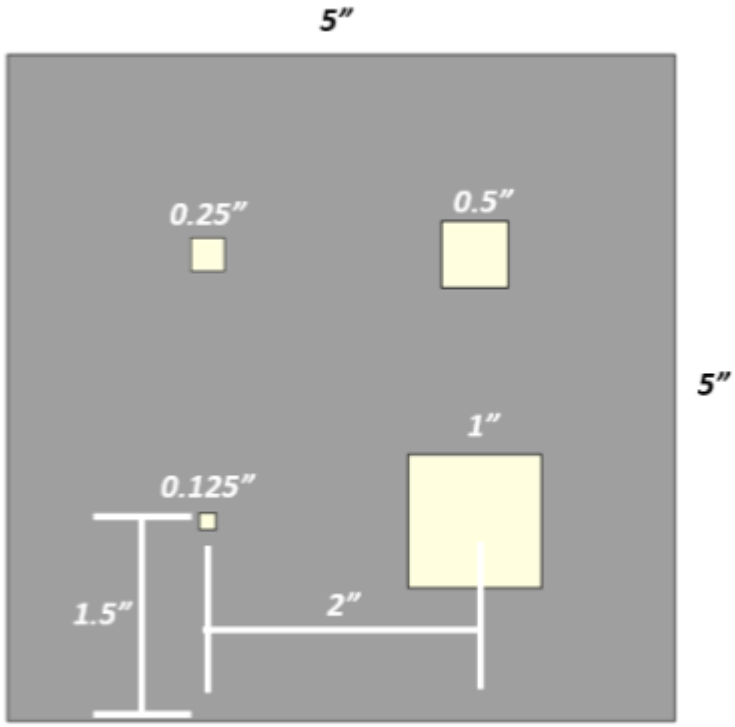

Figure 11: Schematic of Programmed Defect Sample Top View

The position of each of the square Teflon™ simulated delamination defects has the center point of each square 1.5" away from the two closest testing edges. There is also 2" separation of defect center points along each sample side. There are four sizes of defects each decreasing in diameter by 50% in each respective square, 1", 0.5", 0.25" and 0.125" respectively. In this study four similar CFRP specimens were created. In this study four

different CFRP laminates were fabricated with the four different defects. The first sample specimen was assembled from four carbon fiber lamina layers. This would mean that the defect n value is 3, as the defect is positioned between the 3rd and 4th layers. The next few were made with defect depth of 6 layers and total 7 layers, defect depth of 9 layers and total 10 layers, and finally defect depth of 12 layers and total 13 layers. This follows the n and n+1 design seen in Figure 10, with n+1 sealing the programmed defect in between layers n and n+1.

2.2.2 Materials for Creating Test Specimen

When creating the test specimen, Fibre Glast's 3K, Plain Weave Carbon Fiber Fabric was used for the laminates. This laminate material is used for lightweight aerospace applications and provides uniform strength in both horizontal and vertical directions. Gougeon Brothers Inc.'s super low viscosity PRO-SET Infusion Expoxies were used as the matrix medium. The very low viscosity allowed for the rapid saturation of the carbon fiber laminate with infused expoxy during the VARTM layup. The INF-114 Infusion Resin allowed both ambient and elevated tempature curing and the INF-211 nfusion Hardener allowed a medium cure speed. For the delamination defects an adhesive backed DuPont Teflon™ Poly Tetra Flouroethylene (PTFE) tape was used. It is made with a glass fiber yarn soaked with Teflon™ emulsion, dried and coated with a silicon adhesive. The Teflon™ tape is stable and chemical corrosion resistant, can withstand temperatures up to 500F (260C) and has a thickness of 0.011in (0.28mm).

2.2.3 Pre-Fabrication of Sample

To begin fabrication of the test sample, Fibre Glast's 3K, Plain Weave Carbon Fiber roll was placed onto a large cutting surface. A pair of scissors for cutting the roll carbon fiber were used. A 1" wide adhesive tape was utilized to bind the lamina edges together to avoid fiber fraying is used. A metallic sheen marker and straightedge machinist scale were used to mark the laminate surface as a cutting guide. The fiber roll and tools used are showen in

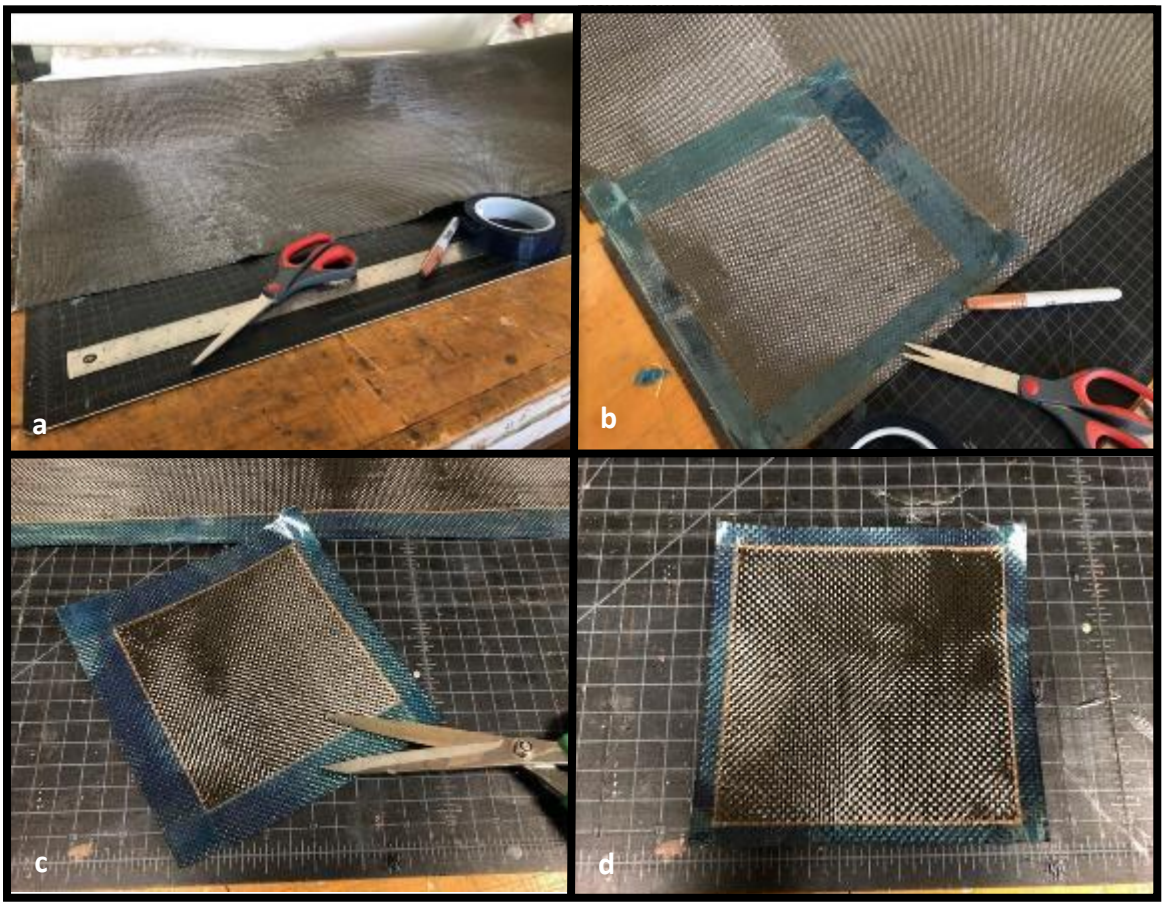

Figure 12: Initial Fabrication of Laminate Steps (a) Raw Materials (b) Lamina Square Tape Border (c) Cut Lamina (d) Trimmed Final Lamina

Figure 12 (a). In Figure 12 (c) it shows the outlines of the shape marked leaving 1" on all edges for adhesive tape. This marking was done using the straightedge machinist scale and the ruler. Additional lines were created 2" away from the 5" desired sample defining lines

as to leave room for 2 lines of 1” tape on the edges in order to ensure that the CF Weave does not pull apart in the desired 5”x5” sample. Once the defining lines are created tape is laid across the outside edge as close as possible to the line as depicted in Figure 12 (b). Next the carbon fiber square was cut from the roll. Note the 1” of tape left from the 2” tolerance in Figure 12 (c). Last, the cut lamina square was trimmed along the 1” tape edges down to 0.5” on all sides to create a final 6x6” square as seen in Figure 12 (d). This was to reduce the area taken in the mold during the resin infusion process while allowing some area for a trim cut of the laminate.

2.2.4 Defects Induced During Initial Fabrication

During the fabrication of the sample the Teflon™ squares were introduced to simulate interlaminar delamination defects. This was accomplished by applying the adhesive backed Teflon™ sheets, cut to the four sizes, as aforementioned in section 2.2.2, to the n^{th} lamina. A metallic marker was used to create guiding lines. The center of each of the four Teflon™ simulated defect squares would fall 1.5” x 1.5” horizontal and vertical distance from each edge respectively as depicted in Figure 13. Then the adhesive backed Teflon™ defect squares were applied to the surface such that the edges of each square aligned with the guiding marks. This lamina layer with the defect squares formed the lowest layer on the mold and then the n^{th} lamina was stacked upon this base lamina as seen in Figure 10 from section 2.2.1.

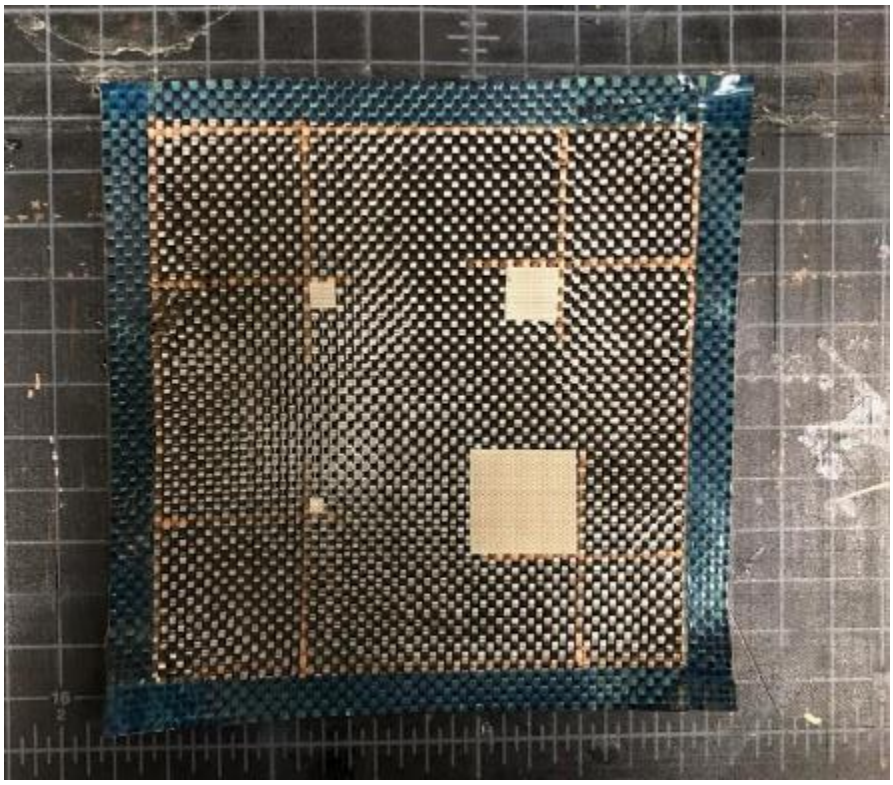

Figure 13: Designated Defect Layout Created in Prefabrication

2.2.5 1st Stage: VARTM Layup/Mold Process

Vacuum-Assisted Resin Transfer Molding (VARTM), a common low-pressure closed molding method was utilized to assemble the four CFRP samples used for comparative NDT. VARTM is conducted by assembling fibers in a desired configuration and enclosing in a vacuum bag to allow a vacuum to be applied to the mold exit vent. Outer atmospheric pressure compresses the composite laminates while the vacuum assists the flow of low viscosity epoxy resin from one side of the mold to the other side with vacuum and simultaneously wetting the lamina layers.

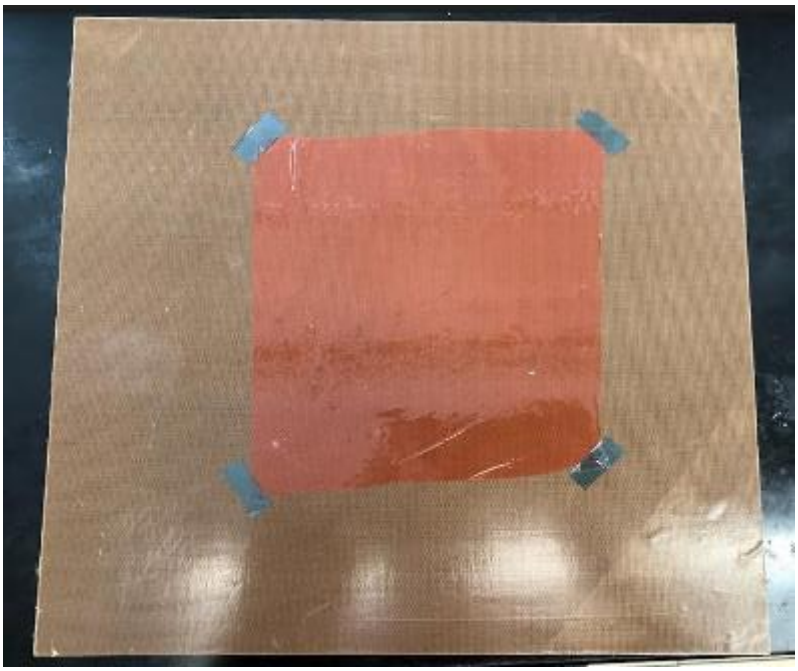

Figure 14: 6x6" Release Film Layer

To begin the VARTM layup of the CFRP samples, a 12x12" fine polished aluminum plate was used as the base mold. To protect the aluminum plate, it was covered with a sheet of the same Teflon™ tape used for the interlaminar defects. Next, a rough 6x6" layer of red release film (6x6" to account for the tape binding the edges of the CFRP weaves) is centered on the aluminum plate on top of the Teflon™ surface and taped on

each corner. On top of the red release film a peel ply was applied. It was pulled taut after each corner is secured to ensure minimal wrinkles as seen in Figure 14.

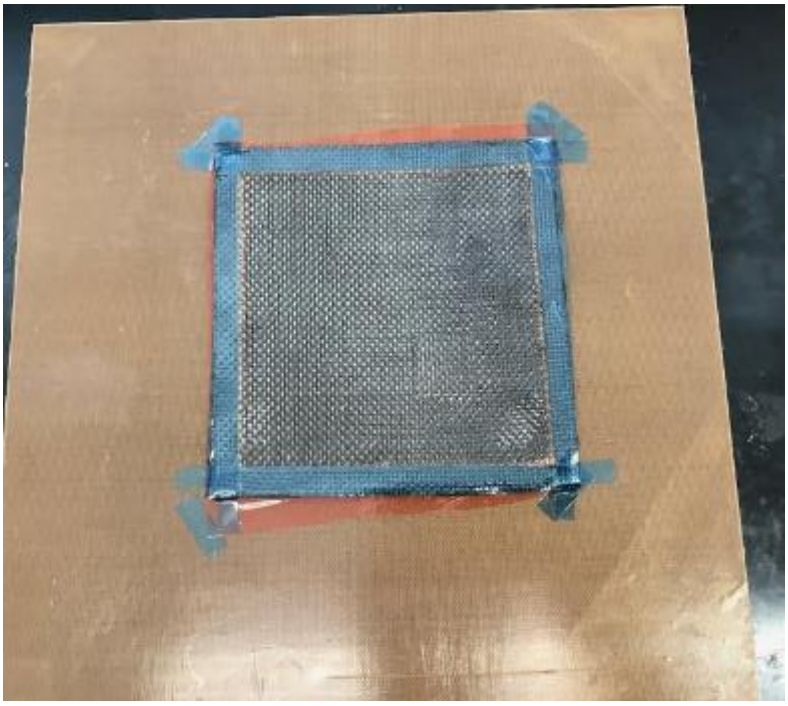

Figure 15: Ply Stack Up on Release Film

Next, the plies of 3K Plain Weave Carbon Fiber are laid onto the peel ply. The lamina were laid in order from largest to smallest in size, this accounts for slight variations in the sizes in each cut lamina. These are taped at the corners ensuring that the stack is tightly secured to the protected mold surface and is not wrinkled as depicted in Figure 15.

After laying the correct number of lamina for each desired CFRP sample a top layer 6”x6” peel ply layer is applied to the stacked lamina and taped at the corners and along the edges where the infused resin will flow as seen in Figure 16. Getting this peel ply fabric as tight as possible across the surface was important to ensure high surface quality.

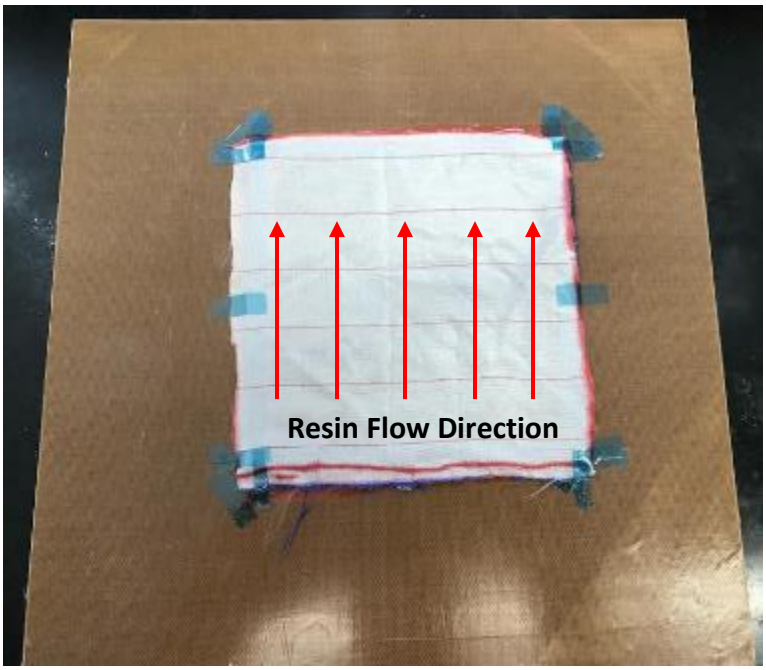

Figure 16: Peel Ply Layer

After the top peel ply layer was installed, a small 1” strip of distribution media was taped along the edge which the infusion resin would enter seen in Figure 17. Then, around the perimeter, a lining of tacky tape was placed with the backing still applied overlapping at the corners. Then the flow tubing was placed with flow holes, spaced 1” apart, facing the VARTM assembly entrance as well as exit locations as shown in Figure 18. The entrance tubing was cut to 20” in length while the exit tubing was cut to 45” in length. The additional length of the exit tubing allows for longer vacuum time before any resin would reach and thereby ruining the vacuum trap. Then, a 4” strip of tacky tape was wrapped around the tubing, aligning with the rest of the tacky tape as shown in Figure 18.

Figure 17: Distribution Medium at Infusion Entrance Edge

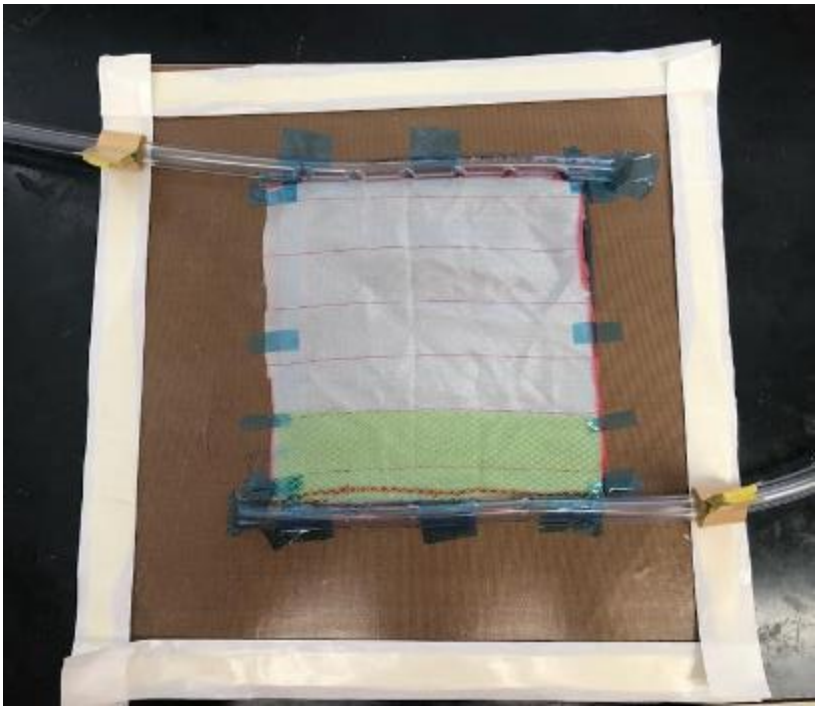

Figure 18: Tacky Tape Perimeter and Resin Flow Tubes

The next step is to peel back the tacky tape backing along the edge and remove the backing completely from the tacky tape wrapped around the tubing as seen in Figure 19 (a) to expose the tape perimeter lining and tape around the tubing. Then the tubing with the tape around it was pressed into the perimeter tacky tape and the long seam was pressed in towards the center of the tooling, depicted in Figure 19 (b). During this process it is important to not contact the tacky tape directly to prevent its compromise. The tape backing, which was previously removed, was reused to apply pressure to the tape. This was done to reduce the potential for compromise of the tape which would result in a failure to achieve and maintain vacuum during the molding process. Once this has been completed the tubing was re-covered with the wrapping which was previously peeled back along the edge as in Figure 19 (c). This step ensured that any potential contact with the perimeter will not contact the adhesive.

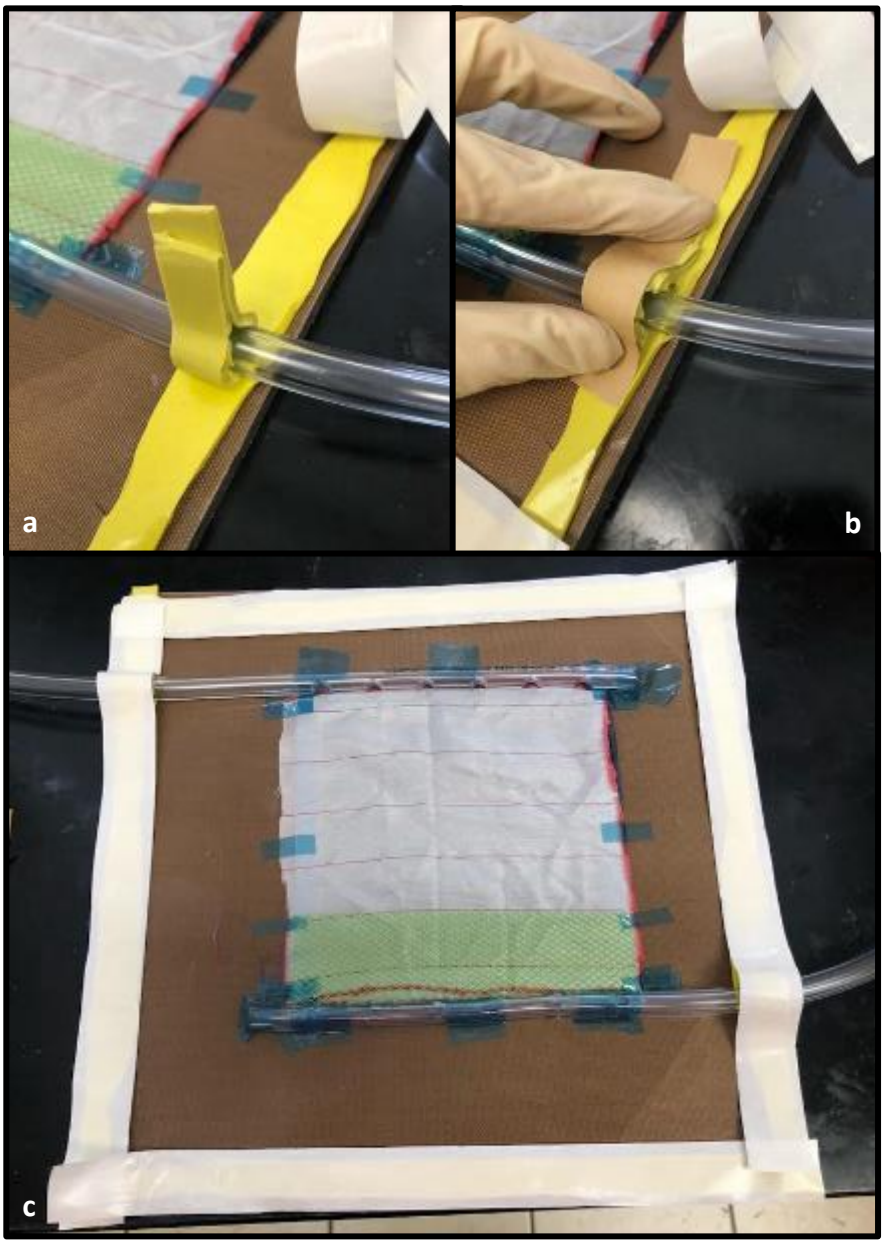

Figure 19: Tacky Tape Cover Around Tubing Peeled Back (a) Tacky Tape Around Tubing Compressed (b) Tacky Tape Peel Around Tubing Reapplied (c)

A 6”x7” piece of release film was then placed over the top surface of the layup and the tubing. This extra 1” in length allows for the release film to form a complete seal along where the tubing meets the layup. The release film is taped along the back side of the tubing as seen in Figure 20.

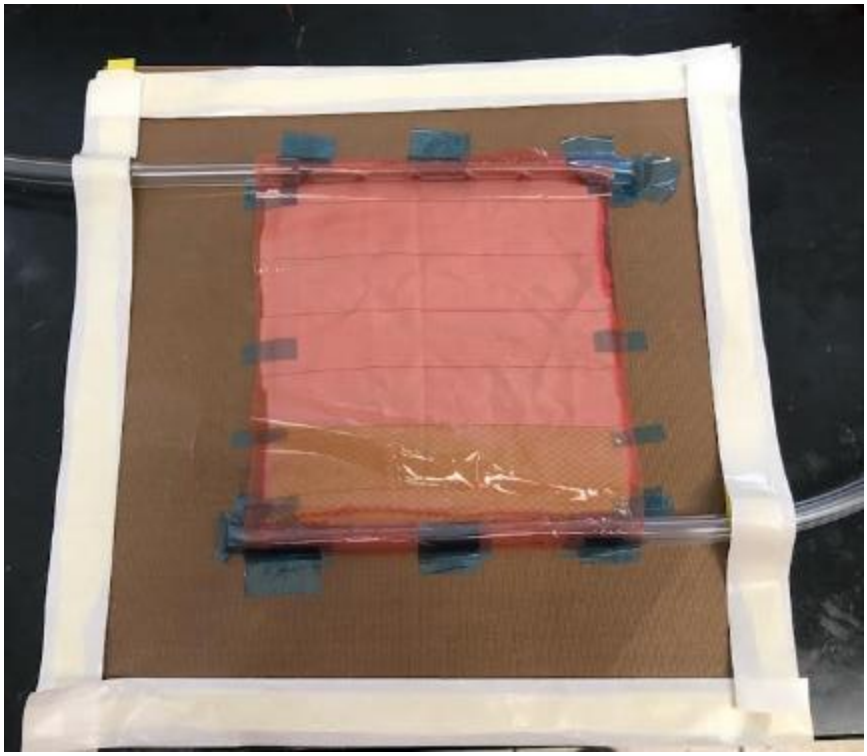

Figure 20: 6x7” Release Film Applied Over Tubing

As the last part of the mold assembly process, the backing was removed from the tacky tape on all edges and place a large vacuum bagging sheet over the top of the tooling as seen in Figure 21 (a). If recreating it is recommended to be best done one edge at a time to avoid unwanted creasing of the bag that can be difficult to seal for the vacuum pull. As a next step the mold entrance tube was sealed with a clamp. A vacuum could then be pulled from the exit tubing, the end result should be something similar to that seen in Figure 21 (b) with the bagging sheet pulled taut by the inner vacuum and outer atmospheric pressure.

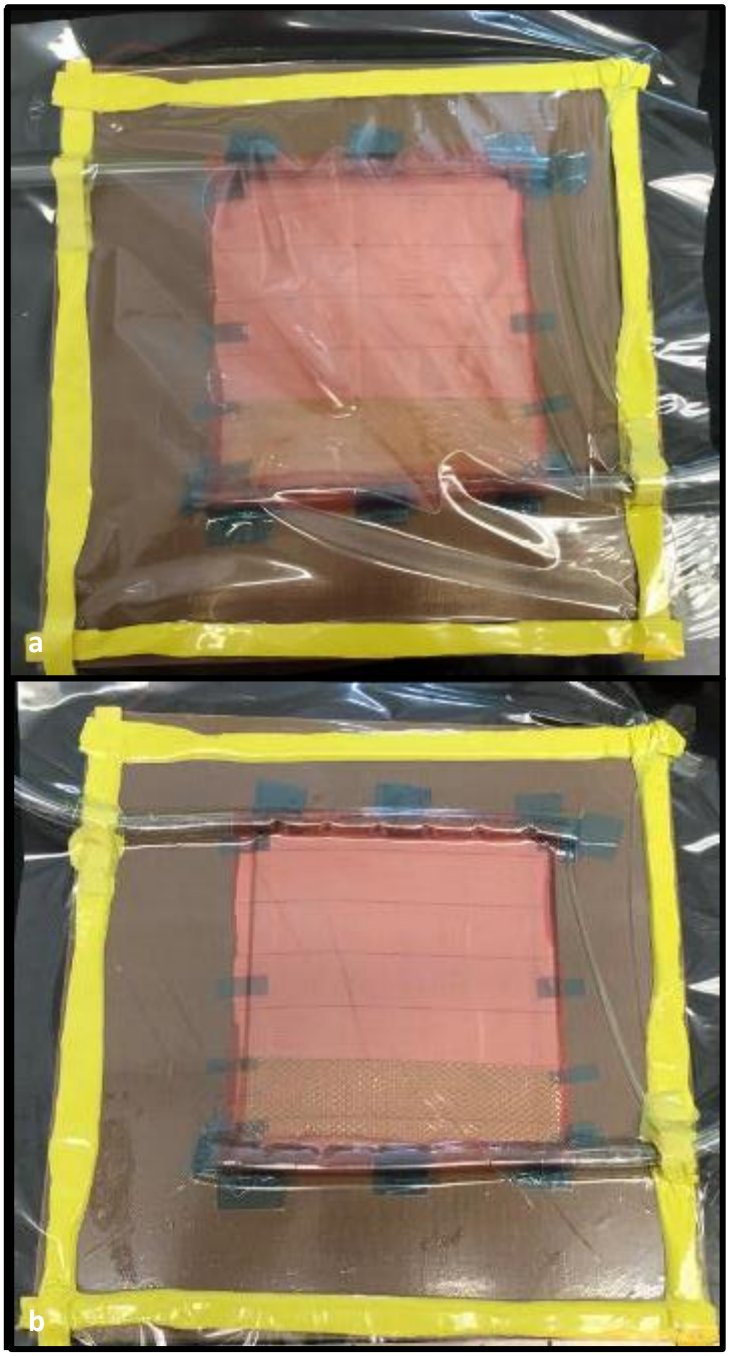

Figure 21: Vacuum Bag Adhered to Tacky Tape (a) Vacuum Bag when Vacuum is Pulled (b)

2.2.6 2nd Stage: Resin Mixing

Before infusion the epoxy infusion resin was carefully mixed. The Gougeon Brothers Inc.'s PRO-SET Infusion Epoxy INF-114 Infusion Resin and INF-211 Medium Infusion Hardener being used, seen in Figure 22, have an overall density of 1.14g/cc.

Figure 22: Gougeon Brother's Infusion Resin

In order to determine the quantity of resin needed for each sample, the following volume and density to mass equation was utilized:

$$\boldsymbol{m} = V * \rho * V_m$$

This can be solved easily since the theoretical volume and area are already known. A is the 6x6" area of the laminate, n is the desired thickness in the scanning direction (3,6,9,12) and t is the theoretical thickness of each laminate after infusion and V_m is the matrix volume fraction, which in the laminates for this study is 40%.

$$\boldsymbol{Resin\ Mass}\ (\boldsymbol{m_T}) = \big((A)(n+1)(t)\big) * (\rho) * (V_m)$$

For the purposes of the samples used in this study, the base thickness per lamina layer was found to be 0.28333cm thick in preliminary studies using this method. Additionally, the

area of the fiber sheets must be converted to centimeters to keep the unit system constant. The final equation used in this study follows this form:

$$\boldsymbol{m_T} = ((6in^2)(2.54cm^2)(n+1)(0.28333cm)) * (1.14g/cc) * (0.4)$$

The hardener to resin ratio for this particular epoxy is 1:3.65. In order to determine the proper quantity of each part (resin and hardener) the following expression was used:

$$\boldsymbol{m_R} = \frac{3.65\boldsymbol{m_T}}{4.65} * SF$$

$$\boldsymbol{m_H} = \frac{\boldsymbol{m_T}}{4.65} * SF$$

Where $\boldsymbol{m_R}$ is the mass of the base resin $\boldsymbol{m_H}$ is the mass of the resin hardener and SF is the desired safety factor for the VARTM system. For the laminate samples made for this study with the aforementioned setup from section 2.2.5, a SF value of 3 was used. So, the resulting final equation for determining the mass of resin and hardener can be written as:

$$\boldsymbol{m_R} = 3\frac{3.65(A)(n+1)(t)(\rho)(V_m)}{4.65}$$

$$\boldsymbol{m_H} = 3\frac{(A)(n+1)(t)(\rho)(V_m)}{4.65}$$

Once the respective masses of the resin and hardener were obtained, the two were combined within a plastic mixing cup utilizing a sheer mixer set at medium speed (800 RPM) for 5 minutes. This length of time ensures thorough mixing of the resin and hardener components. However, sheer mixing does introduce a substantial quantity of air. Therefore, this requires the resin was degassed and a second vacuum chamber was used for this step. This infusion epoxy has a medium cure speed hardener (INF-211) which provides 100 to 115 minutes of infusion time at 72°F (22°C) if resin feed pot stays under

100°F (38°C). Vacuum off time at 72°F (22°C) is 9¾ hours in a typical laminate. Given this cure window the recommended time for degassing can vary, but a safe point found and utilized was 30 minutes. This does give the resin enough time for the majority of the air to escape the resin without gelling. Removing air in these samples was important as the introduction of unplanned defects can result in false positives or a poor test specimen for characterizing programmed defects.

Figure 23: Resin Degassing in Vacuum Chamber

2.2.7 3rd Stage: Resin Infusion

Once the infusion epoxy resin mixture has finished degassing it was immediately infused into the VARTM assembly. The longer the resin sits the higher risk of gelling and a resultant poor infusion. Once the resin was removed from the vacuum chamber the end of the clamped entrance resin flow tube was inserted into the resin pool as seen in Figure 24. Then slowly the intake clamp was loosened to allow for the vacuum pressure fed from

the exit to pull the resin up through the intake tube. The resin flowed through the system, seen in Figure 25, once the resin has reached 3/4 of the length of the laminate area the intake clamp is once again be tightened to stop the flow of resin. The resin with the mold was then be pulled through the system and fully wet the fibers throughout the VARTM. Before any resin reached the end of the exit flow tube it was clamped similarly to the entrance to avoid contamination in the trap valve. The system is then left to sit for 8 hours in total as that is the appropriate gel time at room temperature for the resin used. It is then placed into an oven at 180°F (82°C) for an additional 8 hours which will harden the resin more quickly and increase its tensile and flexural strength compared to room temperature sure.

Figure 24: Resin Flow Tube in Resin Pool

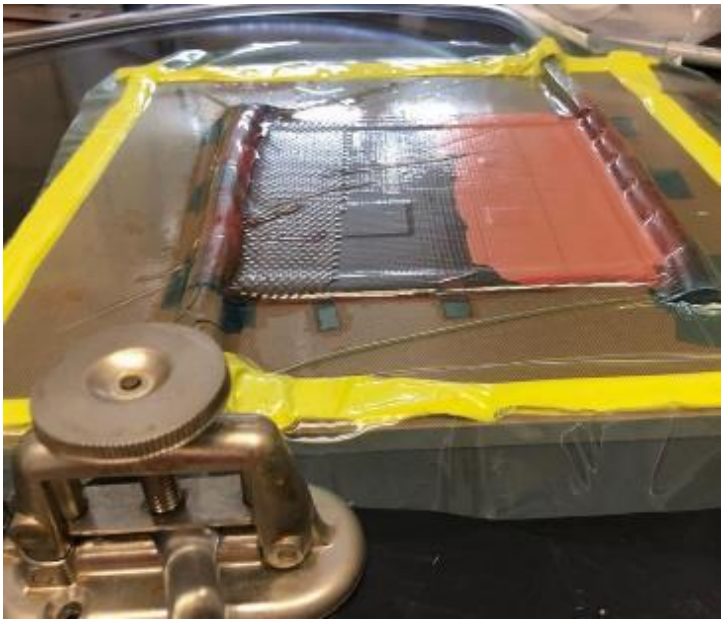

Figure 25: Resin Infusion Process

Figure 26: Fully Wetted Layup

2.2.8 4th Stage: Post Processing

The final stage in creating the test sample was to remove all of the excess resin and boundaries. First, the VARTM system was removed from the oven after the 8-hour window had expired. Once cooled the vacuum bag system was removed and all of the additional layers of release film, peel ply, etc. were removed. Then, using a FELKER TM-75 circular saw, the laminate edges are trimmed to the 5”x5” size. A hose is used to apply water to the blade while cutting the carbon fiber laminate. The water assists in cleaner cuts on the laminates. A 90-degree tracing tool was used to ensure that the cuts were consistent and outlined in metallic marker for high contrast. The markings were left to sit for at an hour prior to trimming as to not wash off when cutting the sample with the FELKER saw.

Figure 27: Untrimmed Laminate on Cutting Table

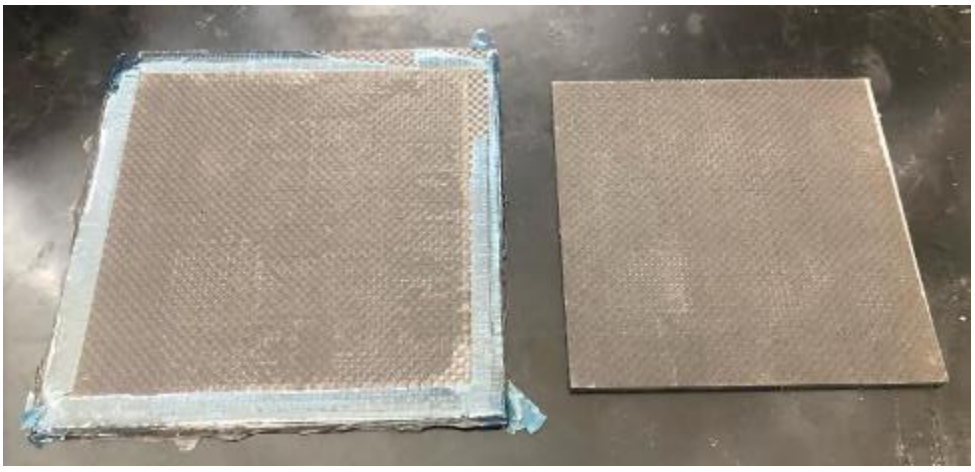

Figure 28: Composite Sample Before and After Post Processing

2.3 Sample Identification

The four NDT samples created for this study were labeled in metallic marker according to their ply count. In Figure 29 the lamina count can be seen that the respective test laminates. Labels are 3(4), 6(7), 9(10) and 12(13) respectively for the complete set. The first digit indicates the number of plies between the Top Test Surface which will be closest to the scanning tool for all but the CT scan (indicated by FRONT in the bottom left corner of the laminate) and the last digit in parentheses indicating the total number of plies in the given laminate. For example, the laminate schematic in Figure 10 would be named laminate 5(6), as there are 5 plies (n) between the Top Scanning Surface and the defects and 6 plies in total, hence 5(6).

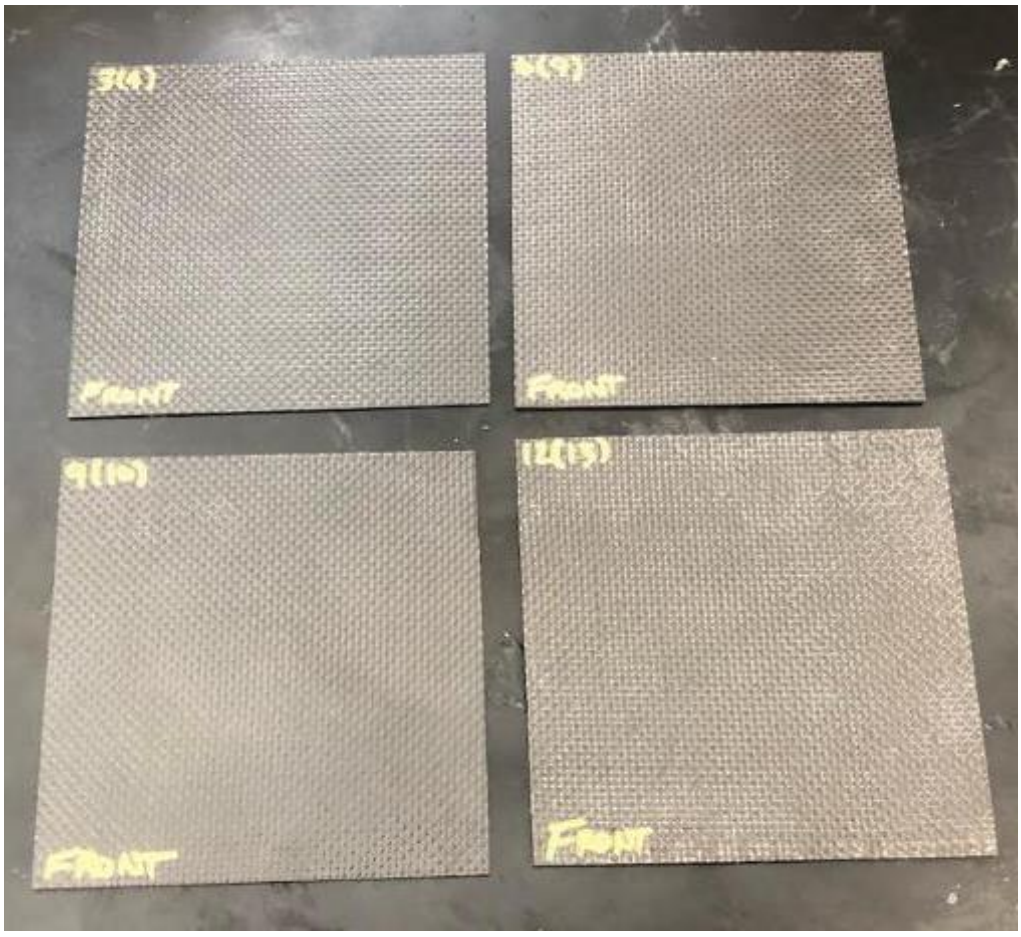

Figure 29: Final Labeled Composite Test Specimen Set

Chapter 3: Non-Destructive Testing

3.1 Ultrasonic C-Scan

3.1.1 Ultrasonic C-Scan of Composite Samples

As introduced in Section 1.3.3 Ultrasonic C-Scanning is a process which involves the mapping of the Time of Flight (TOF) of an ultrasonic wave through a material [17]. This is done via a probe which passes above the surface of the test specimen while pulsing ultrasonic waves. The Ultrasonic C-Scanner tracks the TOF while maintaining its x-y position information. The primary limitation of these systems comes down to the resolution. Ultrasonic testing equipment is typically lower resolution than the majority of other available NDT methods. The resolution limit comes down principally to probe accuracy, as the emitting probe has a specific scanning area. Additionally, more detailed scans require much longer exposure times, and in a fast-moving industry like aerospace, time is key. So, the typical ultrasonic system runs at a lower resolution to sacrifice for faster testing times. The machine being used to test the programmed defect specimens is the MATEC TTU, with a resolution of 13.337 px/in for this particular test. The test took a total of 1 hour to complete for all four panels. The raw results for the scan can be seen below in Figure 30.

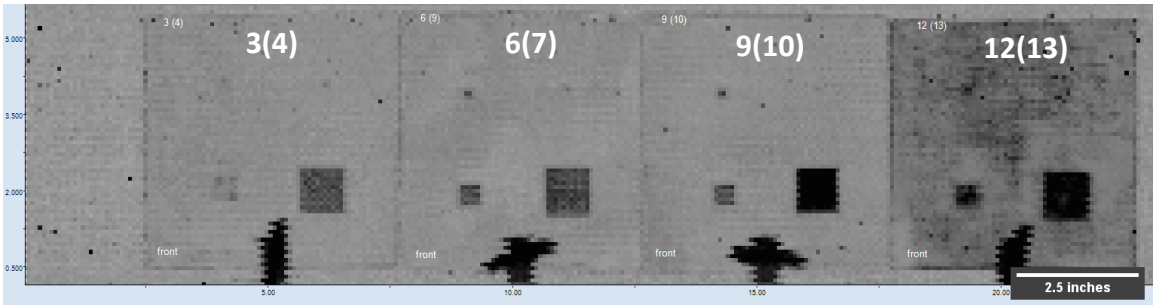

Figure 30: MACTEC TTU Ultrasonic C-Scan Raw Data

The mapping in Figure 30 makes it plainly obvious where the largest two defects, defects 1 & 2, are located in all four samples. This is due to darker regions of the scan indicating areas in which the ultrasonic sound waves hit an inner surface, were reflected and were received earlier than other – simply a lower TOF for the wave. However, the smallest of the two defects, defects 3 & 4, seem both much smaller and inconsistently revealed compared to the largest two simulated delamination defects. This can be explained by the geometry of the defects themselves. Given the low resolution of the scan and the hard edges of the defect, there will be areas in a given relatively large pixel where there is both a scanned pixel with some of the programmed defect area and some without. This mixing of TOF returns results in the color gradient as seen in Figure 31. Black indicates regions in where the relative TOF compared to the rest of the scan was low 100% of the time. Portions where there are lighter shades indicate reductions in relative TOF compared to light grey from the back of the sample. The light grey indicates that there was a uniform TOF between that area and the longest TOF of the scan. Light grey indicates the back wall, or Bottom Test Surface, of the test specimen. Utilizing Ultrasonic C-Scanning there are regions called "dead zones" which occur towards the surface of thinner material being scanned. With reduced depth the ultrasonic signals echo off of each other producing inconsistent TOFs in the material [33]. This explains why in samples 3(4) and 6(7) the programmed defects appear lighter than in 9(10) and 12(13) due to this dead zone manipulating the waves for detecting the defects which are closer to the scanning surface. An additional note is that the black portion seen

Figure 31: Ultrasonic C-Scan Gradient

in Figure 30 at the lower section of each panel is an artifact from the scanning and not a programmed defect.

3.1.2 Ultrasonic C-Scan Results Area Results Methodology

As seen in Figure 31 from section 3.1.1, there is a gradient in shading indicating concentration of ultrasonic waves. For this study we assume that the darkest portion of each defect is the effective "center" of the scanned defect and then the area outside of regions seen in the black or dark grey coloring being the border of the defect interfacing with the rest of the bulk material. Concessions were made if the darkest color is lighter than dark grey. At these interfacing regions the area per pixel will be cut off 50% of the way between the "center" border and the interface. With this being the assumption that it is approximately half programmed defect and half bulk CFRP, as it is near impossible to know how much crossing there is at these zones. This is yet another limitation of the ultrasonic method, there is a reliance on assumptions that create an imprecise measurement from the resolution (down to 0.075 inches). The ImageJ image processing software was used to conduct this image analysis. The equation used to determine the error in area is:

$$\%Error = \frac{A_i - A'_i}{A_i}$$

In this equation A_i is the programmed defect theoretical area and A'_i is the scanned defect error. This equation is used in all theoretical error analysis for all methods.

3.1.3 Laminate 3(4) Ultrasonic C-Scan Results

The thinnest laminate test sample scanned is laminate 3(4), seen in Figure 32.This sample resulted in the C-Scanner having the most trouble discerning between the smaller simulated

defects. As previously stated, this was likely due to the ultrasonic dead zone phenomena. The 0.25” square defect, defect 3, is borderline indistinguishable from the 0.125” square defect 4. Another issue that arose when testing this laminate was that the programmed defects inserted could be misdiagnosed, or at the very least confused with the small void defects more commonly scattered across the edges, particularly the top edge of the laminate sample. However, since the defect location is roughly known based off of the programmed layout the defects in each sample, the 0.25” and 0.125” were observed. In Figure 33 the outlines of defects as observed by this study are highlighted used the methodology shown in section 2.2.1. The defects are designated 1-4, 1 being the largest 1” sided square defect and 4 being the 0.125” sided square defect. The detected areas for the 3(4) sample can be found in Table 1.

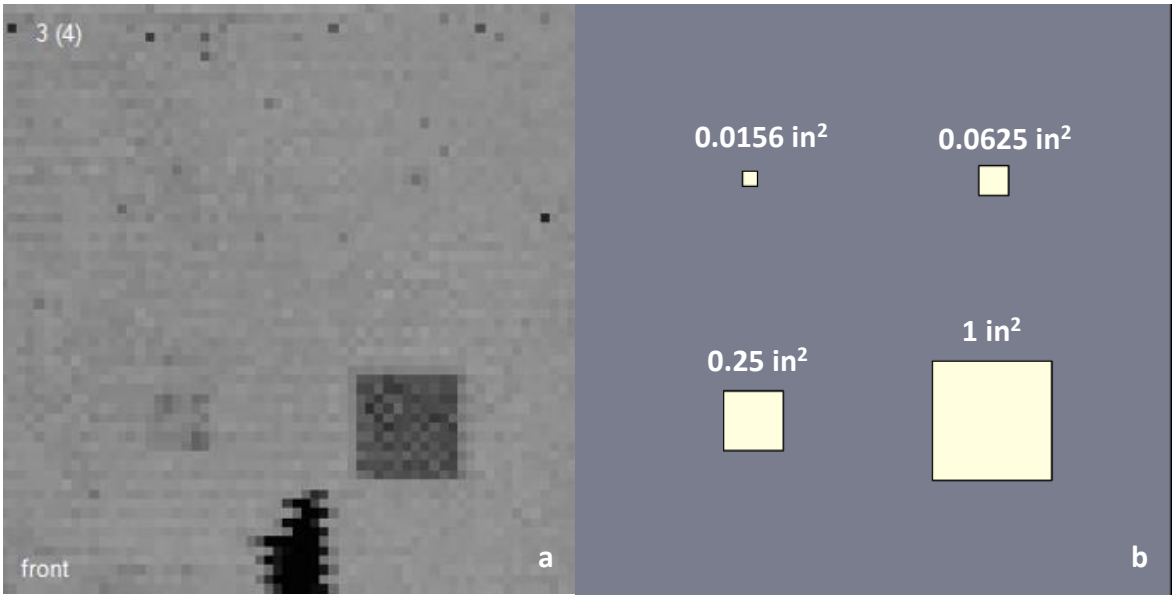

Figure 32: Raw C-Scan with Programmed Defect on 3rd Layer (a) and Laminate 3(4) Schematic (b)

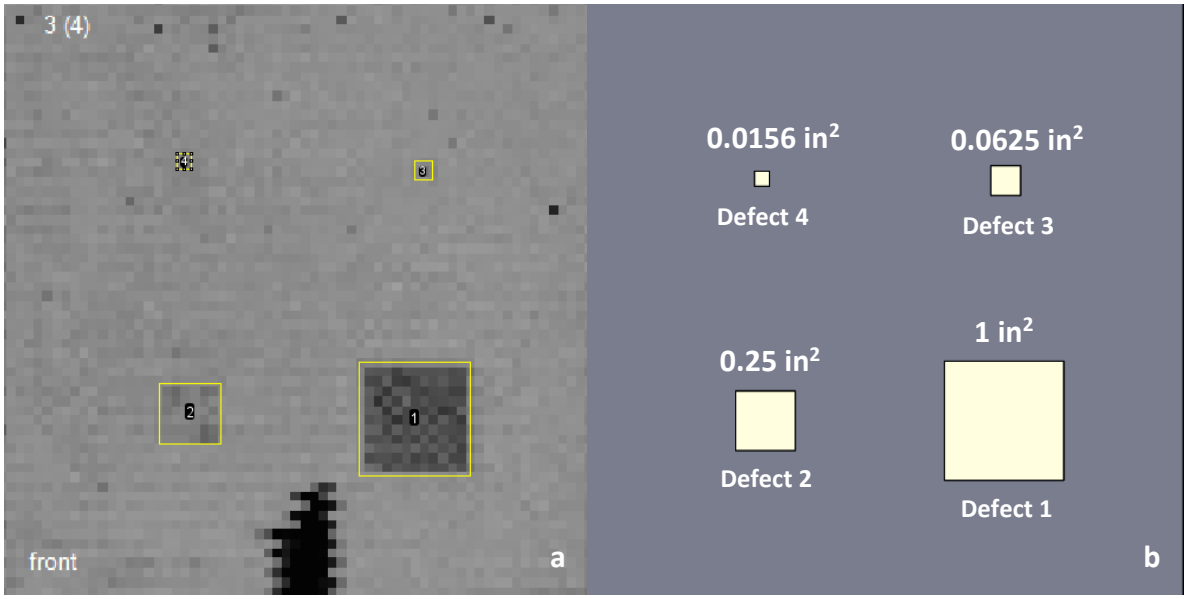

Figure 33: C-Scan Area Analysis with Defect on 3rd Layer (a) and Laminate 3(4) Schematic (b)

Table 1: C-Scan Areas Laminate 3(4)

Defect	Programmed Area (in^2)	C-Scan Detected Area (in^2)	Detection %Error	Visibility
1	1.000	0.924	-7.6%	High
2	0.250	0.282	12.8%	Low
3	0.0625	0.029	-53.6%	Minimal
4	0.0156	0.019	21.6%	Minimal

In Table 1 the theoretical area is given based off of the ideal dimensions for each of the Teflon™ defect squares cut and installed during the CFRP fabrication process. This is compared to the defect area, which generally speaking falls remarkably close for the given resolution for Defects 1,2 and 4. The reason that Defect 3 is very inaccurate, by more than 50% expected area, while Defect 4 is quite close to the desired value is due to the size of a

single pixel cell is over half of the diameter of defect 4. Therefore, any signature picked up during the C-Scan around Defect 4, assuming it is approximately one pixel wide, would always be the correct approximate size given our analysis methodology given the constraints of the scanner resolution. Following this logic, with more partial pixels, Defect 3 is less accurate. The ultrasonic edge or partial pixel dead zones combined with the small signature leads to the determination of a substantially smaller area than the defect truly was for Defect 3. The qualitative defect visibilities were also apparent. These values were roughly based on the darkest corresponding gradient color in the overall detected area. Additionally, it should be noted that in laminate 3(4) the observed defects 3 and 4 are opposite to laminates 6(7), 9(10) and 12(13).

3.1.4 Laminate 6(7) Ultrasonic C-Scan Results

With increased depth the Laminate 6(7) test sample showed much clearer defect areas. This resulted from the defects being further away from the ultrasonic dead zone near the Top Test Surface. However, the areas defined in the scanned image weren't ideally square as planned as seen in Figure 34. Once again this is explained by the resolution limitations of the ultrasonic system, given its placement on the scanning surface there is potential for the x-y position of the defect to appear rectangular as either x or y is more dominated with TOF feedback.

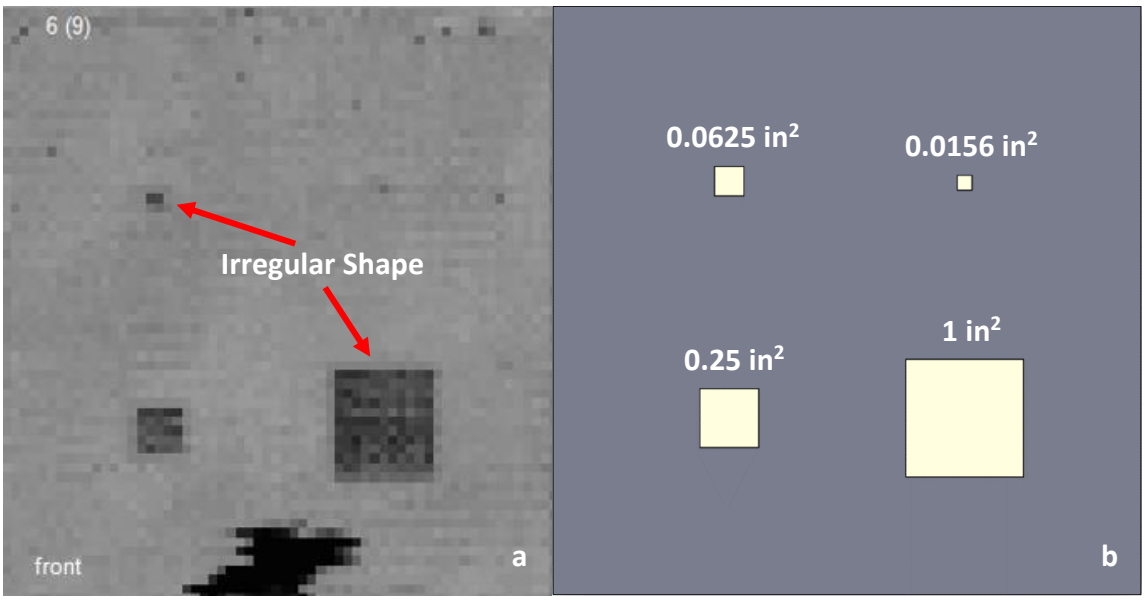

Figure 34: Raw C-Scan with Programmed Defect on 6th Layer (a) and Laminate 6(7) Schematic (b)

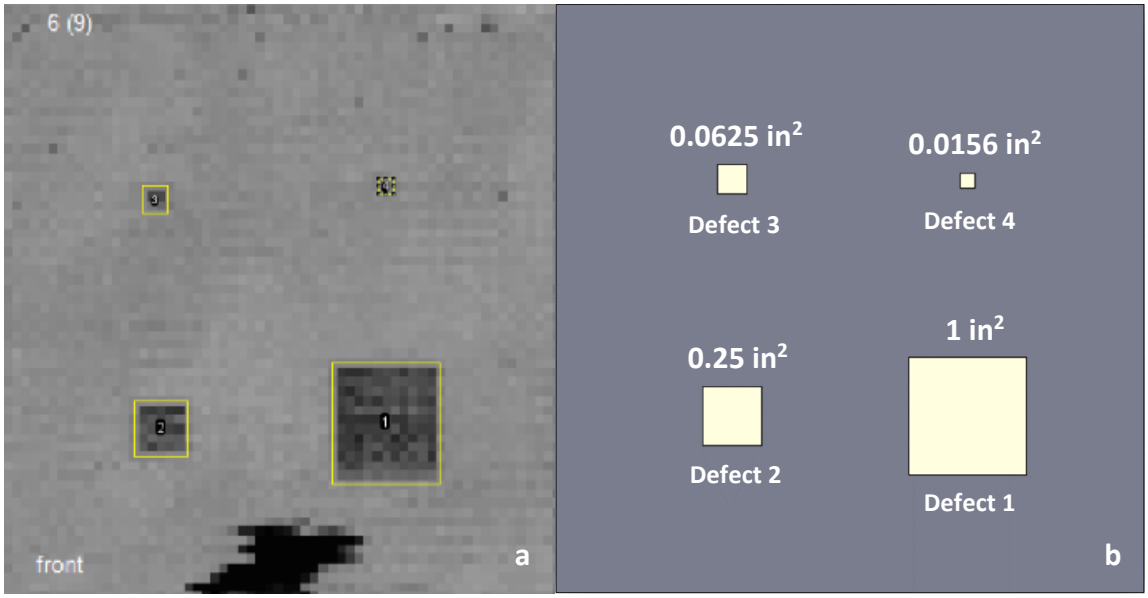

Figure 35: C-Scan Area Analysis with Defect on 6th Layer (a) and Laminate 6(7) Schematic (b)

Table 2: C-Scan Areas Laminate 6(7)

Defect	Programmed Area (in^2)	C-Scan Detected Area (in^2)	Detection %Error	Visibility
1	1.000	1.027	2.7%	High
2	0.250	0.235	-6.0%	High
3	0.0625	0.057	-8.8%	Medium
4	0.0156	0.019	21.6%	Low

In Table 2 the scanned values for Defects 1 and 2 remain relatively similar in accuracy when compared to those in the thinner Laminate test sample 3(4). Larger defects have much clearer signatures due to not being as heavily impacted by the ultrasonic scatter that happens as an ultrasonic wave travels through a material. Composite materials are notorious for this scatter as the fiber and epoxy material itself is nonhomogeneous. High frequency waves, such as ultrasonics, scatter when exposed to nonuniform mediums [34]. The identified Defect 3 in this sample is much closer to the actual size than in sample Laminate 3(4), while the smallest, Defect 4, appearance largely unchanged due to the resolution limitations of the C-Scan device utilized. The qualitative visibility for these defects was much clearer across all defects, with the largest defects (1 and 2) being highly visible while Defect 3 gives a clearer signature. Defect 4, however, given its small size retained low test visibility and is indistinguishable from other unprogrammed noise seen in the scan. Defect 4 itself is scanned close to the approximate size due to the aforementioned pixel resolution more closely matching system resolution and analysis methodology for this study.

3.1.5 Laminate 9(10) Ultrasonic C-Scan Results

Interestingly, Laminate 9(10), the third thickest test laminate studied, is the clearest scan of the set utilizing the Ultrasonic C-Scan NPT. As seen in Figure 36 Defects 1 through 3 are obvious. On the other hand, Defect 4 begins to become even harder to detect. Intuitively this makes sense as detecting smaller defects would become more difficult as the depth of a given defect was increased. This is also the first scan where a defect shows up completely without any sort of relevant scattering effect as indicated by the black gradient color on the Defect 1 area. This effect depreciates as the area of the defects become smaller, however.

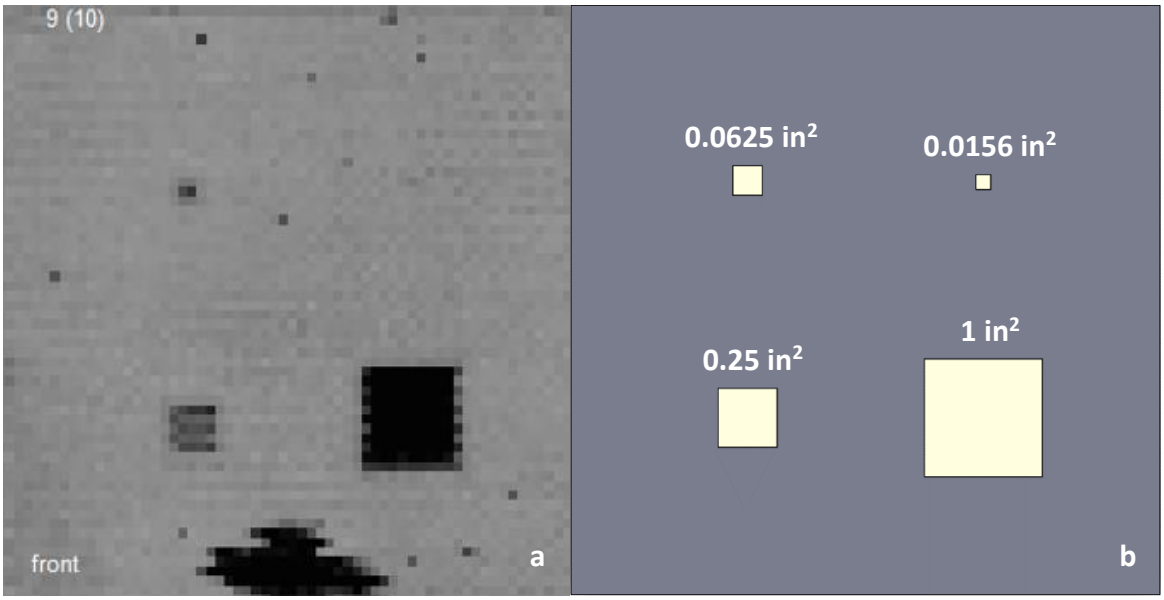

Figure 36: Raw C-Scan with Programmed Defect on 9th Layer (a) and Laminate 9(10) Schematic (b)

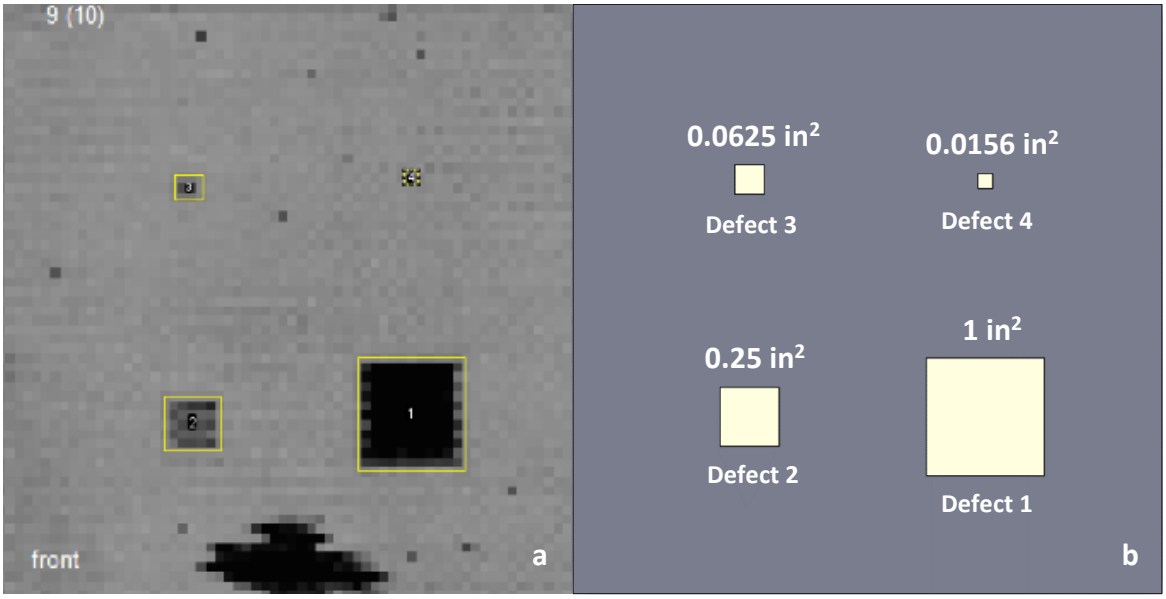

Figure 37: C-Scan Area Analysis with Defect on 9th Layer (a) and Laminate 9(10) Schematic (b)

Table 3: C-Scan Areas Laminate 9(10)

Defect	Programmed Area (in^2)	C-Scan Detected Area (in^2)	Detection %Error	Visibility
1	1.000	0.924	-7.6%	Very High
2	0.250	0.235	-6.0%	High
3	0.0625	0.053	-15.2%	Medium
4	0.0156	0.015	-4.0%	Minimal

In Table 3 the detected areas of the defects remain largely consistent to that of sample 6(7) in that, all of the detected area values fall fairly close to that of the programmed values of the associated Teflon™ delamination defects. It is clear from this image that the smallest size defect, number 4, does not improve in visibility like the other defects. The smallest defect, Defect 4, becomes even fainter as the laminate becomes thicker. This clearly

indicates a relationship between the resolution of the scanner as well as defect depth for detecting small macroscopic delamination defects.

3.1.6 Laminate 12(13) Ultrasonic C-Scan Results

Laminate 12(13) testing highlighted the effect of ultrasonic laminate scattering and noise that become more pronounced in thicker laminates. This scattering is a product of the ultrasonic frequency traveling through the non homogenous medium of the composite versus the dead zone near the Top Scanning Surface. It was seen that the larger defects allowed for the ultrasonic probe to easily descern between the composite and the defect. As these larger areas catch and reflect more waves passing through the material, whether they scatter or not. This can be seen by the higher contrast of the lighter grey areas surrounding each of the larger defects, since the relative differential TOF is easier to contrast between the back wall of the composite and the defect itself. The defects with smaller area had no such lighter grey area, Defect 3 itself appeared to just stick out enough

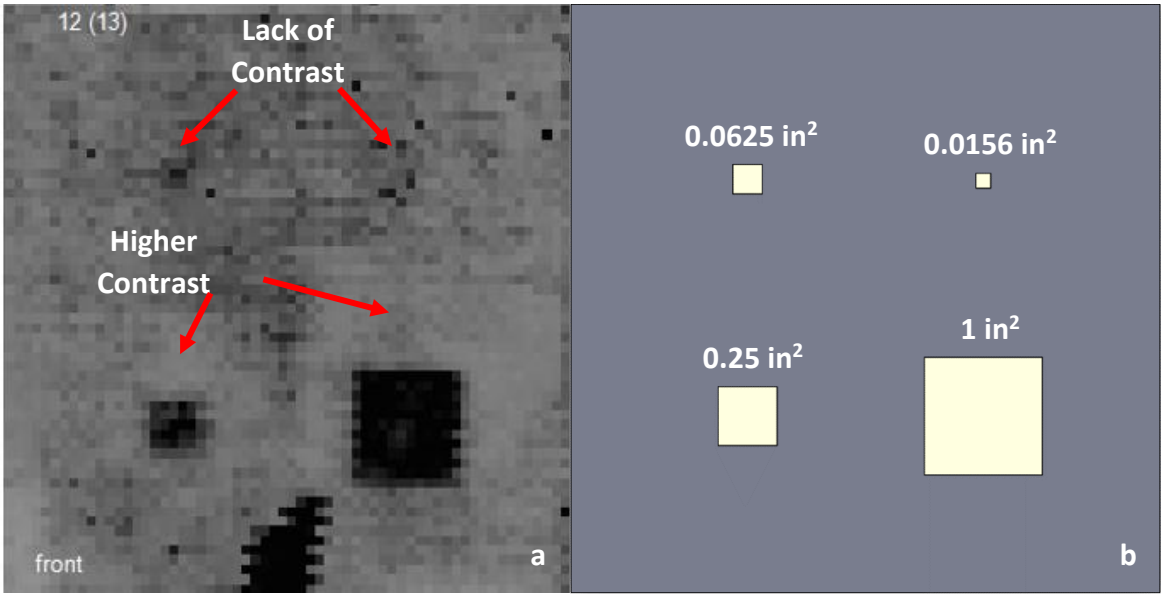

Figure 38: Raw C-Scan with Programmed Defect on 12th Layer (a) and Laminate 12(13) Schematic (b)

from the noise that it can be detected while the area around Defect 4 could be interpreted as a number of smaller defects clustered in that area or the also likely scenario that the rougher Bottom Test Surface (backside) of the sample proved difficult for the C-Scanner to differentiate at this composite thickness.

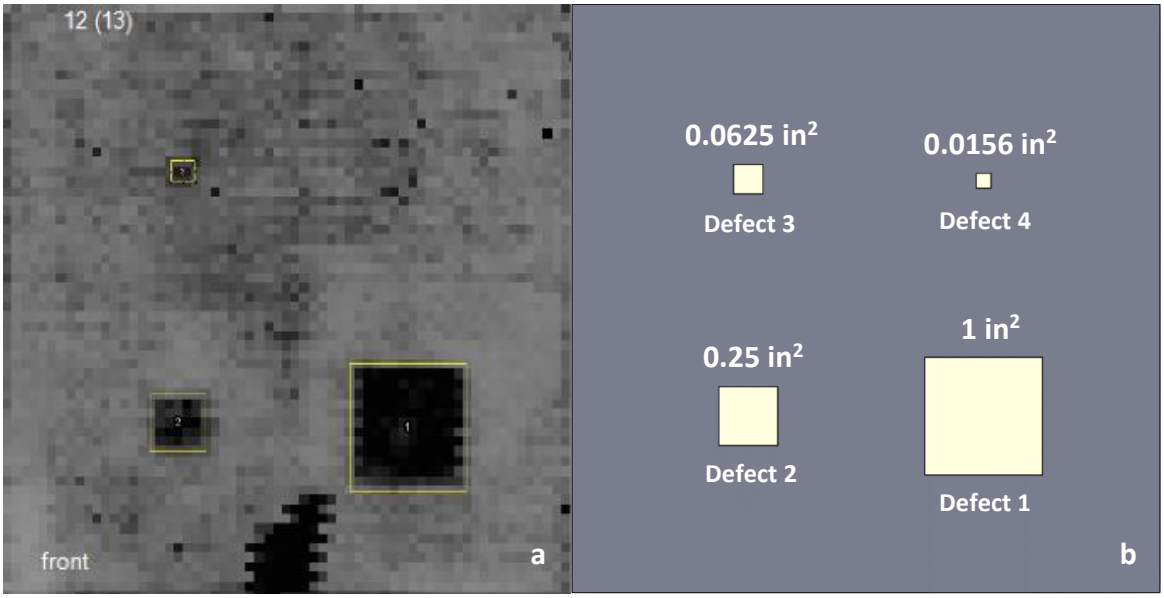

Figure 39: C-Scan Area Analysis with Defect on 12th Layer (a) and Laminate 12(13) Schematic (b)

Table 4: C-Scan Areas Laminate 12(13)

Defect	Programmed Area (in^2)	C-Scan Detected Area (in^2)	Detection %Error	Visibility
1	1.000	1.116	11.6%	Very High
2	0.250	0.238	-4.8%	Very High
3	0.0625	0.043	-31.2%	Low
4	0.0156	N/A	N/A	Undiscernible

In Table 4, once again, there was little deviation from the programmed target area between the 3 thickest test samples for the 2 largest defects. This demonstrated consistent detection for defects that are larger than 0.250 in^2. Defect 4 is not visible in any meaningful way in Figure 38. A machine operator would likely find the area of little concern as the overall mapping of the area appears noise heavy versus having a concerning delamination. Ultrasonic testing itself is very useful at identifying composite porosity. However, if the CFRP contains a potentially more problematic structural defect, like delamination, its usefulness is reduced. If the primary objective is to detect structural defects, this could result dire consequences [35]. Relying on C-Scan NDT is potentially problematic and shows this study demonstrates there is a limit to the effectiveness of these scanners the thicker the CFRP laminate becomes. While this may be intuitive and follow the common trends of UT, composites themselves come in a variety of weave patterns and fiber volume fractions. Given this relatively simple weave the scanning accuracy could be further impacted by different fiber to epoxy volume fractions or quasi-isotropic weave patterns.

3.1.7 Thickness Effect on UT for CFRPs

For ultrasonic scanning, the results across the various laminate thicknesses remained relatively steady, lacking any remarkable trends. Considering the near surface laminate dead zone limitations which impacts the thinnest and thickest samples respectively the results stay remarkably steady throughout, as seen in Figure 40. These finding are corroborated by a number of studies analyzing simulated delamination in CFRPs using ultrasonic scanning [17, 19]. The issues highlighted in the majority of these studies are the resolution of the scan and requiring some sort of image processing algorithm to predict what the scanned signature is more accurately. Within this study's data set we

see a number of issues beyond simple resolution flaws. The ultrasonic dead zone effect on area detection in near surface defects as it correlates to defect size is a parameter that has been identified through this study. Defects 1 and 2, being the largest, retained detectability throughout all of the samples whereas the smaller, Defects 3 and 4, had the most fluctuation and volatility across the Ultrasonic C-Scan tests. The range of thicknesses for the laminates used in this study are aimed to reflect actual use cases of aircraft skin assemblies, versus merely going to the extremes of CFRP thicknesses. A practical tool used in industry for

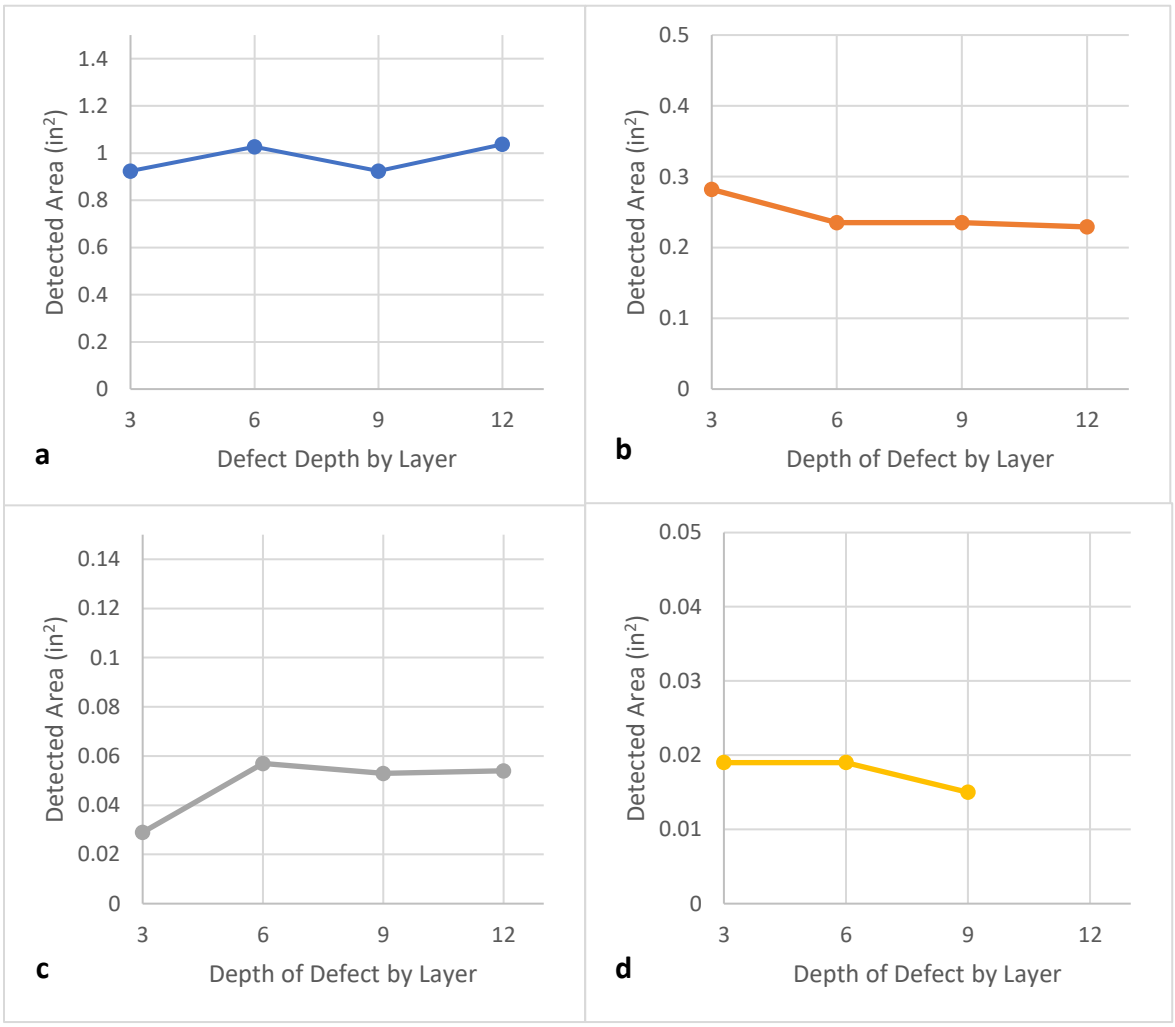

Figure 40: Ultrasonic C-Scan Defect 1 (1 in^2) Detected Areas (a) Defect 2 (0.25 in^2) Detected Areas (b) Defect 3 (0.0625 in^2) Detected Areas (c) Defect 4 (0.0156 in^2) Detected Areas (d)

UT being the MACTEC TTU was utilized for this study as to accurately reflect the current aerospace industry capabilities.

3.1.8 Ultrasonic C-Scan Summary

The collected data from C-Scanning the set of test laminates brought forward a few interesting takeaways. As identified in the study CFRPs with small near surface defects have trouble being identified if below a quarter inch in area. This is due to the ultrasonic near surface dead zone of the interrogating probe. Another point highlighted by this study is the effect of nonhomogeneous materials on defect detection. UT requiring large penetration depths result in more noise interpreted by the UT probe as defects. Despite this, for large delamination defects around 1 in^2, which would be critical to detect in aircraft maintenance, ultrasonic testing shows reliability with relatively small fluctuations in defect signature capture. For smaller defects, less than 0.25 in^2, the dead zone is a major issue in identification. Once past the surface dead zone the Defects 2 through 4 can be detected up until laminate 12(13). In this laminate the smallest defect is lost to the ultrasonic noise from the fiber/matrix configuration. The four Ultrasonic C-Scans used in this study took a total of 1 hour to complete. This time accounted for both setup as well as sample scanning time. While this NDT method is not the quickest of the rapid inspection tools, the level of consistency at each depth seen for all but the smallest delamination defects make UT an option for CFRP testing [35].

3.2 Shearography Testing

3.2.1 Shearography Scan of Composite Samples

Optical Shearography utilizes the interference of laser speckle patterns on a surface to identify minute strain changes in a material. There are multiple forms of material excitation for shearography, the most common of which are thermal and vacuum excitation. In this study both thermal and vacuum excitation shearography were utilized on the samples. The tests were conducted utilizing the Laser Technology Inc. LTI 5100HD shearography system. In order to reduce surface reflection, the standard florescent penetrant inspection (FPI) method C spray penetrant was used.

3.2.2 Thermal Excitation Shearography

Under thermal excitation it was found that none of the laminates gave any signature indicating a composite defect. This is likely due to the thermal loading on the composite surface was inadequate to achieve thermal expansion on the level of the composite defect. The Teflon™ tape simulating an actual delamination may well have performed differently than air when subjected to heat. There are a number of factors which contribute to this, one of the major ones being the thermal diffusivity. Fiber volume fraction is a primary contributor to the propagation of heat through the system. Higher fiber volume fractions contribute to higher thermal conduction into a material [37]. Epoxy resins are not efficient conductors of heat thus thermal processes rely on the carbon fibers in the laminate to provide the majority of the thermal conduction.

3.2.3 Vacuum Excitation Shearography

Under vacuum excitation some of the larger defects were detected. Additionally, the role of surface finish comes into play impacting the effectiveness of the collection of shearography data. This was demonstrated in Figure 41. The vacuum excitation shearography setup and scanning were conducted in a total of 30 minutes time. The partial vacuum level was 50 in/H_2O with a shearing direction of +45°. As aforementioned, shearography data can be difficult to interpret given the low contrast visuals presented. Defect signatures can be seen in laminates 3(4), though obstructed by surface glare due to the weave pattern in the field of view. Laminate 6(7) had multiple defects visible and Laminate 9(10) Defect 1 can be easily identified and a very slight trace of defect 2. The thickest, strongest test sample, Laminate 12(13) did not reveal any defects in either applied vacuum or thermal excitation test scenarios. These defects are highlighted in the overview in Figure 42.

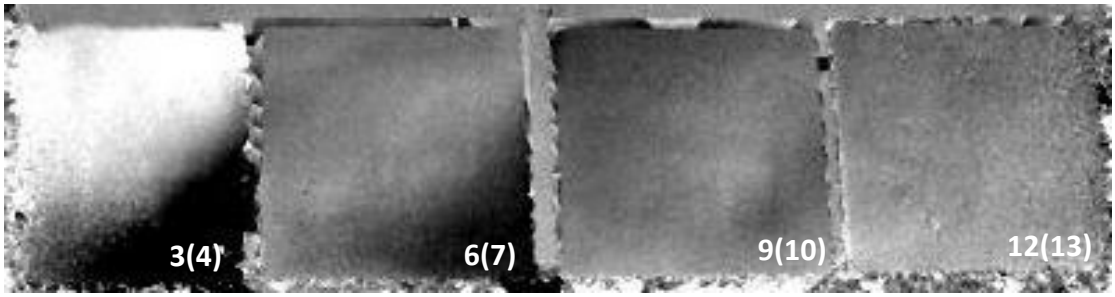

Figure 41: LTI 5100 HD Vacuum Excitation Shearography

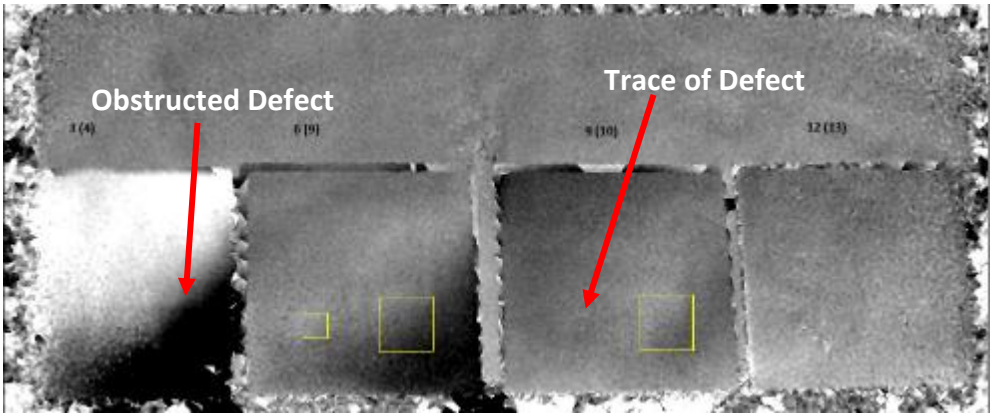

Figure 42: Vacuum Excitation Shearography Highlighted Delamination

3.2.4 Laminate 3(4) Vacuum Excitation Shearography Results

Laminate 3(4) experienced issues with the laser shearography system being used due to reflections. Even after application of an industrial-grade coat of matte spray penetrant to reduce glare, the surface was unable to be read well. The shearing angle of +45° can be observed given the reflections exhibited in Figure 43. The outline of the largest Defect 1's top left corner can be observed, however the glare resulting from the composite surface obstructs visual detection of the majority of the delamination defect. In a pure sense the largest defect was detected, however it is undiscernible that there are any other defects given the glare. It is likely that Defect 2 could be found given if surface finish was less problematic for the scanning device as it could be detected in Laminate 6(7) as well as trace

in 9(10). It is impossible to tell if Defect 3 or 4 could be detected at this thickness laminate sample.

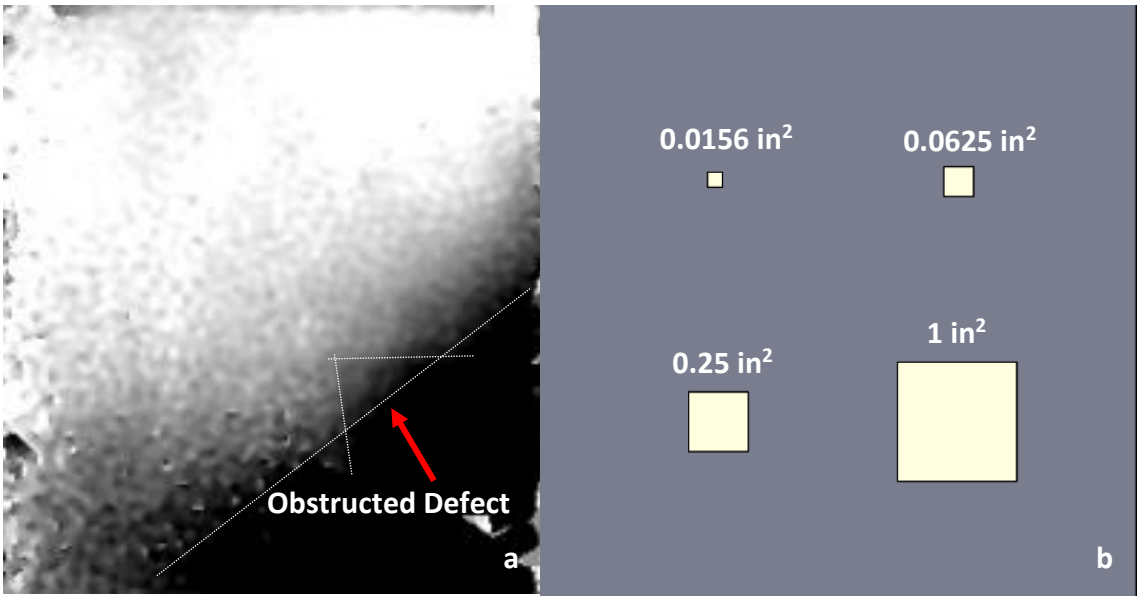

Figure 43: Raw Shearography Data with Programmed Defect on 3rd Layer (a) and Laminate 3(4) Schematic (b)

3.2.5 Laminate 6(7) Vacuum Excitation Shearography Results

Laminate 6(7) presented the strongest raw vacuum excitation shearography detection results across the four test samples . Both Defect 1 and Defect 2 are detectable on the surface. There is minimal surface glare on this sample as compared to laminate 3(4). With image processing technology utilized by the LTI 5100HD highlights increased detected surface gradients, similar to how ultrasonic scanning would highlight the relative TOF as seen in section 3.1.

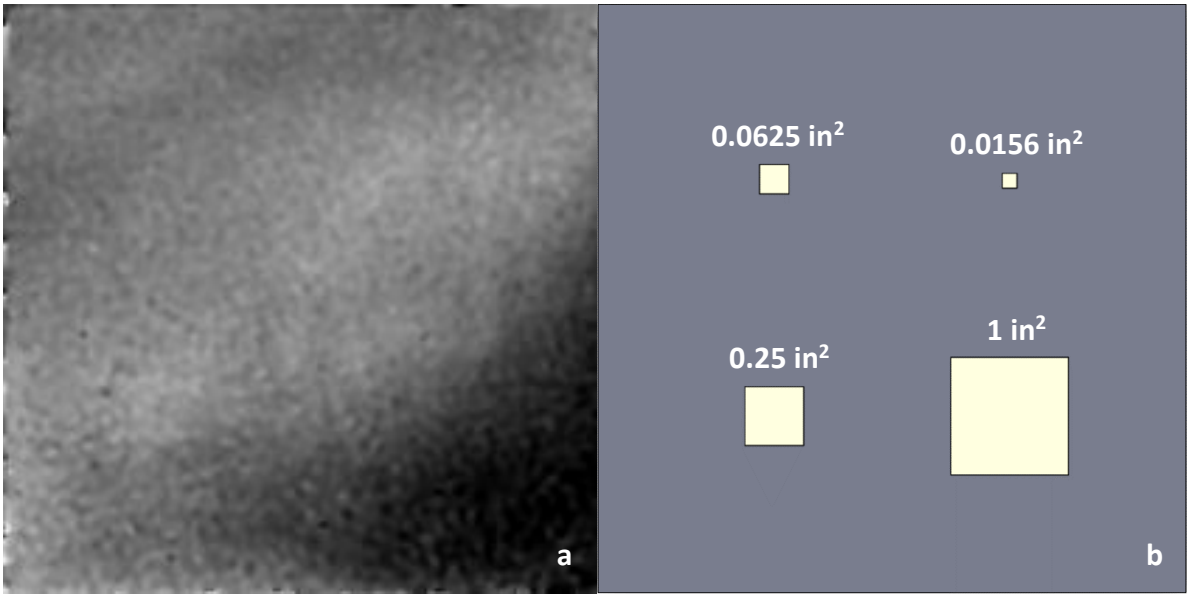

Figure 44: Raw Shearography Data with Programmed Defect on 12th Layer (a) and Laminate 12(13) Schematic (b)

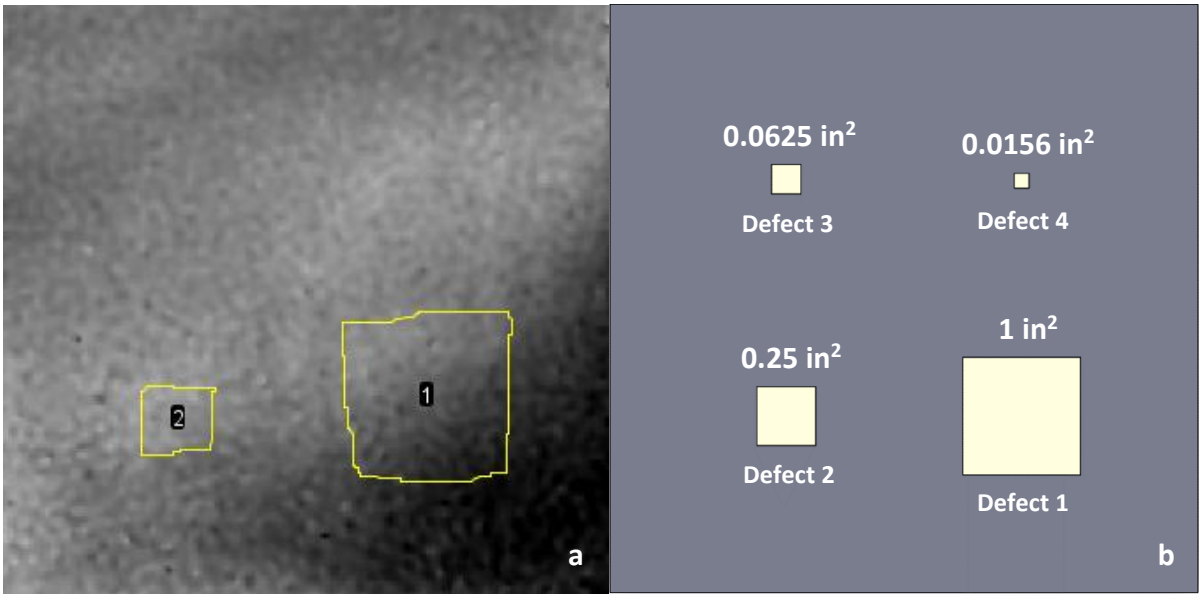

Figure 45: Shearography Area Analysis with Defect on 6th Layer (a) and Laminate 6(7) Schematic (b)

Defect areas 1 and 2 were found utilizing ImageJ processing software. The outlines were created by outlining the highlighted area; however, these highlighted areas were very difficult to detect precisely and required meticulous overview to create. Defect 1 was found

to have an area of 1.700 in^2, much greater than the actual 1 in^2 programmed area with 70.0% error. Defect 2 was found to be 0.321 in^2, greater than the actual 0.25 in^2 programmed area, a 28.4% error. This larger than actual area can be attributed to the flexing of the bulk material from the vacuum generated strain. , unlike some other methods of NDT. Thinner cross section of material will flex to a greater extent about the defect area, given the reduced area moment of inertia, to create the visual of a larger area.

3.2.6 Laminate 9(10) Vacuum Excitation Shearography Results

Laminate 9(10) gave a relatively clear image of Defect 1; Defect 2 was visually decipherable. However, in order to not confirm experimental bias, it was not included as it is nearly invisible unless looking at the known programmed defect location.

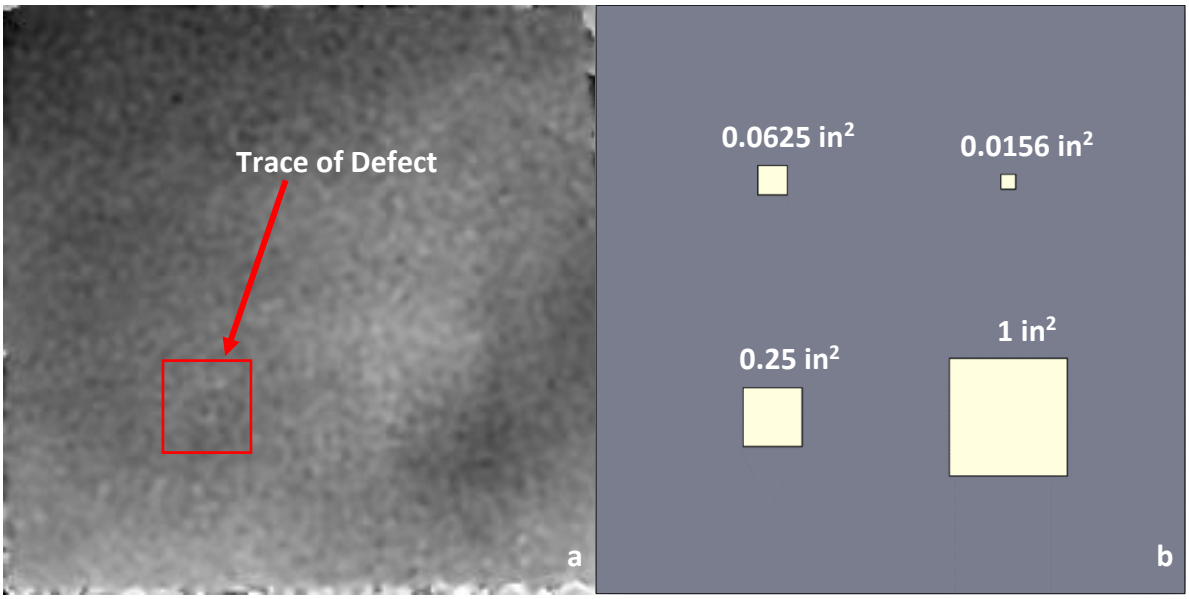

Figure 46: Raw Shearography Data with Programmed Defect on 9th Layer (a) and Laminate 9(10) Schematic (b)

Defect 2 is indicated in Figure 46, though almost indistinguishable from the surrounding area. The defect is somewhat easier to visualize in Figure 41 in section 3.2.3. The only defect with a detectable area, Defect 1, was found to have an area of 1.445 in^2, which is

greater than the theoretical 1 in^2 programmed area defect with 44.5% error. The smaller Defects 2, 3, and 4 were undetectable using this NDT process.

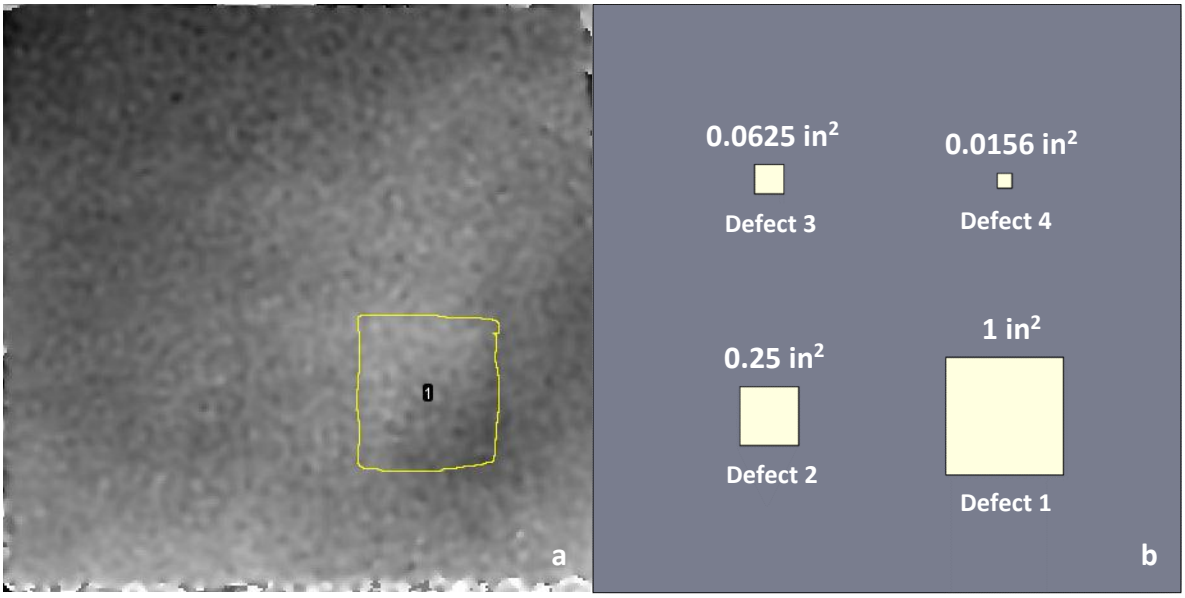

Figure 47: Shearography Area Analysis with Defect on 9th Layer (a) and Laminate 9(10) Schematic (b)

3.2.7 Laminate 12(13) Vacuum Excitation Shearography Results

Laminate 12(13) has no detectable defects on this thickest, most rigid test sample. This laminate additionally shows some haziness on the edge, indicating that the edge was at the end of the shearography equipment FOV. This is the only sample seen that has no trace of defects, indicating that this thickness is too great for the 50 in/H_2O partial vacuum to produce any identifiable shearing strain.

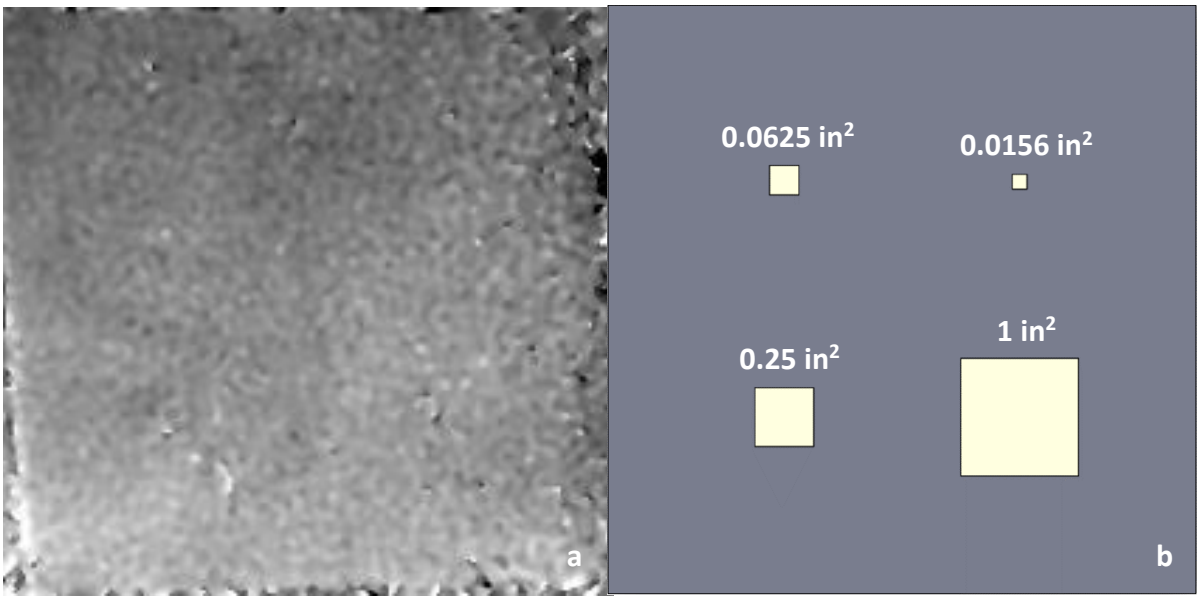

Figure 48: Raw Shearography Data with Programmed Defect on 12th Layer (a) and Laminate 12(13) Schematic (b)

3.2.8 Thickness Effect on Shearography for CFRP

Unlike UT, shearography demonstrated a relationship between observed area and composite thickness. Defect 1 appears clearly in both 6(7) and 9(10), which had detected values of 1.700 in^2 and 1.445 in^2 respectively. The values are much greater than the actual 1 in^2 area measure, demonstrating that shearography reports delamination defect areas larger than the actual defect itself. The detection results appear to become closer to the actual defect size the stiffer the material (thicker) it gets. Additionally, Defect 2 in laminate 6(7) appears as 0.321 in^2 versus the actual 0.250 in^2. Defect 1 is also detectable in Laminate 3(4), however area is indecipherable. Given the trend seen it is likely to assume Defect 2 in Laminate 3(4) would also be visible under correct surface conditions. For defects of areas 0.250 in^2 there appears to be a point where they can no longer be excited by the shearography process between the 6- and 9-layer lamina depths. There is potential for this

method to overcome the lack of depth information through the understanding of these trends. This would be valuable as one of the primary drawback of shearography is the missing depth information.

3.2.9 Shearography Summary

Shearography proves to be somewhat limited due to the methods of excitation utilized and the surface properties. Thermal excitation of the CFRP laminate set resulted in the detection of no programmed defects. This is most likely attributed to the lack of thermal diffusivity through the laminates themselves. There is potential for stronger heat sources to allow delamination defects to be drawn out. Results of other NDT methods will reveal it may be worth utilizing alternative methods to heat excitation shearography. Additionally, Teflon^{TM} could be a poor test case for this particular method of excitation since its thermal expansion characteristics are different than a traditional air-filled delamination. Vacuum excitation did allow detection of delamination defects. Limiting though, the size of defects drawn out were primarily limited to the largest defects, 1 and 2. The smaller defects did not appear to be drawn out by the partial vacuum pressures excitation utilized. Stronger vacuum pressures may draw out the smaller defect areas, but further testing would be required. Additionally, shearography is very susceptible to missed or flawed readings due to the surface finish of the test sample. Despite the use of surface matte spray to reduce reflections, the weave pattern of the CFRP laminate 3(4), though identical to the other laminates, resulted in a much harsher glare which obstructed the detection of the programmed defects. There is evidence that is encouraging about vibration excitation of CFRP laminates being able to detect defects of smaller sizes [39]. What makes Shearography appealing is its non-contact methodology, where inspecting large swaths of

area is advantageous, as aero structures have many large skin sections. Shearography is an ideal tool for relatively rapid detection of some larger defects in a CFRP skin panel [39].

3.3 Thermography Testing

3.3.1 Thermography Scan of Composite Samples

Thermography involves the measurement of differences in the thermal characteristics of a material. In this study pulsed thermography was used, specifically Thermal Wave Imaging, Inc.'s EchoTherm Flash Thermography System. This process utilizes an optical heat flash to the surface of the material as well as an infrared imaging system to track the heat flow through the system [40, 41]. In this study each laminate was

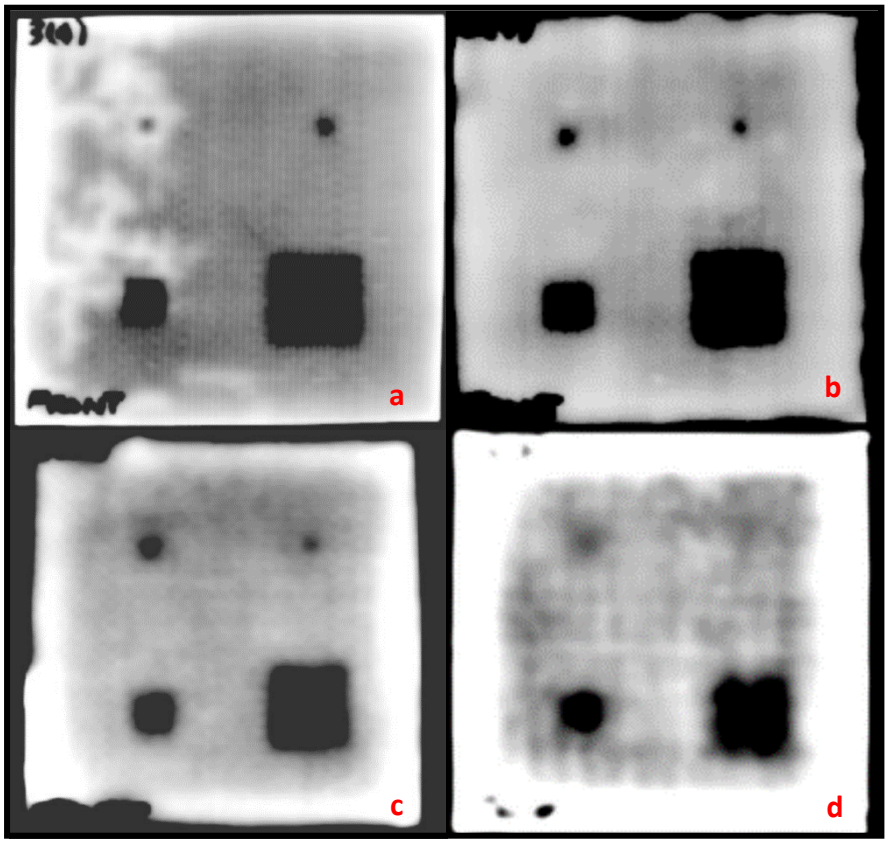

Figure 49: TWI EchoTherm Thermography Laminate 3(4) (a) Laminate 6(7) (b) Laminate 9(10) (c) Laminate 12(13) (d) Raw Data

scanned individually as only one interrogated depth is visible at a given time for each image. The total length of time for scanning was just over 3 minutes accounting for setup time for the camera and scanning of the four test laminates. The raw images of these scans are seen in Figure 49. The contrast shown in these test sample laminate images indicate the areas in which the programmed defects obstruct the flow of heat through the material, and which were observed by the scanner. The edges of the embedded square defects are not particularly sharp. This lack of edge contrast is due to the way in which corners will lose heat faster due to the greater exposure to the bulk of the material at the vertices of the defects. This lack of contrast appears to become more significant as the composite laminate becomes thicker.

3.3.2 Laminate 3(4) Thermography Scan Results

The pulsed thermography scan of Laminate 3(4) shows that all embedded delamination test defects can be observed. The thermography scan was also able to detect a region of the laminate which was resin starved. The area of resin starvation appears to have impacted the area detection of the programmed defects in that respective region slightly. Each defect was clear and was analyzed using the ImageJ processing software similarly to the other methods studied. The white edges seen on the border are a thermal artifact from the exposed edge with air being a strong insulator. In a scan of an aircraft skin on an assembled aircraft this would not be present. The scanning time for this sample took a total of 5 seconds once setup was completed.

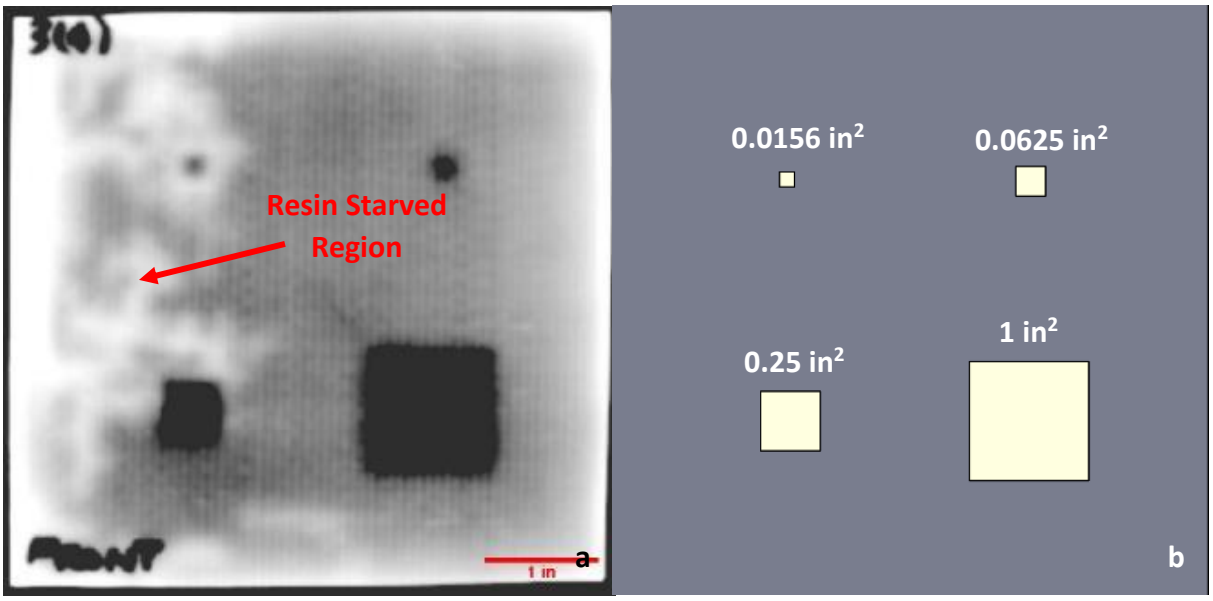

Figure 50: Raw Thermography Data with Programmed Defect on 3rd Layer (a) and Laminate 3(4) Schematic (b)

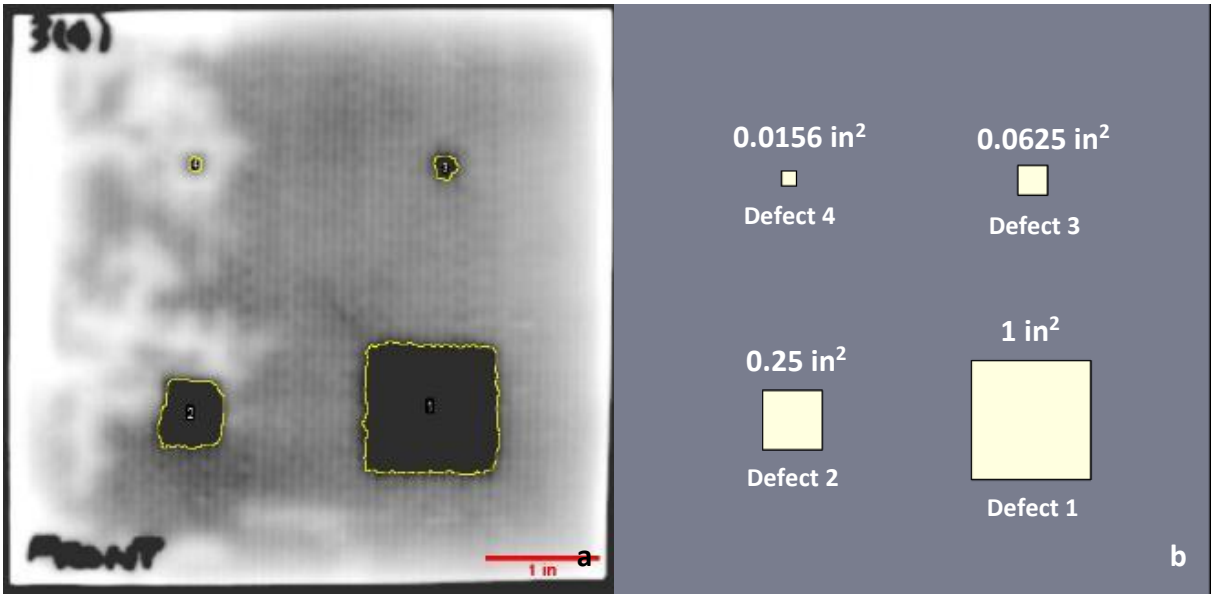

Figure 51: Thermography Area Analysis with Defect on 3rd Layer (a) and Laminate 3(4) Schematic (b)

Table 5: Thermography Areas Laminate 3(4)

Defect	Programmed Area (in^2)	Thermography Scan Area (in^2)	Detection %Error	Visibility
1	1.000	1.262	26.2%	Very High
2	0.250	0.290	16.0%	Very High
3	0.0625	0.032	-48.8%	Very High
4	0.0156	0.010	-36.0%	Medium

Figure 50 shows the effect of the resin starved region on the scan of Defect 2 in particular. The scalped corner of that sample would indicate that some of the sample is obscured by this region. If that is the case then it is safe to assume the calculated scanned error would be higher than the 16% seen in Figure 51. Additionally, the smaller defects have the most trouble distiguishing the square shape as programmed. This detection challenge for share is due to the lack of bulk material to disrupt the heat transfer through the laminate. This resulted in a significant underprediction in the area of the defects.

3.3.3 Laminate 6(7) Thermography Scan Results

The thermography scans show that all programmed defects are detectable for Laminate 6(7) seen in Figure 52. When compared to laminate 3(4), the defects are all highly visible. The edge detection for the smaller Defects 3 and Defect 4 become more rounded, showing that the effect seen in area reduction from laminate 3(4) is further aggravated by increase defect depth. The scan conducted on Laminate 6(7) took 10 seconds to complete.

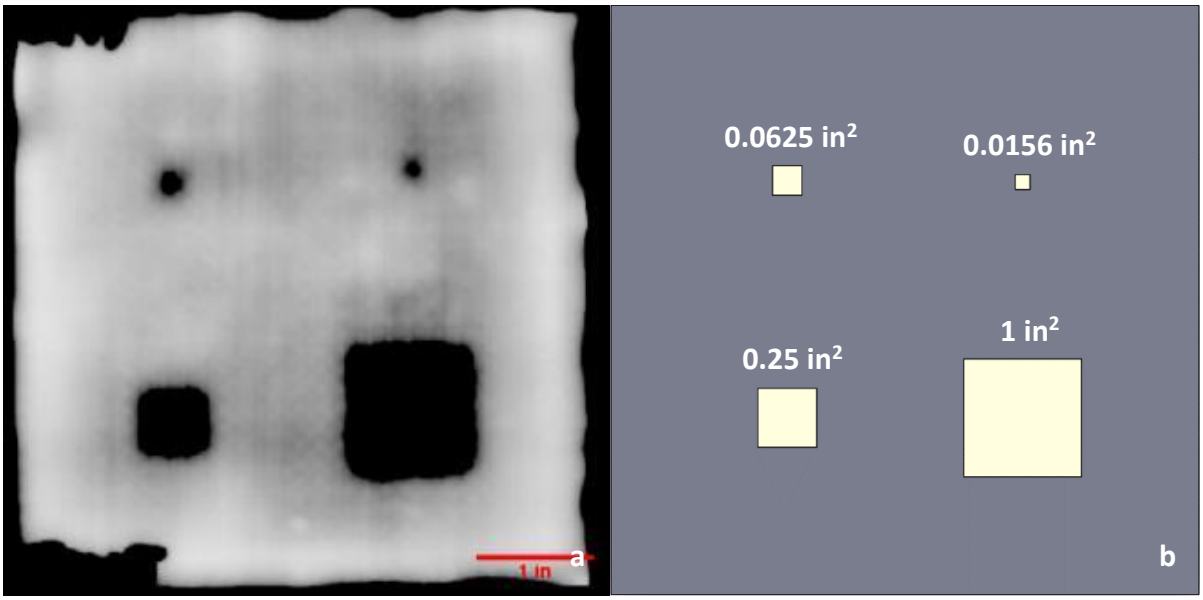

Figure 52: Raw Thermography Data with Programmed Defect on 6th Layer (a) and Laminate 6(7) Schematic (b)

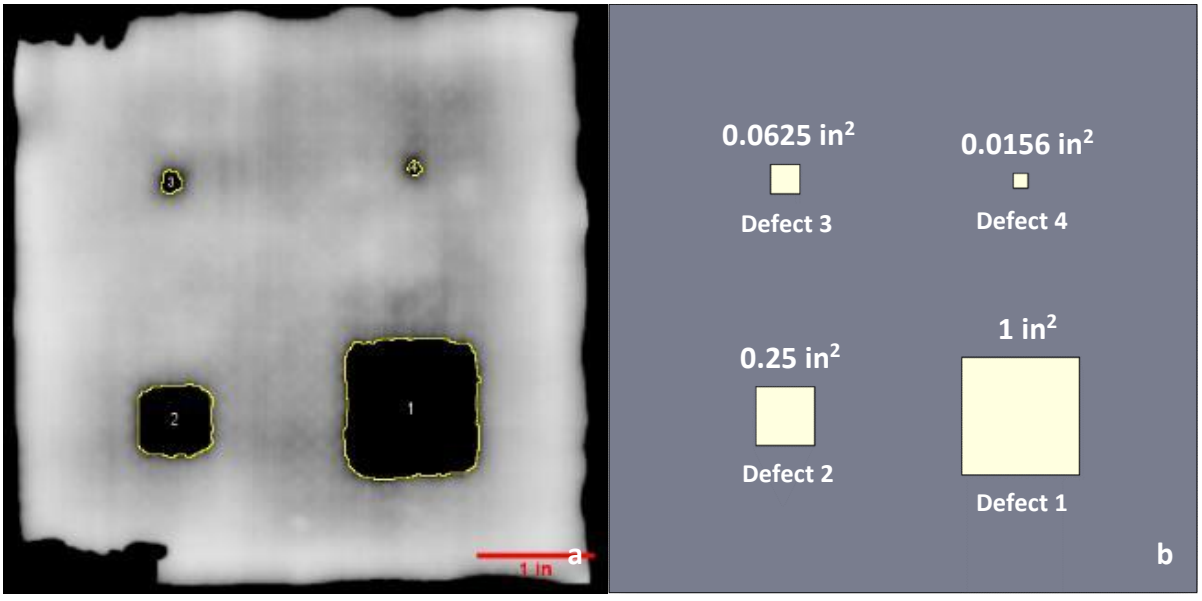

Figure 53: Thermography Area Analysis with Defect on 6th Layer (a) and Laminate 6(7) Schematic (b)

The detection effectiveness for Laminate 6(7) was very similar to that of Laminate 3(4). The larger defects, 1 and 2, are overpredicted while the smaller of the defects, 3 and 4, are heavily underpredicted. As previously shared, the edge detection for thermography worsens even on the largest defects as depth of the defect was increased. However, there are "shadows" around the scanned area which give some sense of the true shape. These shaded areas are not accounted for as the only the black regions are considered in the detected area calculations.

Table 6: Thermography Areas Laminate 6(7)

Defect	Programmed Area (in^2)	Thermography Scan Area (in^2)	Detection %Error	Visibility
1	1.000	1.255	25.5%	Very High
2	0.250	0.345	38.0%	Very High
3	0.0625	0.026	-58.4%	Very High
4	0.0156	0.01	-36.0%	Very High

3.3.4 Laminate 9(10) Thermography Scan Results

The thermography scans of Laminate 9(10) demonstrated in Figure 54 that all programmed defects are detectable. When compared to Laminate 6(7), the embedded delamination defects' edges and shape become increasingly blurred as the thickness continues to increase with this sample. The scan conducted on Laminate 9(10) took 15

seconds to complete. The noticeable white edges, on prior, thinner tested laminate samples, sample grow ever larger the thickness of the samples increases. With larger edge surface edge area more heat is trapped with insulating air. These thermography scans demonstrate air is a poor medium for heat conduction.

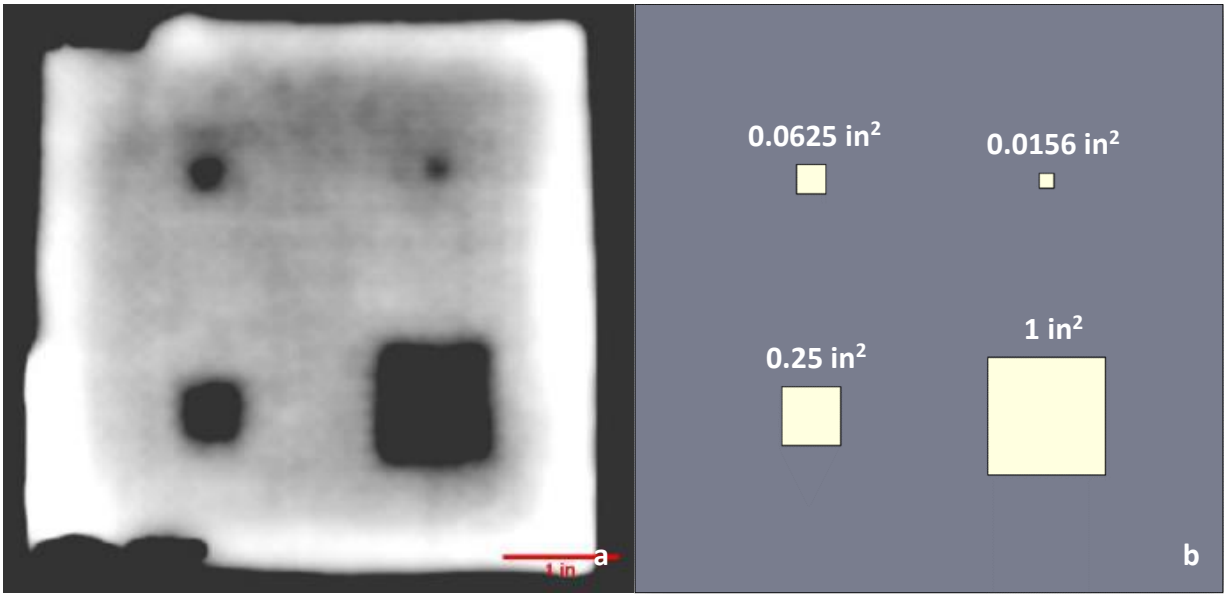

Figure 54: Raw Thermography Data with Programmed Defect on 9th Layer (a) and Laminate 9(10) Schematic (b)

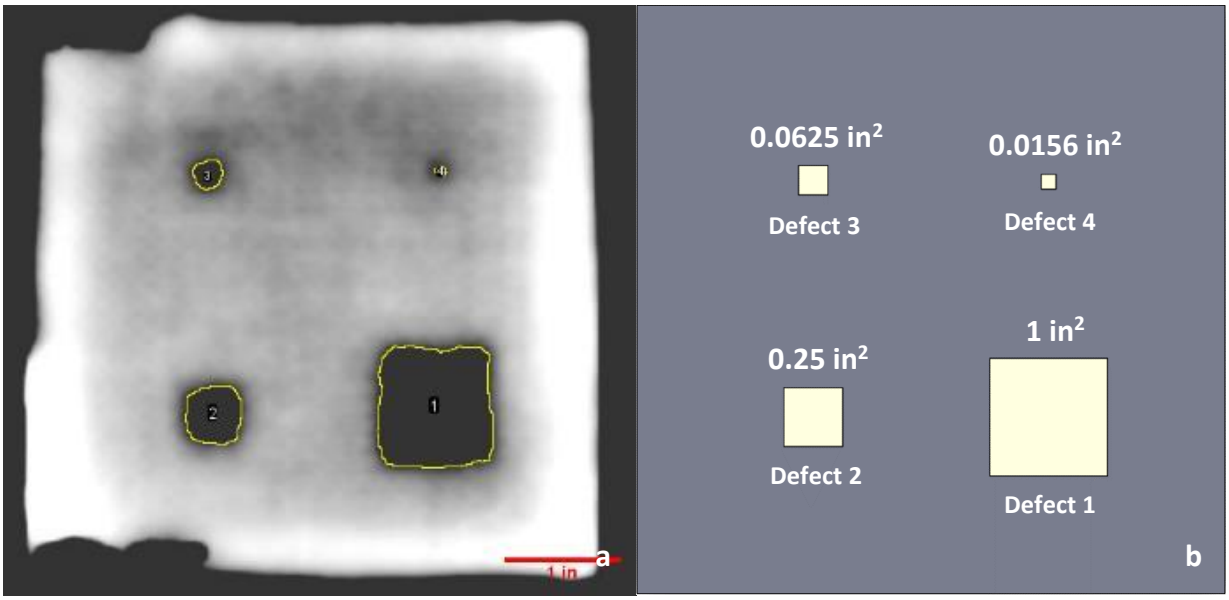

Figure 55: Thermography Area Analysis with Defect on 9th Layer (a) and Laminate 9(10) Schematic (b)

Table 7: Thermography Areas Laminate 9(10)

Defect	Programmed Area (in^2)	Thermography Scan Area (in^2)	Detection %Error	Visibility
1	1.000	0.949	-5.1%	Very High
2	0.250	0.205	-18.0%	Very High
3	0.0625	0.049	-21.6%	Very High
4	0.0156	0.006	-61.6%	High

Sample 9(10) marks the first thermography sample in which both Defect 1 and Defect 2's areas are underpredicted. The edge detection of the defects steadily degrades with increased thicknesses as the programmed defect square shape is increasingly lost. Defect 4 is severely underpredicted, this demonstrates the nonlinearity of the area loss in the thermography scan as it relates to defect area.

3.3.5 Laminate 12(13) Thermography Scan Results

In Figure 56, the heat trapped along the borders of Laminate 12(13) become quite substantial. This is due to the much greater depth and associated volume of this sample. This required increase application of heat, meaning more heat is stored in the sample and its escape is increasing difficult along the edges. This is the first laminate in which not all defects can be interrogated. Additionally, the blur brought about by the decay in edge quality through thickness becomes particularly apparent for the second smallest defect, Defect 3. Laminate 12(13) took a total of 30 seconds to scan, double the time to scan Laminate 9(10). This was a sharp increase relative to the 5 second increments from previous test samples as thickness increased 3 lamina.. However, the time of scanning still remains incredibly slim, still under a minute in total.

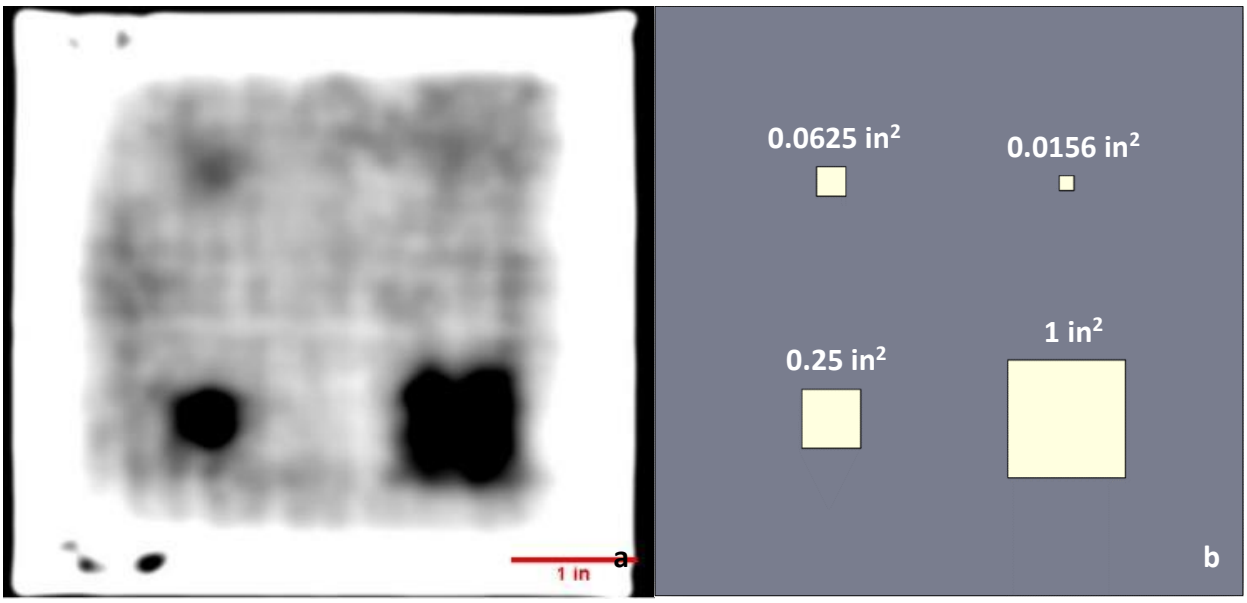

Figure 57: Raw Thermography Data with Programmed Defect on 12th Layer (a) and Laminate 12(13) Schematic (b)

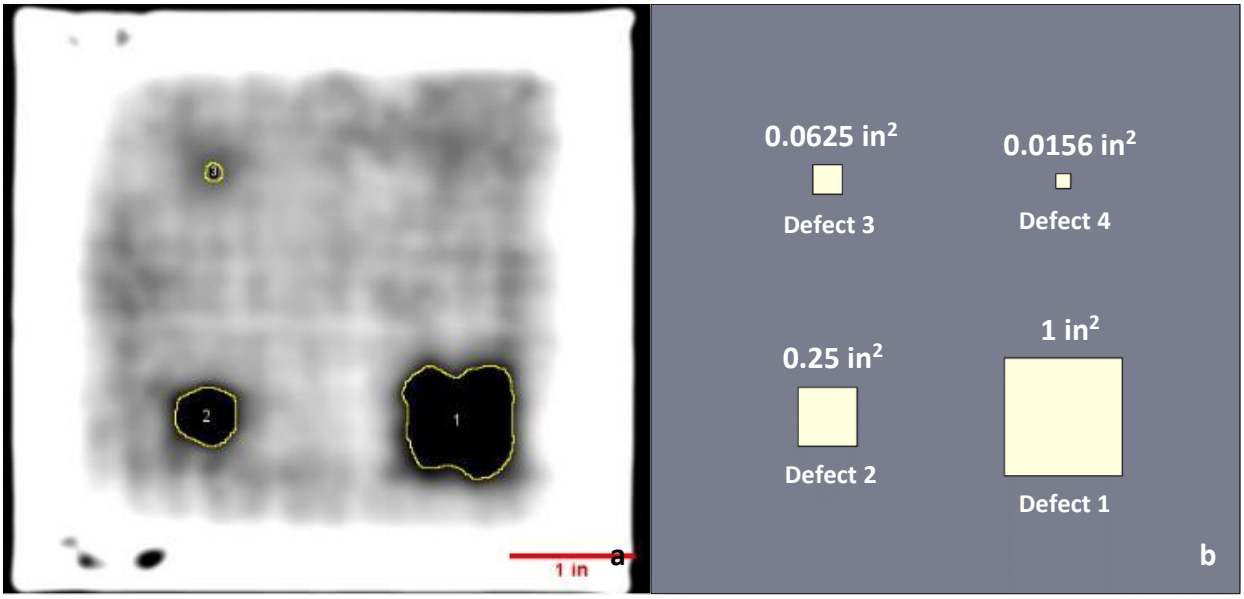

Figure 58: Thermography Area Analysis with Defect on 12th Layer (a) and Laminate 12(13) Schematic (b)

Table 8: Thermography Areas Laminate 12(13)

Defect	Programmed Area (in^2)	Thermography Scan Area (in^2)	Detection %Error	Visibility
1	1.000	0.633	-36.7%	Very High
2	0.250	0.175	-30.0%	Very High
3	0.0625	0.015	-76.0%	Low
4	0.0156	N/A	N/A	Undiscernible

Laminate 12(13), as seen in Figure 59, shows a substantial drop off in edge quality. Defect 4 becomes lost in this scan, and Defect 3 has very little discernable edge. Defects 1 and 2 remain highly visible, however the error seen in their edge detection grew substantially at this depth. The heat storage at the edge is an artifact from heat trapped at the transition between the exposed laminate edge and the surrounding environment.

3.3.6 Thickness Effect on Thermography for CFRP

As previously shared, there is a relationship between the delamination edge detection error and the depth of the composite defect observed. This can be observed the various size delamination defects across the variety of laminates analyzed in Figure 58 below. The TWI EchoTherm thermography system, which utilizes pulsed thermography, shows an increase in defect detection area as the thickness of the composite laminate increases. There is some volitility in these metrics likely due to the test samples having a variety of unplanned defects induced during fabrication which impacted the interrogation of the programmed defects. However, this survey shows how, particularly for large defects such as Defect 1 seen in Figure 58 (a), the reduction in area becomes substantial. For smaller defects there appears to be some uncertainty. This variance is likely due to the complex nature of heat propogation through nonhomogenous materials, and why certain defects appear as outliers from the overall trends. Thicker laminates with programmed defects have been experimentally determined to underpredict defect dimensionality due to the thermal diffusivity properties of composites [43]. Overall, smaller defects are generally underpredicted, while the larger defects appear to have a greater size closer to the surface, then past a threshold begins to shrink in detected area reported vs actual defect size.

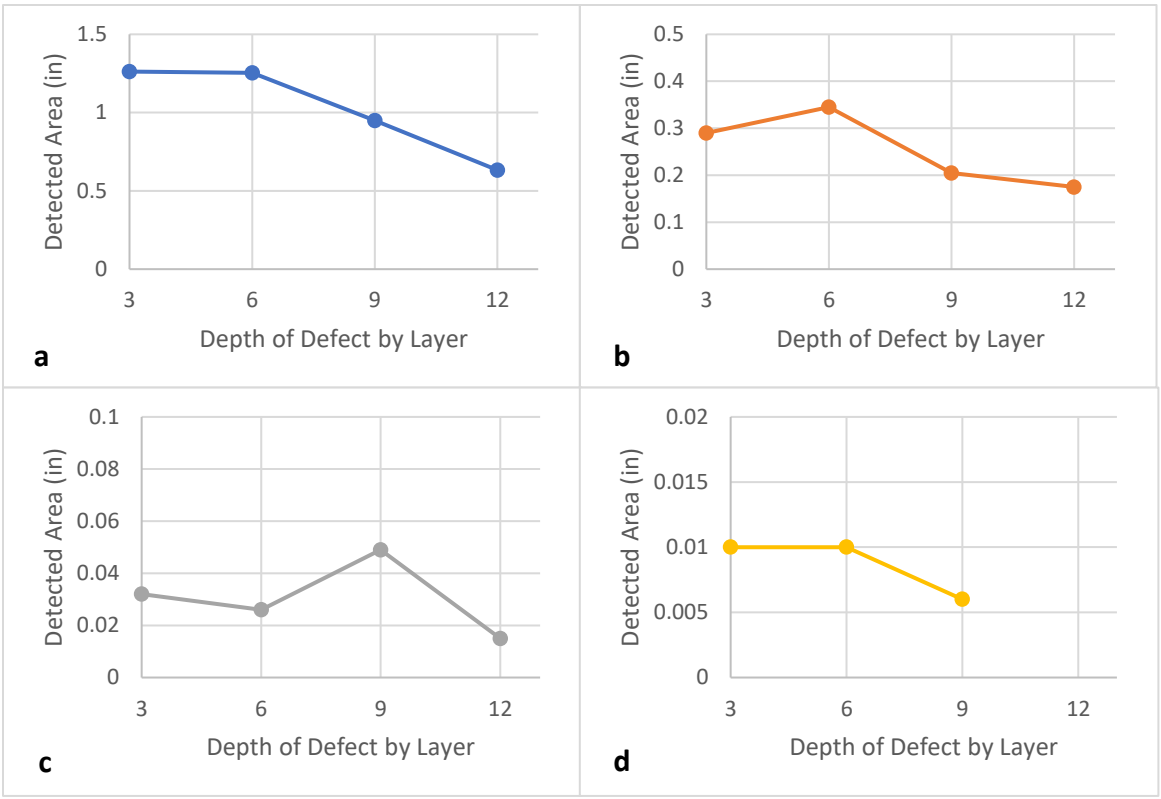

Figure 58: Thermography Defect 1 (1 in^2) Detected Areas (a) Defect 2 (0.25 in^2) Detected Areas (b) Defect 3 (0.0625 in^2) Detected Areas (c) Defect 4 (0.0156 in^2) Detected Areas (d)

3.3.7 Thermography Summary

Thermography proves to be an extremely rapid and reliable method for detecting a wide range of defect sizes through a variety of thicknesses. Thicker laminates require greater exposure time in order to interrogate for defects. There is a drop off in defect edge detection as the size of the defect increases as well as when the depth of the defect inside of the laminate increases. Visibility of smaller defects becomes problematic as a result if there are composite inconsistencies, at great depths in the CFRP or close to an insulated panel edge,. It was demonstrated there is a point where a defect can be missed if the thickness is too great relative to the diameter of the defect.

3.4 Computed Tomography Testing

3.4.1 CT Scan of Composite Samples

Computed Tomography (CT) utilizes a controlled array of x-ray images to compose a 3-dimensional model of the subject being tested. For this study a Perkin Elmer Quantum FX Micro CT was used. Each of the performed scans were performed at 70 kV, with a current of 200 µA. The FOV for each scan was 2.87" x 2.87" (73 mm x73 mm), limiting the possible scanning area of each section to a bit less more than ¼ of each laminate sample. The CT scanner being used was set to provide the largest FOV achievable. The downside of the large FOV setting was of lower delivered resolution. This FOV restriction combined with the additional restriction of the CT scanner housing proved difficult to host the entire sample's 5" x 5" size. Consequently, each programmed defect was targeted individually for the purpose of identification. Each of the 16 resultant scans required approximately 4.5 minutes each to complete When combined with setup times a total of 3 hours was required to complete one round of scans. Each scan was constructed from 7904 frames of x-ray images, starting at 0° and ending at 360°.

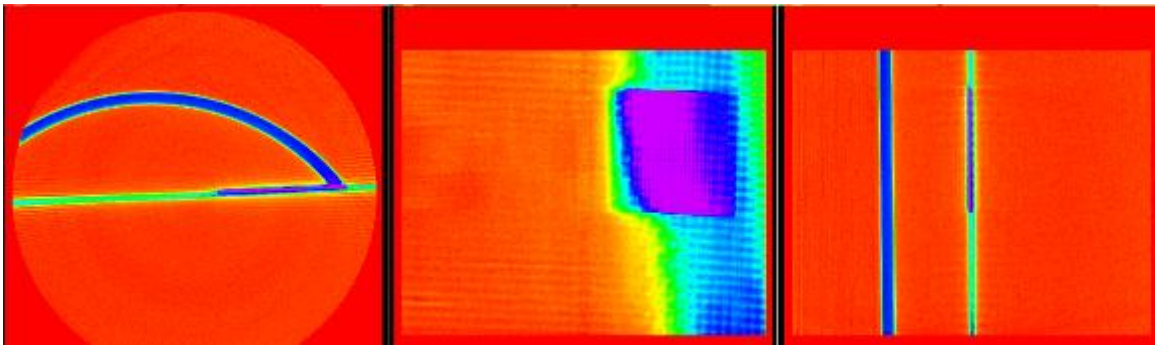

Figure 59: Example: Laminate 3(4) Defect 1 CT Scanned Raw Data Views

3 views are obtained utilizing this method, each with 512 segments at a resolution of 148 µm/px and each slice segment having a thickness of 118 µm. This type of resolution allows for unparalleled detection of these delamination defects with exceptionally high precision – despite the FOV-resolution trade-off. Samples of these slices can be seen in Figure 59, where the blue arch in Figure 59 (a) is the CT scanner's stage upon which the sample were placed. The purple segments are the observed strong shadow of the programmed defect. Defect depth is also easily and precisely observed through this method.

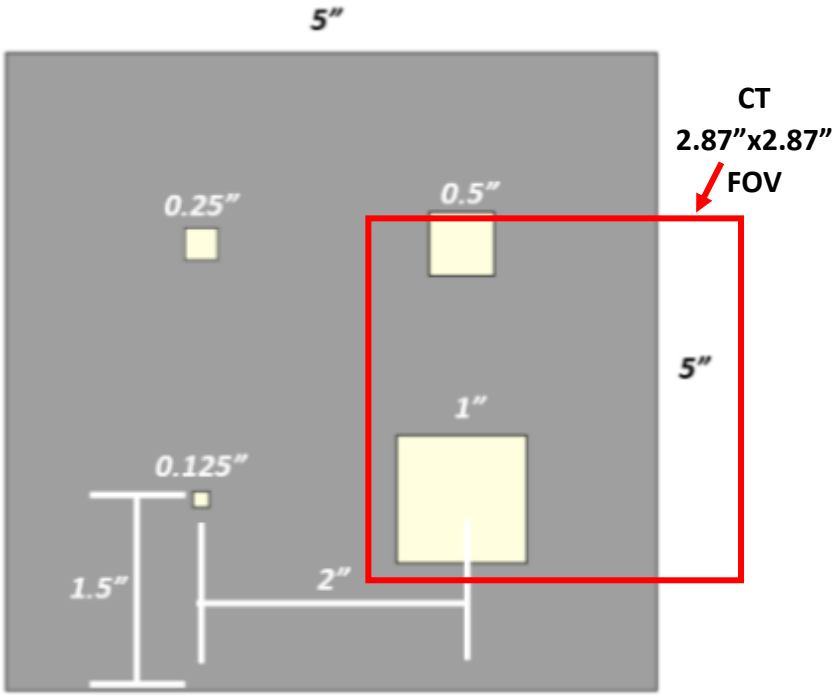

Figure 60: CT Scan Example Laminate 3(4) Defect 1 Targeted Area Schematic

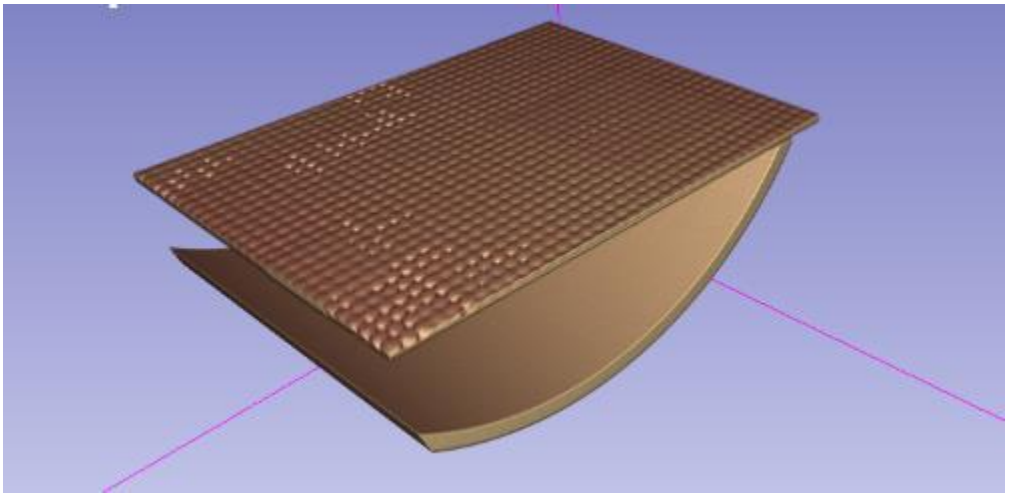

Figure 61: Laminate 3(4) Defect 1 Area Unfiltered CT Reconstruction

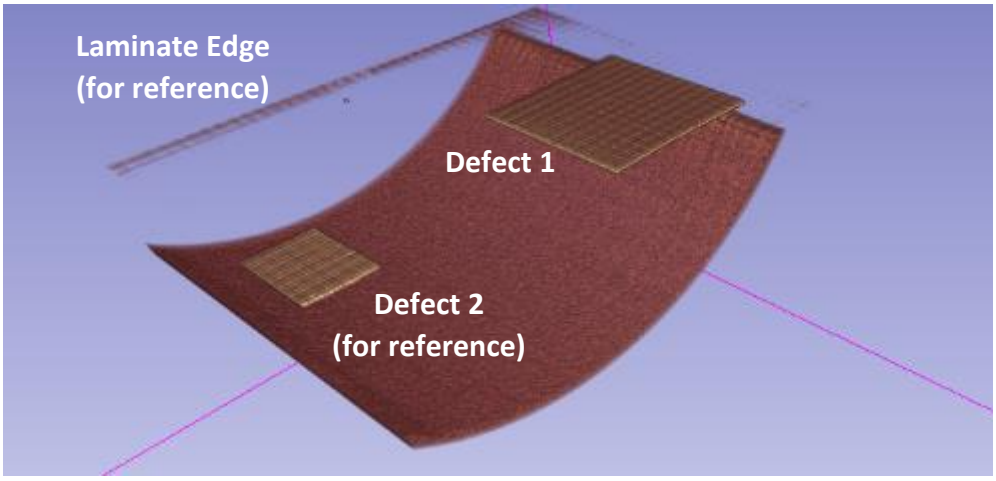

Figure 62: Laminate 3(4) Defect 1 Area Filtered Defect Isolation

The scanned CT images were next processed using 3D Slicer software to reconstruct the 3-dimensional model. 3D Slicer is a free open-source software used for the 3D reconstruction and visualization. This software enables the user to filter CT image sets and reconstruct the test specimen. In Figure 61 the laminate portion of the laminate being scanned can be seen in its entirety, including detail of the woven fabric's surface porosity information. By filtering out the the CFRP components of the x-ray the Teflon™ programmed defects were isolated, as seen in Figure 62 above the curved CT scanner's stage.

3.4.2 CT Area Analysis and Depth Methodology

As mentioned, 3D Slicer software was used for the reconstruction of the CT scans. This software also was used to create a scale for the images to be analyzed in a similar fashion to the other methods evaluated. This was done with the ImageJ software to determine the defect area, similar to previous sections, and depth is also determined using this software utilizing the base CT scan views of the samples. For depth determination it was assumed that all defects have the same y-axis depth, which is the depth axis in this CT system. Defect 1 was used for depth determination for all of the sample depths in each respective laminate sample.

3.4.3 Laminate 3(4) CT Area Analysis and Depth Results

Laminate 3(4) scanned defects were isolated in Figure 63. Immediately it was clear from the CT reconstruction that the simulated Teflon™ delamination defects cut, laid and VARTM processed into CFRP were not perfect squares. This is to be expected given the

nature of manufacturing. Defects 1-4 in this thinnest laminate sample are all clearly distinct in the scans and can be filtered using the 3D Slicer CT image processor. The detected areas for the programmed defects are 636.127 mm^2 or 0.986 in^2 for Defect 1, 168.387 mm^2 or 0.261 in^2 for Defect 2, 34.193 mm^2 or 0.053 in^2 for defect 3 and 14.194 mm^2 or 0.022 in^2 for Defect 4. The areas analyzed for the respective defects can be found in Figure 64 (a) through Figure 64 (d). Table 9 also lists these defects with the associated error from the programmed defect area. The assumption of these results is that the CT scanned images are precise and should be the benchmark for the true size of the programmed defects rather than the programmed values assigned in manufacturing. The detected depth was determined from the default y-z plane cross section delivered from the Perkin Elmer CT system's scan on Defect 1, the detected depth was found to be 0.787 mm or 0.031". The determining distance can be observed in Figure 66. This value will also be used as the base depth assumption for further analysis of defects in Laminate 3(4).

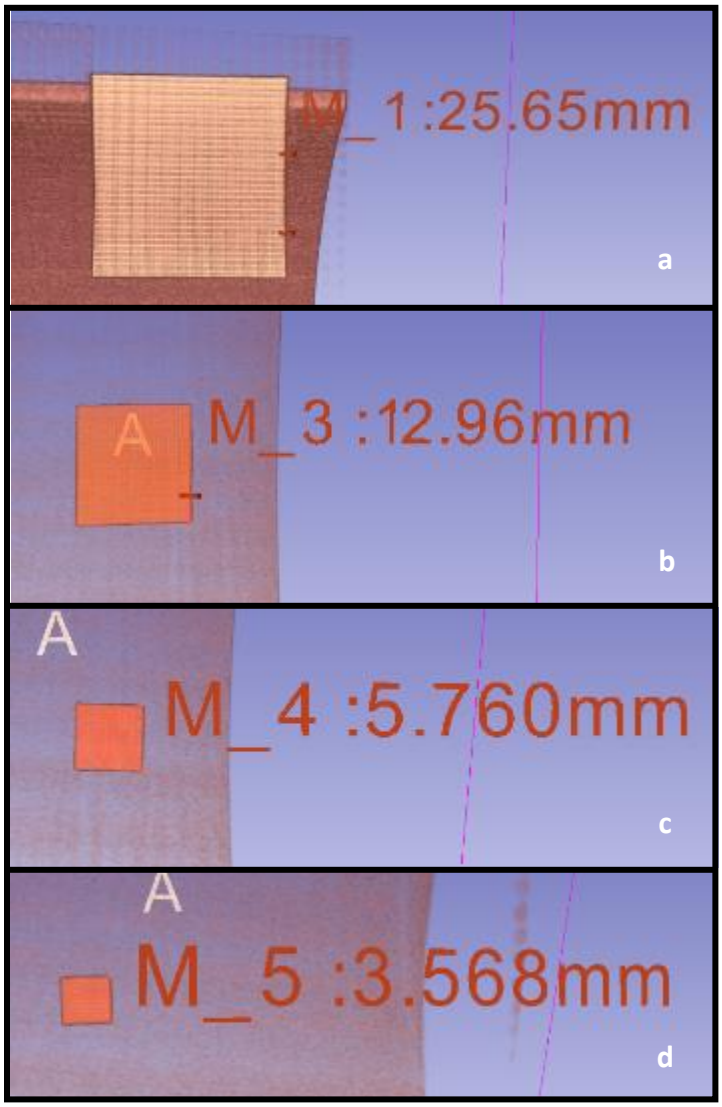

Figure 63: Laminate 3(4) Defect 1 (a) Defect 2 (b) Defect 3 (c) Defect 4 (d) Raw Data (w/ Scale)

Table 9: CT Scan Areas and % Error of Programmed Defect in Laminate 3(4)

Defect	Programmed Area (in^2)	Detected Area (in^2)	Defect %Error
1	1.000	0.986	-1.4%
2	0.250	0.261	4.4%
3	0.0625	0.053	-15.2%
4	0.0156	0.022	40.8%

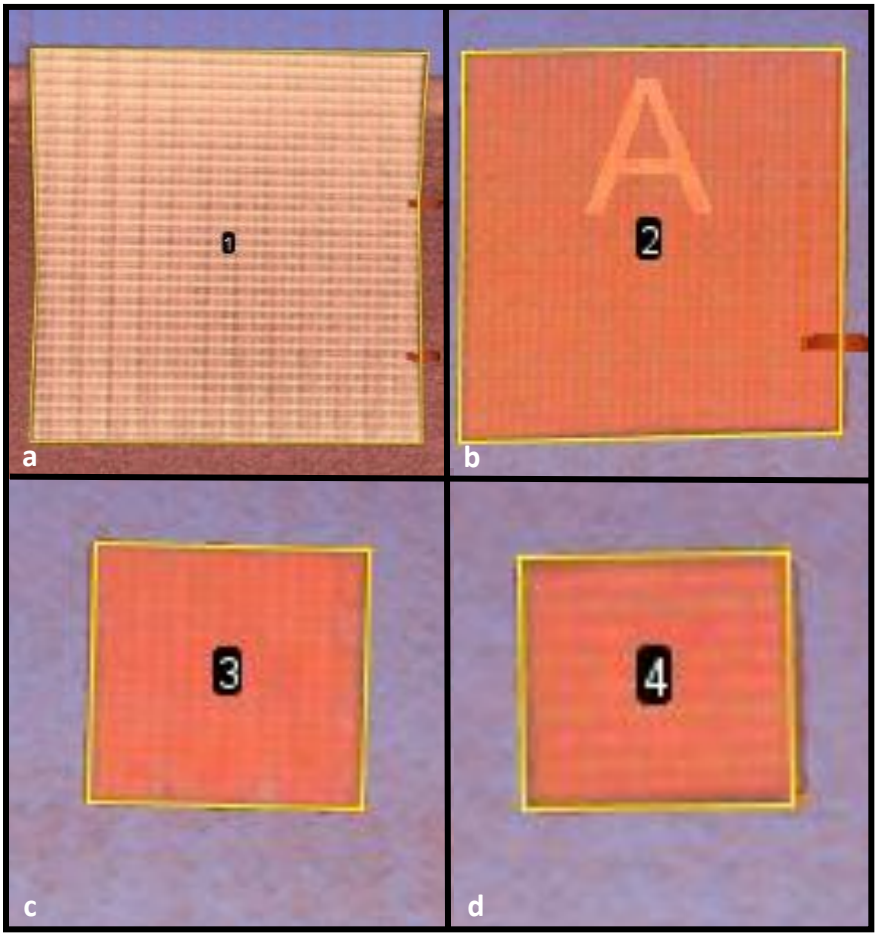

Figure 64: Laminate 3(4) Defect 1: 1 in^2 (a) Defect 2 (b) Defect 3 (c) Defect 4 (d) Detected Area

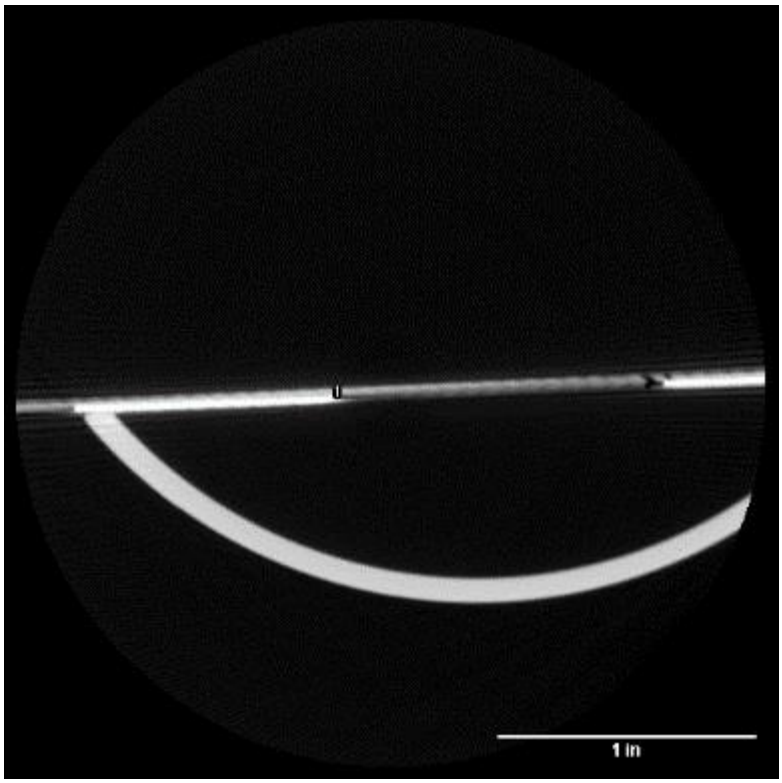

Figure 65: Laminate 3(4) Z-Y Axis Image

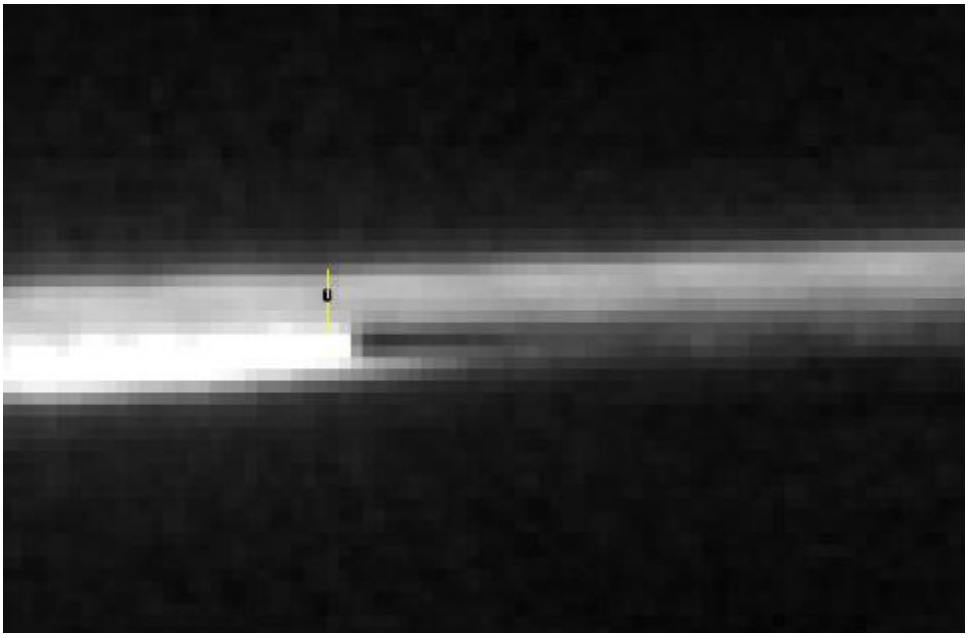

Figure 66: Laminate 3(4) Detected Depth

3.4.4 Laminate 6(7) CT Area Analysis and Depth Results

Laminate 6(7) defects show signs of pores developing along the edges of the Teflon™ delamination defect sheets. Similar to Laminate 3(4), the introduced defects were once again found to be imperfect squares, which again could be observed easily with the CT reconstruction. The detected areas for the programmed defects are 715.482 mm^2 or 1.109 in^2 for defect 1, 167.742 mm^2 or 0.260 in^2 for defect 2, 36.774 mm^2 or 0.057 in^2 for defect 3 and 16.129 mm^2 or 0.025 in^2 for defect 4. The areas analyzed for the respective defects can be found in Figure 68 (a) through Figure 68 (d). Table 10 identifies the error of the programmed defects in laminate 6(7). The detected depth was determined from the default y-z plane cross section of the CT scan based on Defect 1, the detected depth was found to be 1.32 mm or 0.052 in. The detected depth can be observed in Figure 70. The y-z axis contrast seen allows for accurate detection of depth on a micrometer scale.

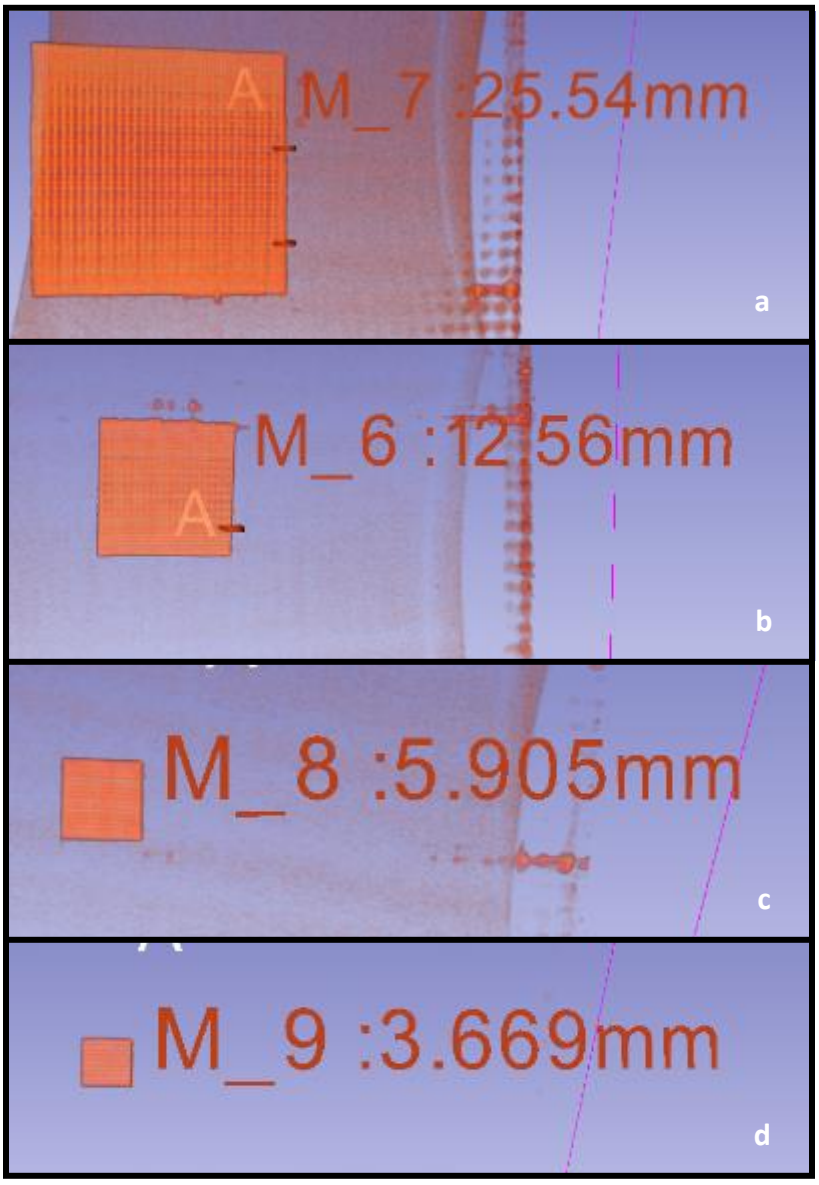

Figure 67: Laminate 6(7) Defect 1 (a) Defect 2 (b) Defect 3 (c) Defect 4 (d) Raw Data (w/ Scale)

Table 10: CT Scan Areas and % Error of Programmed Defect in Laminate 6(7)

Defect	Programmed Area (in^2)	Detected Area (in^2)	Defect %Error
1	1.000	1.109	10.9%
2	0.250	0.260	4.0%
3	0.0625	0.057	-8.8%
4	0.0156	0.025	60.0%

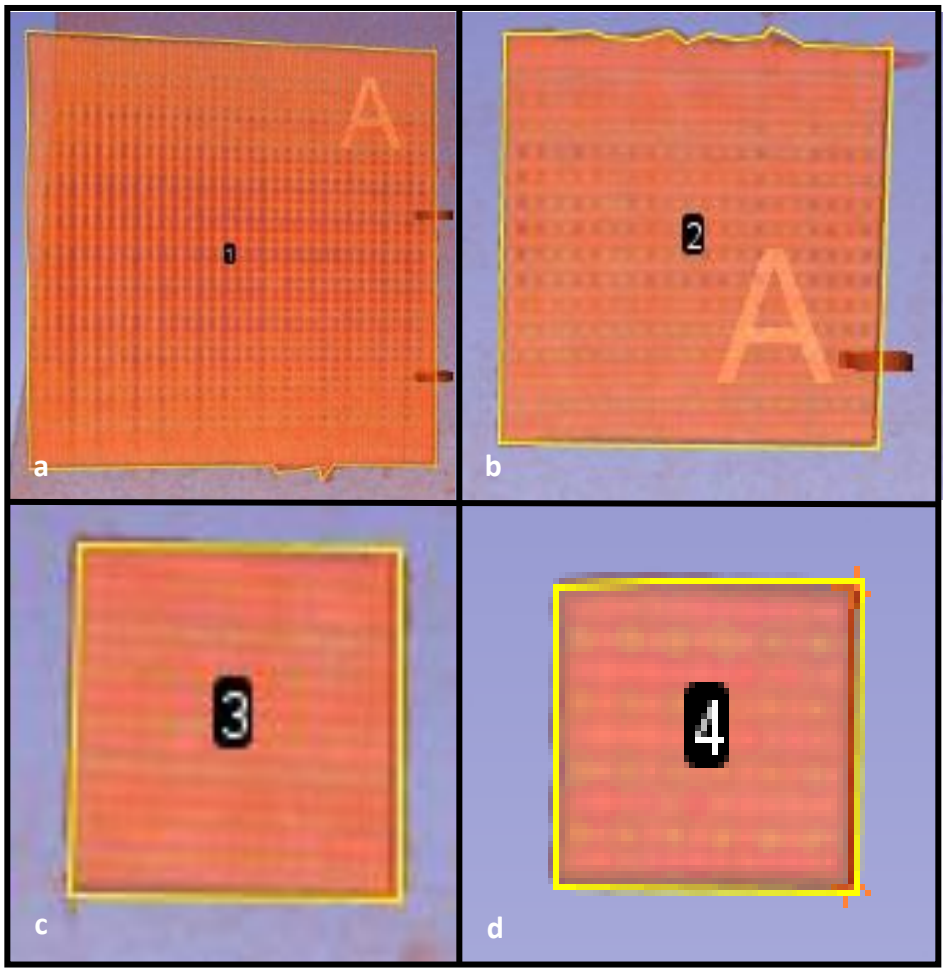

Figure 68: Laminate 6(7) Defect 1 (a) Defect 2 (b) Defect 3 (c) Defect 4 (d) Detected Area

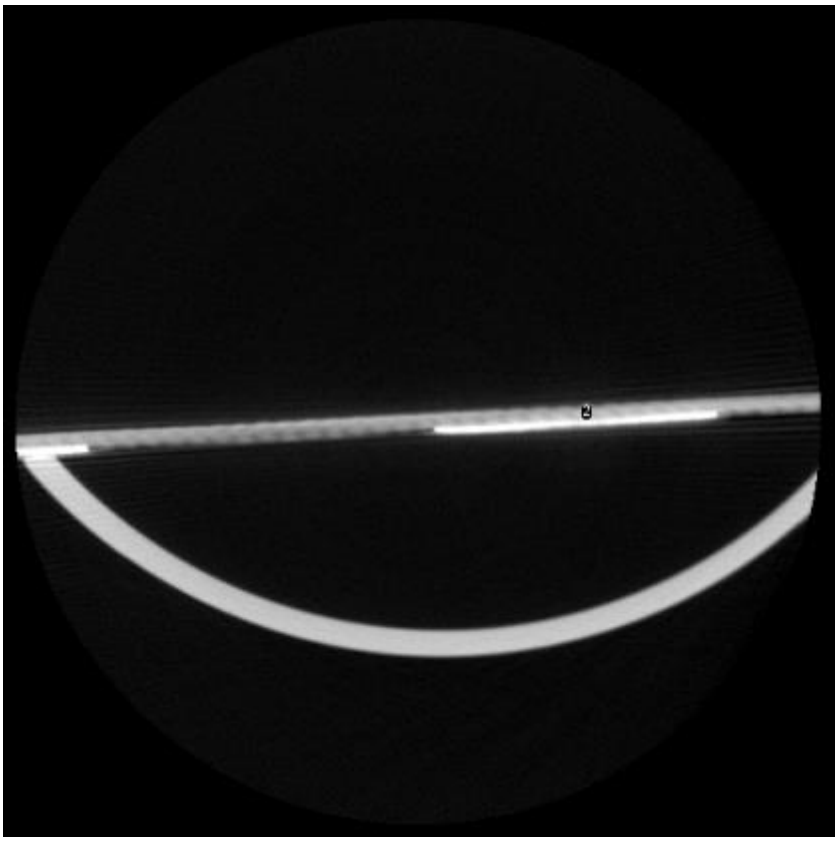

Figure 68: Laminate 6(7) Z-Y Axis Image

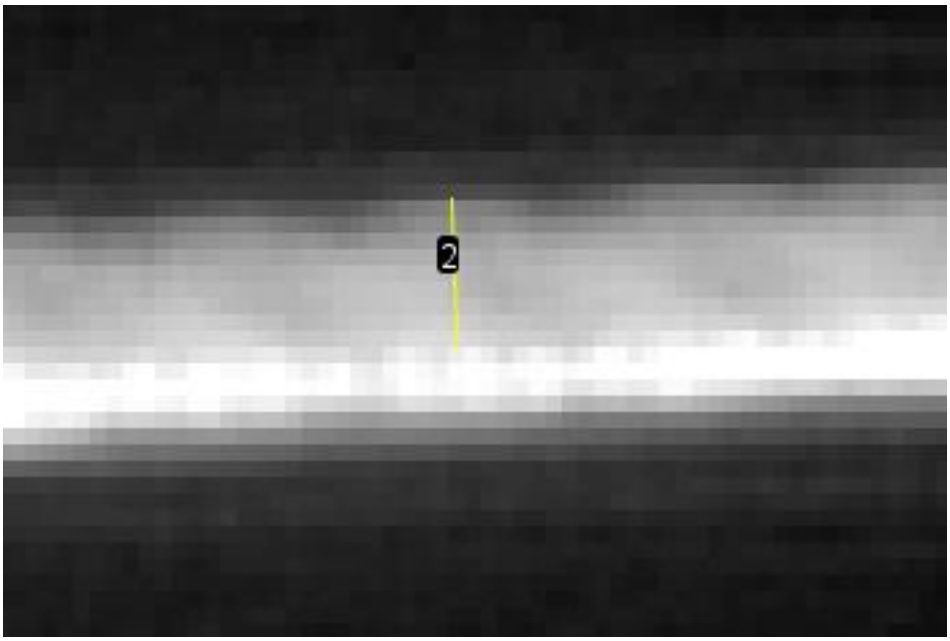

Figure 69: Laminate 6(7) Detected Depth

3.4.5 Laminate 9(10) CT Area Analysis and Depth Results

Laminate 9(10) defects show signs of pores developing along the seam created by the Teflon™ defect sheets. These pores appear on the surface of the rough side Bottom Test Surface of the sample and penetrate down to the depth of the defect layer. This results in a greater quantity of pores developing along the marked guidelines for the defects created in manufacturing. These pores are detected in the CT scan and could alter the programmed defect for scanning in other methods. The detected areas for the programmed defects are 658.063 mm^2 or 1.02 in^2 for defect 1, 170.967 mm^2 or 0.265 in^2 for defect 2, 46.452 mm^2 or 0.072 in^2 for defect 3 and 12.258 mm^2 or 0.019 in^2 for defect 4. The areas analyzed for the respective defects can be found in Figure 72 (a) through Figure 72 (d). Table 11 identifies the error of the programmed defects in laminate 9(10). The detected depth was determined from the y-z plane cross section of the CT scan based on Defect 1, the detected depth was found to be 1.803 mm or 0.071 in. The detected depth can be observed in Figure 74.

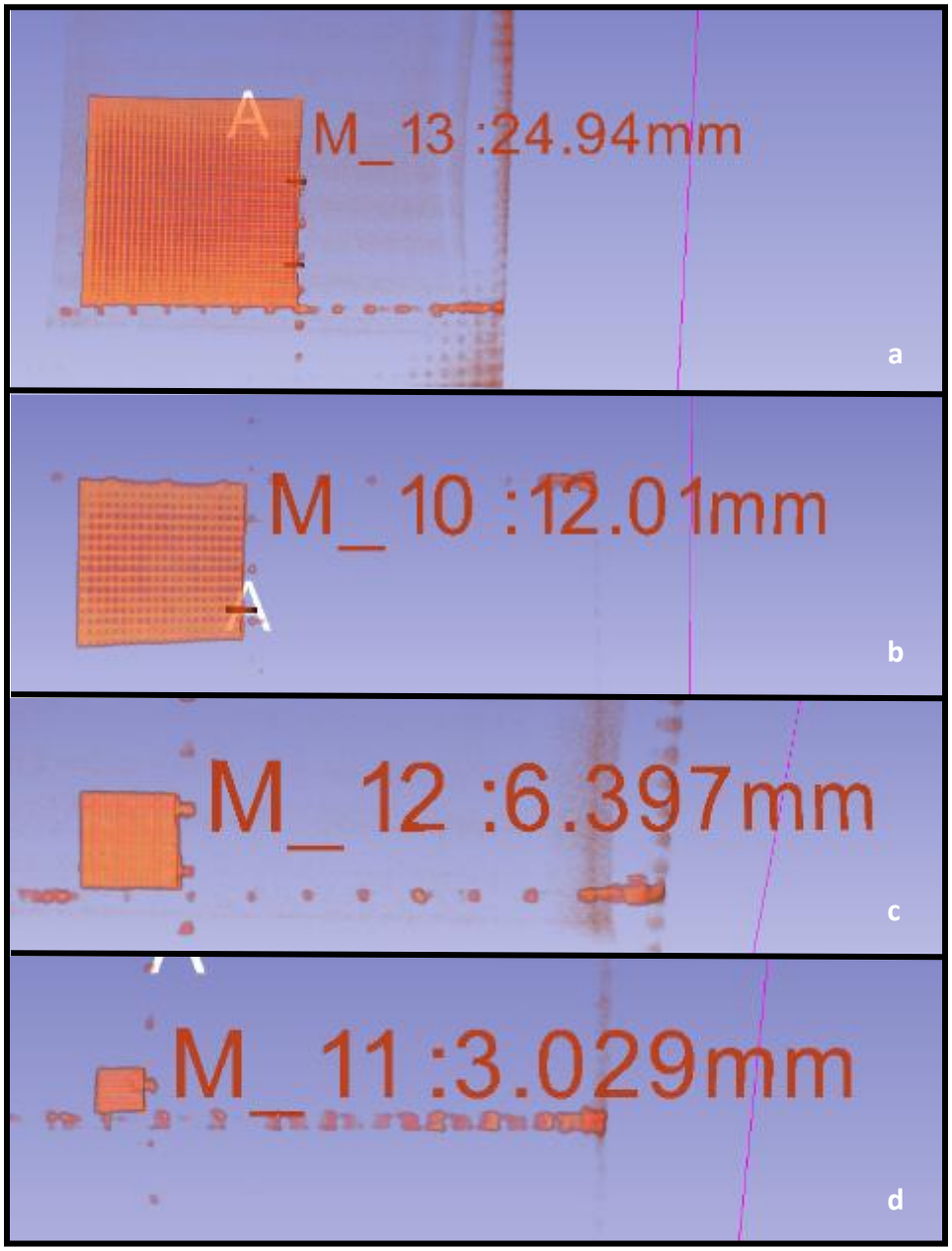

Figure 71: Laminate 9(10) Defect 1 (a) Defect 2 (b) Defect 3 (c) Defect 4 (d) Raw Data (w/ Scale)

Table 11: CT Scan Areas and % Error of Programmed Defect in Laminate 9(10)

Defect	Programmed Area (in^2)	Detected Area (in^2)	Defect %Error
1	1.000	1.020	2.0%
2	0.250	0.265	6.0%
3	0.0625	0.072	15.2%
4	0.0156	0.019	21.6%

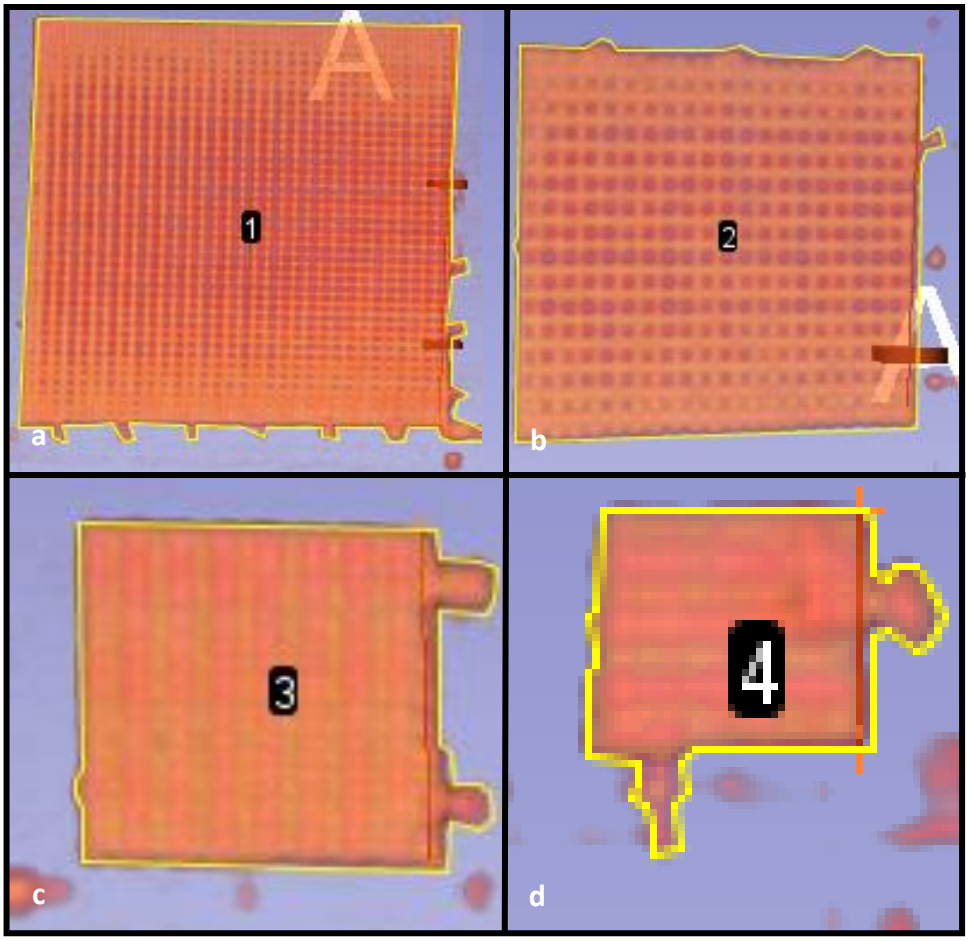

Figure 72: Laminate 9(10) Defect 1 (a) Defect 2 (b) Defect 3 (c) Defect 4 (d) Detected Area

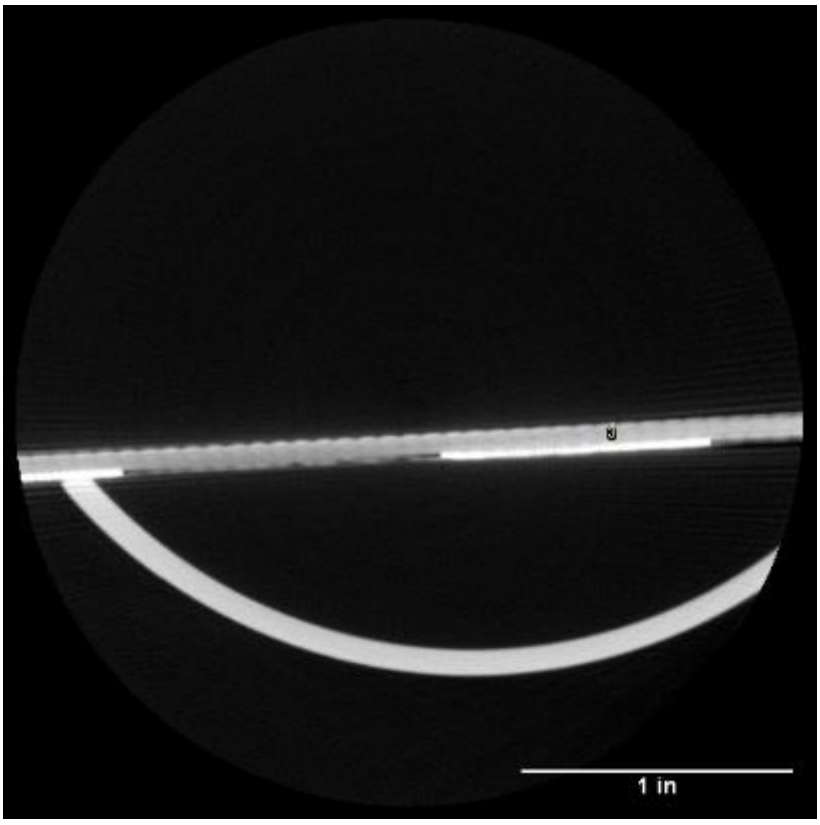

Figure 73: Laminate 9(10) Z-Y Axis Image

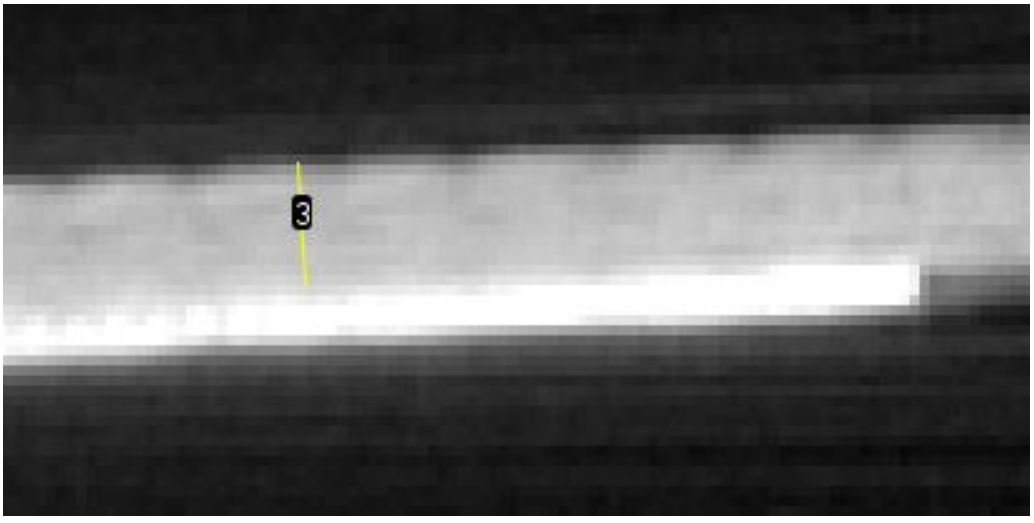

Figure 74: Laminate 9(10) Detected Depth

3.4.6 Laminate 12(13) CT Area Analysis and Depth Results

For Laminate 12(13) the detected areas for the programmed defects are 676.772 mm^2 or 1.049 in^2 for Defect 1, 156.774 mm^2 or 0.243 in^2 for Defect 2, 39.355 mm^2 or 0.061 in^2 for Defect 3 and 12.258 mm^2 or 0.019 in^2 for Defect 4. The areas analyzed for the respective defects can be found in Figure 76 (a) through Figure 76 (d). Table 12 identifies the error of the programmed defects in laminate 12(13). The detected depth was determined from the y-z plane cross section of the CT scan based on Defect 1, the detected depth was found to be 2.515 mm or 0.099 in. The detected depth can be observed in Figure 78. The y-z plane cross section indicates that Laminate 12(13) has a lower fiber volume fraction than the other 3 test sample laminates. This can also be observed from the sample thickness jump between laminate 9(10) and laminate 12(13) being larger than any other samples.

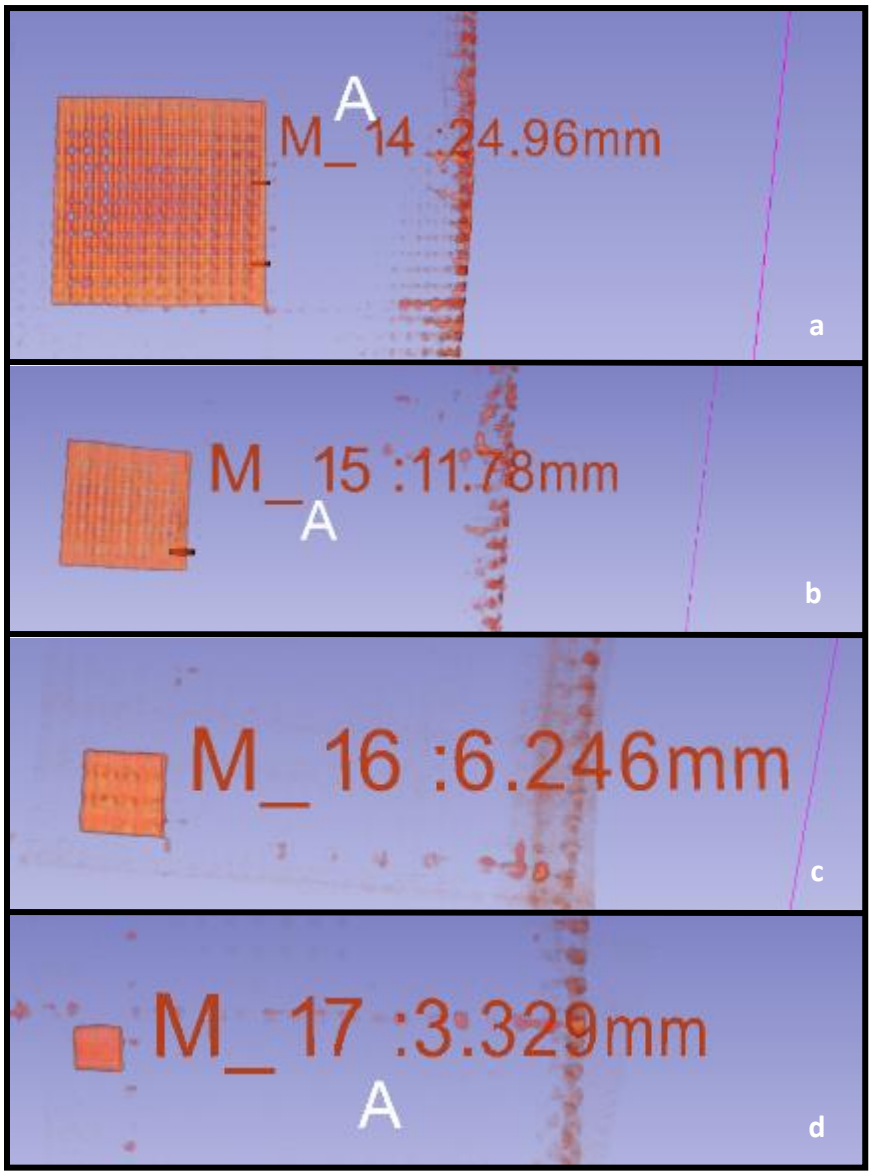

Figure 75: Laminate 12(13) Defect 1 (a) Defect 2 (b) Defect 3 (c) Defect 4 (d) Raw Data (w/ Scale)

Table 12: CT Scan Areas and % Error of Programmed Defect in Laminate 12(13)

Defect	Programmed Area (in^2)	Detected Area (in^2)	Defect %Error
1	1.000	1.049	4.9%
2	0.250	0.243	-2.8%
3	0.0625	0.061	-2.4%
4	0.0156	0.019	21.6%

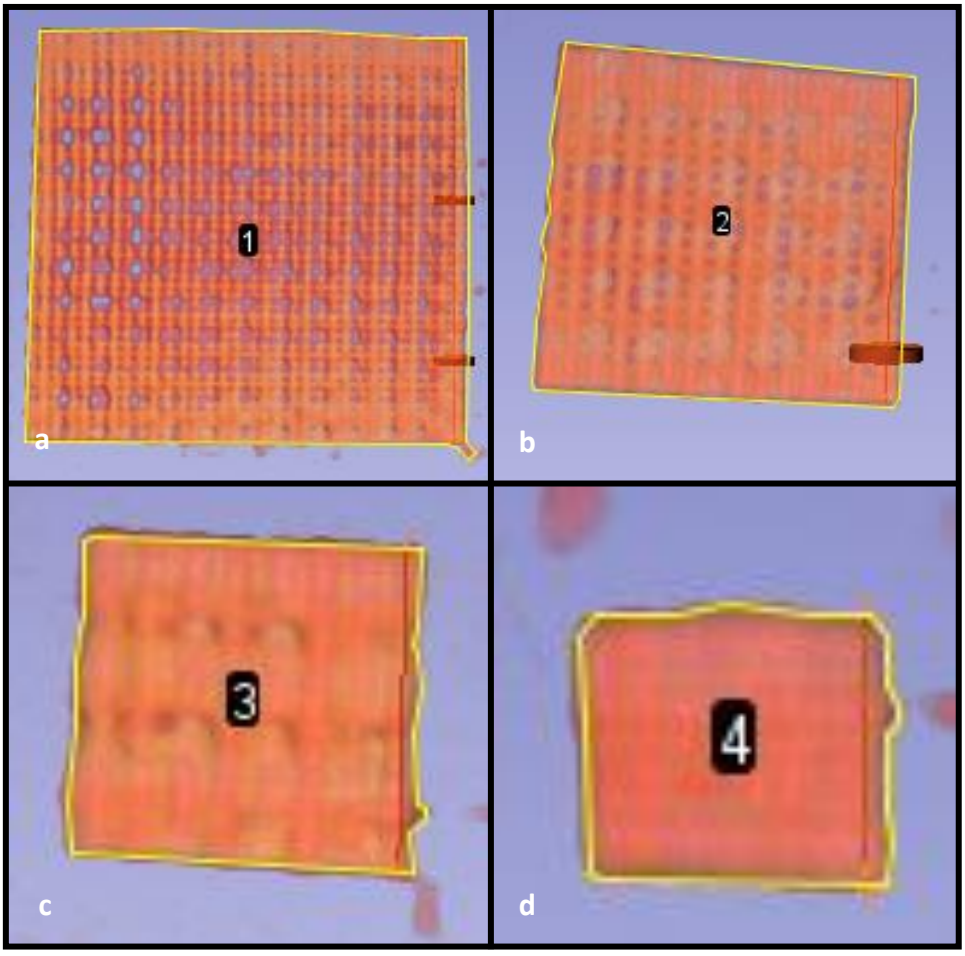

Figure 76: Laminate 12(13) Defect 1 (a) Defect 2 (b) Defect 3 (c) Defect 4 (d) Detected Area

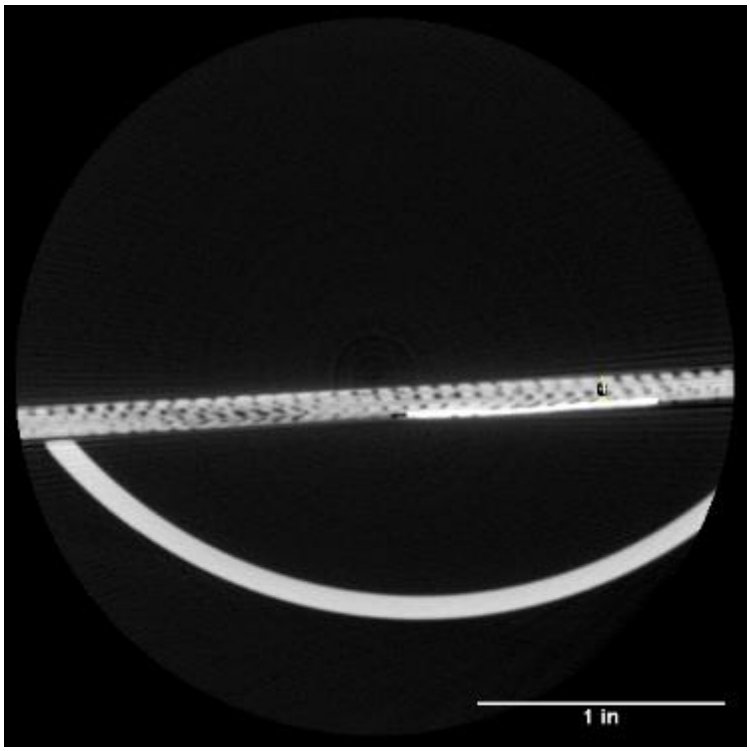

Figure 77: Laminate 12(13) Z-Y Axis Image

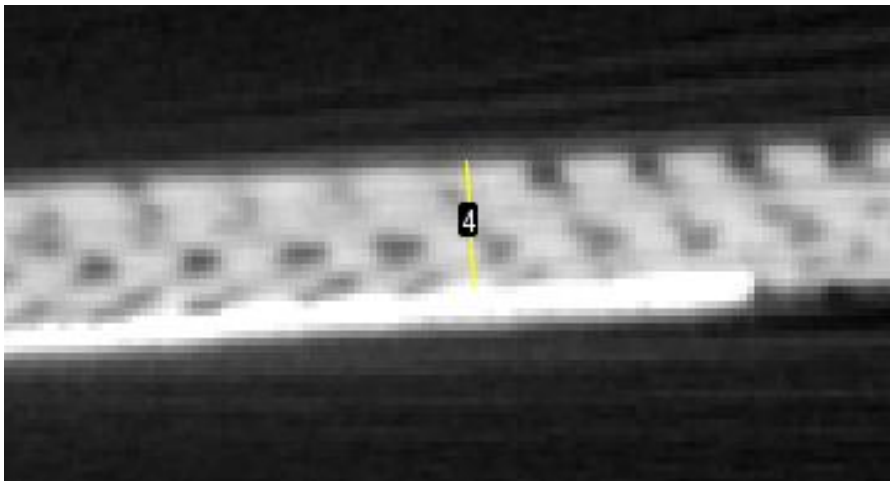

Figure 78: Laminate 12(13) Detected Depth

3.4.7 CT Scan Summary

Computed Tomography is a powerful tool, as it allows for the assessment of defects down to the micron level. This makes it invaluable for studies aiming to create algorithms based on defect dimensions. In the CT scans conducted there are a number of insights gained about the test specimens. The primary one being the defect areas being not as exact as programmed, due to the human error of cutting the Teflon^{TM} sheet during the prefabrication of the CFRP laminates. CT scans also give unparalleled depth information on defect location, as well as the complex geometries which may propagate around a large defect. In this study it was seen that air pockets tended to form along the edges of the programmed defects. The major downside of CT scanning are the geometric limitations. The laminates fabricated in the study measured 5x5 in approximately on each side. The CT scanner housing was just capable of fitting the laminate in the chamber. Meaning larger specimen studies using this machine would be impossible without cutting the laminate into smaller sections, defeating the purpose of the cross-evaluation study. Additionally, on top of the geometric limitations, the micro-CT scanner used has FOV limitations which further reduce the area which can be scanned. Each scan, in order to penetrate the composite effectively, required a total of 4.5 minutes for each scan. Including setup time this took a total of 3 hours. This reasoning alone makes it impractical as a widespread rapid NDT tool. However, CT itself is remarkable for its ability to allow for edge detection and the creation of algorithms or machine learning systems which can better improve the previous systems investigated [21, 42].

3.5 NDT Benchmarking Using CT Scans

3.5.1 CT Benchmarking Methodology

In this portion of the study the goal is to identify the true error in each scanning method, utilizing the true as assembled delamination defect areas revealed utilizing computed tomography scanning. These errors are compared with the theoretical "old" errors from the tests as compared to the true "new" error as determined by CT scanning. By utilizing CT scans area information can be refined and analyzed with accurate depth detection to create precise relationships between rapid scanning methods and defect area/depth. As demonstrated through the CT scans, each composite laminate increases in depth nonuniformly. Therefore, relying on these CT scans for depth baselines rather than initial assembly lamina thickness assumptions (0.2833 mm) can make the refining of NDT technological algorithms for composites substantially more precise. In the benchmarking which follows the CT scans of the laminate test samples will be considered the "source of truth". The equation used to determine the corrected error from the CT scans is the following:

$$\%Error\ (New) = \frac{A_{CT} - A'_i}{A_{CT}}$$

where A_{CT} is the area detected by the CT scan, which is being considered as the true area of the defect area and A'_i remains the scanned error from each associated NDT. The equation used to determine the %Error Improvement is the following:

$$\%Error\ Correction = |\%Error\ (Old)| - |\%Error\ (New)|$$

$$\%Error\ Correction = \left|\frac{A_i - A'_i}{A_i}\right| - \left|\frac{A_{CT} - A'_i}{A_{CT}}\right|$$

This equation utilizes the absolute value of each error measurement in order to determine if the value becomes closer to the CT scanned value. A positive value is indicative of an improvement in area detection precision and a negative value would be indicative of a decrease in area detection precision.

3.5.2 Ultrasonic C-Scan Benchmarking

The following tables indicate the transition from the original experimental assumptions to the new CT scan-based findings for UT. The error improvement highlights how much closer the scans absolute value of error approaches the true area. Error (Old) indicates the error found in the original ultrasonic C-Scans from section 3.1 found in Table 1-4. Error (New) is the error calculation based upon the CT scan areas found in section 3.4.

Table 13: C-Scan Area Benchmarking Laminate 3(4)

Defect	Theoretical Area (in^2)	Area CT Scan (in^2)	C-Scan Area (in^2)	%Error (Old)	%Error (New)	%Error Correction
1	1.000	0.986	0.924	-7.6%	-6.29%	+1.31%
2	0.250	0.261	0.282	12.8%	8.05%	+4.75%
3	0.0625	0.053	0.029	-53.6%	-45.28%	+8.32%
4	0.0156	0.022	0.019	21.6%	-13.63%	+7.97%

Table 14: C-Scan Area Benchmarking Laminate 6(7)

Defect	Theoretical Area (in^2)	Area CT Scan (in^2)	C-Scan Area (in^2)	%Error (Old)	%Error (New)	%Error Correction
1	1.000	1.109	1.027	2.7%	-7.39%	-4.69%
2	0.250	0.260	0.235	-6.0%	-9.62%	-3.62%
3	0.0625	0.057	0.039	-15.2%	-31.58%	-16.38%
4	0.0156	0.025	0.019	21.6%	-24.00%	-2.4%

Table 15: C-Scan Area Benchmarking Laminate 9(10)

Defect	Theoretical Area (in^2)	Area CT Scan (in^2)	C-Scan Area (in^2)	%Error (Old)	%Error (New)	%Error Correction
1	1.000	1.020	0.924	-7.6%	-9.41%	-1.81%
2	0.250	0.265	0.235	-6.0%	-11.32%	-5.32%
3	0.0625	0.072	0.053	-15.2%	-26.38%	-11.18%
4	0.0156	0.019	0.015	-4.0%	-21.05%	-17.05%

Table 16: C-Scan Area Benchmarking Laminate 12(13)

Defect	Theoretical Area (in^2)	Area CT Scan (in^2)	C-Scan Area (in^2)	%Error (Old)	%Error (New)	%Error Correction
1	1.000	1.049	1.116	11.6%	6.39%	+5.21%
2	0.250	0.243	0.238	-4.8%	-2.05%	+2.75%
3	0.0625	0.061	0.043	-31.2%	-29.50%	+1.7%
4	0.0156	0.019	N/A	N/A	N/A	N/A

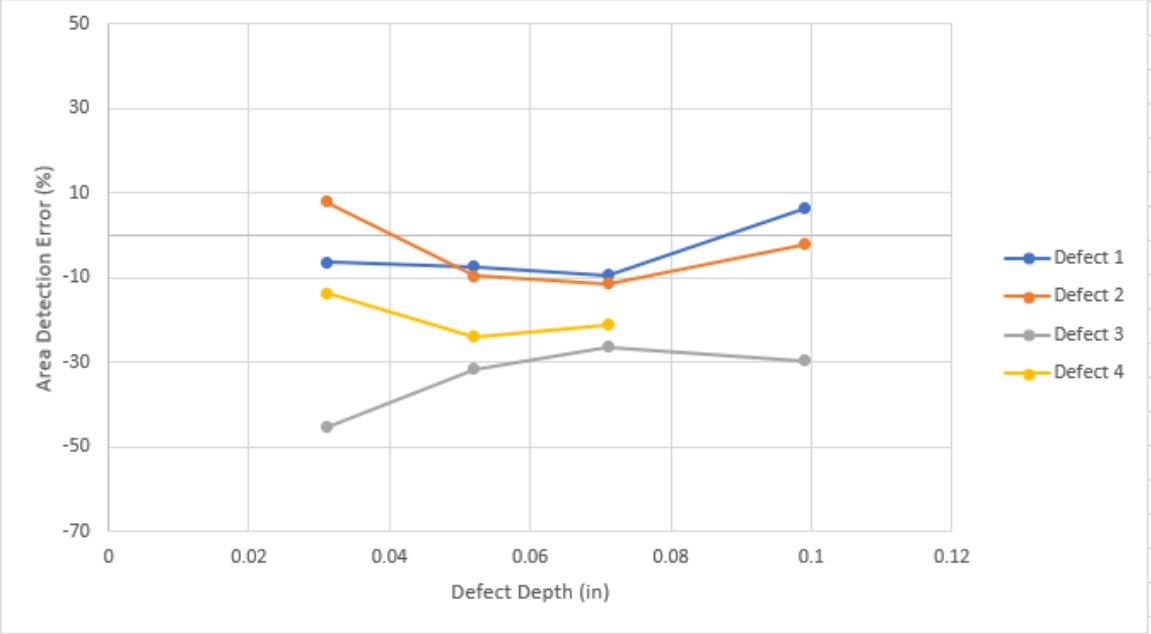

Figure 79: C-Scan Defect Area Detection Inaccuracy Vs. Defect Depth

Figure 78 shows the relationship between depth and the inaccuracy of detecting various similarly defects. The depths of the prescribed defects are those cited in Section 3.5. What is obvious from the data presented is that smaller defects are severely undershot by the interrogating ultrasonic probe. While Defect 4 may appear to have been detected more precisely, this is likely due to the previously discussed resolution limitation of the ultrasonic system, and by being smaller than the resolution the results tend to skew closer to the true value of the defect. Defect 4 was completely undetectable at a depth of 0.099 in with the C-Scan, showing that it is perhaps the least consistently detected defect- which is to be expected. Defect 3 shows high error across all laminates. This seems due to the scattering phenomenon in nonhomogeneous materials, such as composites. Parsing out the actual defect from the noise becomes difficult with this NDT method given the small defect size for both Defects 3 and Defect 4. Defects 1 and Defect 2 show the most stable detection, Defect 1 was found to have an average absolute error of 7.37% $\pm$1.45%, and Defect 2 was found to have an average absolute error of 7.75% $\pm$4.03%. Defects 3 and Defect 4

meanwhile were seen to have 33.19% ±8.34% and 19.56% ±5.34% errors respectively. Ultrasonic C-Scans prove to be able to detect a wide range of macroscopic defects, however there is a substantial decrease in detection accuracy for smaller defects. Ultrasonic C-Scans also struggle with near surface defects given the ultrasonic dead zone phenomenon, specifically for the smaller defects investigated.

3.5.3 Shearography Benchmarking

The following tables, similarly, demonstrate indicate the transition from the original experimental defect area assumptions to the new CT scan base line area findings but for Thermography NDT results. The error improvement highlights how much closer the scans absolute value of error approaches the true area. Error (Old) indicates the error found in the original shearography scans from section 3.2 found in Table 5. Error (New) is the error calculation based upon the CT scan areas found in section 3.4.

Table 17: Vacuum Exited Shearography Area Benchmarking

Defect	Sample	Theoretical Area (in^2)	Area CT Scan (in^2)	Shearography Scan Area (in^2)	%Error (Old)	%Error (New)	%Error Correction
1	6(7)	1.000	1.109	1.700	70.0%	53.29%	+16.71%
2	6(7)	0.250	0.260	0.321	28.4%	23.46%	+4.94%
1	9(10)	1.000	1.020	1.445	44.5%	41.67%	+2.83%

For the laminates tested, the shearography data is limited due to the lack of defect detection from either vacuum or particularly thermal excitation. Shearography shows promise of

rapid detection for large defects in composite laminates over a large area. The defects which were detected appear substantially larger than their true size due to the straining of the surrounding material. This error appears to decrease as laminate thickness increases or as defects decrease in size, however given the lack of data points a trend cannot be accurately prescribed.

3.5.4 Thermography Benchmarking

The following tables indicate the transition from the original experimental assumptions to the new CT scan-based findings for Thermography. The error improvement highlights how much closer the scans absolute value of error approaches the true area. Error (Old) indicates the error found in the original thermography scans from section 3.3 found in Table 6-9. Error (New) is the error calculation based upon the CT scan areas found in section 3.4.

Table 18: Thermography Area Benchmarking Laminate 3(4)

Defect	Theoretical Area (in^2)	Area CT Scan (in^2)	Thermography Scan Area (in^2)	%Error (Old)	%Error (New)	%Error Correction
1	1.000	0.986	1.262	26.2%	27.99%	-1.79%
2	0.250	0.261	0.29	16.0%	11.11%	+4.89%
3	0.0625	0.053	0.032	-48.8%	-39.62%	+9.18%
4	0.0156	0.022	0.01	-36.0%	-54.55%	-18.55%

Table 19: Thermography Area Benchmarking Laminate 6(7)

Defect	Theoretical Area (in^2)	Area CT Scan (in^2)	Thermography Scan Area (in^2)	%Error (Old)	%Error (New)	%Error Correction
1	1.000	1.109	1.255	25.5%	13.17%	+12.33%
2	0.250	0.260	0.345	38.0%	32.69%	+5.31%
3	0.0625	0.057	0.026	-58.4%	-54.39%	+4.01%
4	0.0156	0.025	0.01	-36.0%	-60.00%	-24.00%

Table 20: Thermography Area Benchmarking Laminate 9(10)

Defect	Theoretical Area (in^2)	Area CT Scan (in^2)	Thermography Scan Area (in^2)	%Error (Old)	%Error (New)	%Error Correction
1	1.000	1.020	0.949	-5.1%	-6.96%	-1.86%
2	0.250	0.265	0.205	-18.0%	-22.64%	-4.64%
3	0.0625	0.072	0.049	-21.6%	-31.94%	-10.34%
4	0.0156	0.019	0.006	-61.6%	-68.42%	-6.82%

Table 21: Thermography Area Benchmarking Laminate 12(13)

Defect	Theoretical Area (in^2)	Area CT Scan (in^2)	Thermography Scan Area (in^2)	%Error (Old)	%Error (New)	%Error Correction
1	1.000	1.049	0.633	-36.7%	-39.66%	-2.69%
2	0.250	0.243	0.175	-30.0%	-27.98%	+2.02%
3	0.0625	0.061	0.015	-76.0%	-75.41%	+0.59%
4	0.0156	0.019	N/A	N/A	N/A	N/A

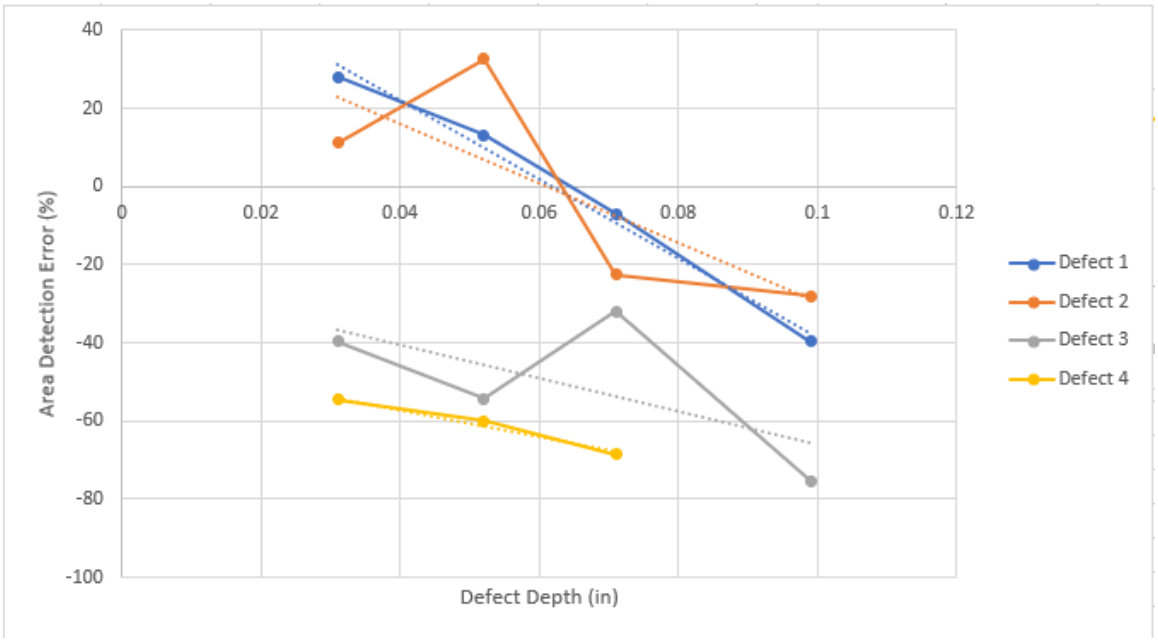

Figure 80: Thermography Defect Area Detection Inaccuracy Vs. Defect Depth

Figure 79 shows the relationship between depth and the inaccuracy of detecting various similarly defects for the thermographic scans conducted. The depths of the prescribed defects are those cited in section 3.5. What is obvious from the data presented is the trend towards undershooting the area prediction as the composite thickness increases. Additionally, smaller defects were under detected as well. The smallest delamination defects, Defect 3 and Defect 4, show high error across all laminates. This high error percent is due to the small defects absorbing larger amounts of heat relative to their size due to the reduction in surface area to volume, as heat conduction relies on surface contact between two mediums. Unlike Ultrasonic C-Scan, the defects observed had obvious trend as a relationship to area. Defect 1 follows a trend of -1007.10x with an R^2 value of 0.9883. Defect 2 was found to have a trend of -759.36x with an R^2 value of 0.5832. Defect 3 was found to have a trend of -420.72x with an R^2 value of 0.4047. Finally defect 4 was found to have a trend of -345.37x with an R^2 value of 0.9772. What is interesting about this is that not only do all defects in thermography experience a drop in area detection through thickness, larger defects experience harsher drop off in edge detection through thickness as well.

3.5.5 CT Scan Benchmarking Summary

Through the use of computed tomography relationships between the true defect area and depth versus the scanning error of the various rapid inspection techniques were analyzed. Ultrasonic C-Scanning was found to have somewhat stable detection regardless of defect depth. Shearography was found to have substantial overprediction in defect size, this error appears to decrease as defect size decreases and depth increases, however given the lack of a significant number of data points this has to be acknowledged as primarily

author's informed speculation. Thermography was found to have a drop in detected area as the thickness increased and the defect size decreased. The defect error trend appears to be more dramatic for larger area defects through thickness than smaller area defects.

Chapter 4: Discussion

4.1 CFRP Test Specimen

The test specimens which have undergone testing for this study, after in depth analysis, were far from perfect subjects. Will there was an attempt to assemble as similar as hand assembly of CFRP via VARTM construction allows there is clearly substantial error in the smallest programed defects, the non-uniform edge geometry of the programed defects, the fiber volume fraction proved hard to precisely control and there are regions in the thicker laminates where there are voids and resin starved regions. All this being shared, the samples themselves, through the use subsequent utilization of CT characterization / baselining, are able to overcome these flaws. Since the error in the defects can be observed, it makes comparison across laminate samples substantially more grounded. In experimental proceedings it is often the easiest option to assume that a perfect test sample has been created, this is generally far from the case. In this study that inaccurate simplifying assumption was not required. Yes inaccuracy has clearly been revealed via the accuracy of CT scanning of NDT test laminates. Yet CT scanning also delivers the ability to utilizes those accurate “as assembled” values for each of the four samples providing a very strong / accurate baseline. By being able to determine exact size and depth, to the micron level, it allows for future research into these NDT methods to come closer to low error prediction of defects in composite laminates.

4.2 Comparison of Methods

4.2.1 Rapid Inspection NDT Methods Defect Detection

Multiple methods of rapid inspection NDT for use in aerospace applications of CFRP delamination detection have been analyzed. Those consisted of Ultrasonic C-Scan, Thermal and Vacuum Excitation Shearography and Thermography. Ultrasonic testing (UT) itself shows detection reliability through thickness, while the detection of defects is impacted by wave scattering it is undeniable that the method itself is robust. What makes UT an appealing technology is also its widespread deployment across the aerospace industry for NDT as well as reliability testing [36]. The resolution limitations of C-Scanning systems are their greatest weakness. The C-Scanning scattering effect this makes the identification of smaller defects quite challenging. The area detection for C-Scans maintains a reasonable detection error window for large delamination defects which would be a primary concern for those in the aerospace industry NDT. Shearography, as demonstrated in this study, is a much less beneficial technology for delamination defect detection in CFRP. Shearography struggles with the detection of small defects and shows the greatest success in thinner laminates or near surface defects. There is also dependence on the method of excitation utilize for achieve even lower accuracy results., as described thermal excitation was not enough to draw out enough strain in the surface to detect the programmed delamination defects. Vacuum excitation shows some promise for the rapid detection of larger defects. The amount of area which can be scanned by a shearography scanners is quite impressive. The entire setup time and testing took 30 minutes for vacuum excitation shearography, quite fast compared to the other methods evaluated. One more issue that shearography faces in delivering accurate results is its dependance on specific

surface requirements. While other optical methods of NDT, such as thermography, does not have such a heavy dependance on specific surface characteristics to perform a successful test scan shearography certainly does. Thermography, the quickest testing method by far at just over 3 minutes total for setup, scanning and processing time, has remarkable results for detecting the programed delaminations considering the speed. Not only is thermography able to detect the same number of programmed defects as ultrasonic, but it can also detect the near surface defects seen in laminate 3(4) more reliably. This is due to thermography not experiencing the same wave disruptions of the ultrasonic wave dead zone.

4.2.2 Rapid Inspection NDT Detection Accuracy

After conducting the error analysis with the CT benchmarking, there are a few main takeaways. Ultrasonic C-Scanning shows relatively consistent area detection through a variety of CFRP laminate thicknesses. This could be used to enhance current C-Scanning systems to predict, within the window of error, what size the defect truly is. The primary drawback of C-Scanning is the resolution of the machine, this makes reliable detection for very small defects a challenge and could lead to false negative or false positive detections. The next takeaway is that shearography vastly overpredicts the size of the defect beneath the surface. Since shearography is not able to measure delamination defect depth, utilizing similar characterization techniques with more data points could provide a way to approximate true defect size with a quick depth reference such as a tap test. Finally, thermography is seen to lose detection accuracy as both delamination defect size decreases and as the depth of defects increase. For near surface defects thermography overpredicts some larger defects but soon those same defects begin to be underpredicted as depth

increases. The reduction in accuracy appears to be sharper for large defects while smaller defects have slower decays.

4.3 Ideal Use Cases for NDT Methods

4.3.1 Ultrasonic C-Scan

C-Scanning is best utilizing its strengths, being the reliable delamination detection through thickness. When inspecting thicker laminates, faster methods of inspection such as shearography or thermography may not suffice. This is particularly true for smaller defect sizes. C-Scanning is also valuable for the built-in scale it can create with the axis position mapping, making interrogation of these composites for stress evaluation much simpler as exact location is known. It can also be used in compliment to a technology like shearography on thinner laminates. Shearography can perform a quick initial inspection for larger defects which might show whether it is worth testing with C-scan for example. C-Scanning could also compliment or substitute for thermography excellently as they appear to have the same detection consistency.

4.3.2 Shearography

Shearography alone may not be a tool which can be relied on exclusively for NDT of composite delamination. However, it has proven to be a quick method to detect large defects close to the surface or in thinner laminates (less than 2 mm). Depending on application it can be paired with other inspection methods as an initial screening of a laminate for large delamination which would warrant further inspection for delaminations. This could be performed by a bond tester to determine depth information whilst having a general understanding of defect area.

4.3.3 Thermography

Thermography is incredibly quick and can be used with the same base detection reliability as ultrasonic. In fact, there have been studies that show pulsed thermography may be superior to ultrasonic for detection of delamination defects [44, 45]. Thermography however has the drawback of high error at large defect depths in CFRPs, thus could be paired with a technology like ultrasonic C-Scan in order to further interrogate those defects. Thermography is also equipped, similarly to shearography, to scan large areas simultaneously, so for rapid inspection of large surfaces for a wide range of delamination is also a very viable option.

4.3.4 Radiography Computed Tomography

Radiography CT is extremely precise, that is its primary benefit. Additionally, being able to filter and isolate specific defects with micron level precision in a scan is incredible for understanding the potential it poses in the failure of a composite laminate. This is where the positives end, as the major geometric restrictions and further restricted view per scan makes it incredibly slow. As seen in this study, it can be used to understand the error in NDT equipment, and with extensive testing could be used to calibrate other NDT machines and anticipate the error to predict the true defect size. So, for NDT application of CT it is best used to benchmark or potentially scan very small composite pieces, such as removable joints or tubing segments.

Chapter 5: Concluding Remarks

In this thesis, composite NDT methods were introduced. The methodology of the creation of the delamination defects as well as subsequent test sample CFRP laminates to be examined was explored in detail as well as the manufacturing process. Next, a number of composite NDT methods were evaluated. The methods compared were ultrasonic C-Scans, thermal and vacuum excitation shearography, and pulsed thermography. All of the technologies used in this study were aerospace industry grade and operated by professionals in their field as to reduce operator error. First, an understanding of delamination detection capability in CFRP laminates was evaluated. Scans with the aforementioned methods on the same set of samples allowed for direct comparison to be drawn. Next, highly accurate Computed Tomography was performed on the composite test samples in order to subsequently benchmark the NDT methods being evaluated with a most accurate baseline. This allowed for an accurate understanding of the inaccuracies of each detected scanned defect across the methods. This demonstrated the viewing of relationships between delamination defect area as well as its depth's effect for delamination detection NDT accuracy. Finally, the results of the study are discussed, and the methods seen throughout the study are compared and recommendation are given for their use to most benefit from their respective strengths.

In conclusion, this study offers a direct comparison between a variety of very popular composite NDT techniques. The hope for this study is to encourage future exploration into the accuracy and creation of algorithms for correcting for defect detection error utilizing more accurate CT data set baselines. The groundwork and techniques are laid out for studies into individual methods with potential for the creation of machine

learning algorithms with further data sets for anticipating true defect size utilizing CT scans for advanced defect characterization.

References

[1] Mrazona Maria, “Advanced composite materials of the future in Aerospace industry”, INCAS BULLETIN, Volume 5, Issue 3/ 2013.

[2] Kesarwani Shivi, “Polymer Composites in Aviation Sector”, IJERT, Volume 6, Issue 6/ 2017.

[3] Lester Clifford., Nutt Steven. “Composite Materials: Advantages and Cost Factors”. 2018 [Online] Available: https://www.elevatedmaterials.com/advantages-and-cost-factors-of-composite-materials/

[4] Nairn John. “A Critical Evaluation of Theories Predicting Microcracking in Composite Laminates”. Journal of Material Science, Volume 28, 1993, 5099-5111.

[5] Wang Bing., et al. “Non-Destructive Testing and Evaluation of Composite Materials/Structures: A State-of-the-Art Review”. Advances in Mechanical Engineering, DOI 10.1177/1687814020913761

[6] Djordjevic B., Boro, “Nondestructive Test Technology for The Composites”. International Conference of the Slovenian Society for No Destructive Testing. 2009.

[7] Tol S.L., et. al. “Application of Shearography in Nondestructive Testing of Composite Plates”. Journal of Materials Processing Technology, 23, 1990, 267-275.

[8] Steinchen W., et al. “Non-Destructive Testing of Aerospace Composite Materials Using Digital Shearography”. Proc Instn Mech Engrs, Volume 212, Part G, 1998.

[9] Zhao Qihan, et al. “Digital Shearography for NDT: Phase Measurement Technique and Recent Developments”. Applied Sciences, 2018, 8(12), 26-62.

[10] Yang Ruizhen, He Yunze. “Optically and Non-Optically Excited Thermography for Composites: A Review”. Infrared Physics & Technology, Issue 75, (2016), 26-50.

[11] Bai W., Wong B.S. “Evaluation of Defects in Composite Plates Under Convective Environments Using Lock-In Thermography”. Measurement Science and Technology, 12, (2001).

[12] Mandal Sefa K. “Damage Detection in Carbon Fiber Reinforced Polymeric Composites and Honeycomb Sandwich Panels by Active Thermography”. Sabanci University. December 2019.

[13] Ahmed Junaid., et al. “Sparse Ensemble Matrix Factorization for Debond Detection in CFRP Composites Using Optical Thermography”. Infrared Physics & Technology, Issue 92, (2018), 392-401.

[14] Roach Dennis P., Rice Thomas M. “A Quantitative Assessment of Advanced Nondestructive Inspection Techniques for Detecting Flaws in Composite Laminate Aircraft Structures”. Sandia National Labs, (March 2016), DOT/FAA/TC-15/4.

[15] Roach Dennis P. “A Quantitative Assessment of Advanced Nondestructive Inspection Techniques for Detecting Flaws in Composite Honeycomb Aircraft Structures”. Sandia National Labs, (December 2016), DOT/FAA/TC-15/63.

[16] Hay Thomas R., et al. “Rapid Inspection of Composite Skin-Honeycomb Core Structures with Ultrasonic Guided Waves”. Journal of Composite Materials, Volume 37, No. 10, 2003.

[17] Hasiotis Theodoros., Badogiannis Efstaratos, Tsouvalis Nicolaos G. “Application of Ultrasonic C-Scan Techniques for Tracing Defects in Laminated Composite Materials”. Journal of Mechanical Engineering, 57, (2011), 192-203.

[18] Hsu D.K., “Non-Destructive Evaluation of Aerospace Composites: Ultrasonic Techniques”. Woodhead Publishing Series in Composites Science and Engineering, 2013, 397-422.

[19] D’Orazio T., et. al. “Automatic Ultrasonic Inspection for Internal Defect Detection in Composite Materials”. NDT&E International, 41, (2008), 145-154.

[20] Davi S., Et Al. “Correction of B-Scan Distortion for Optimum Ultrasonic Imaging of Backwalls with Complex Geometries” Insight- Non-Destructive Testing and Condition Monitoring, Volume 62, No. 4, Apr 2020, 184-191.

[21] Katunin Andrzej., et al. “Impact Damage Evaluation in Composite Structures Based on Fusion of Results in Ultrasonic Testing and X-Ray Computed Tomography.” *MDPI, Sensors 2020, 20,* 1867, March 27, 2020.

[22] Kastner Johann., et al. “Defect and Porosity Determination of Fibre Reinforced Polymers by X-Ray Computed Tomography”. 2nd National Symposium on NDT in Aerospace 2010 – We.1.A.2.

[23] Prade F., et al. “Nondestructive characterization of Fiber Orientation in Short Fiber Reinforced Polymer Composites with X-ray Vector Radiography”. NDT&E International 86, (2017), 65-72.

[24] Rus J., et al. “Qualitative Comparison of Non-Destructive Methods for Inspection of Carbon Fiber Reinforced Polymer Laminates”.

[25] Parks ET. “Computed Tomography Applications for Dentistry”. Dental Clinics of North America. 2000 Apr;44(2):371-394. PMID: 10740774.

[26] Kalender Willi A., “X-Ray Computed Tomography”. Phys. Med. Biol., 51, (2006), R29-R43. http://dx.doi.org/10.1088/0031-9155/51/13/R03.

[27] Stoessel Rainer, et. al. “Analysis of Inner Fracture Surfaces in CFRP Based on µ-CT Image Data”. Wels, Austria, (2012).

[28] Liu Xueshu, Chen Fei. “Defect Characterization in CFRP Using X-Ray Computed Tomography”. School of Automotive Engineering, Dalian University of Technology, (2016). https://doi.org/10.1177/096739111602400210

[29] Aldave Jorge I., et al. “Review of Thermal Imaging Systems in Composite Defect Detection”.

[30] Han Dae-Hyun., Kang Lae-Hyong. “Nondestructive Evaluation of GFRP Composite Including Multi-Delamination Using THz Spectroscopy and Imaging”. Composite Structures, 185, (2018), 161-175.

[31] McElroy M., et. al. “Simulation of Delamination-Migration and Core Crushing in a CFRP Sandwich Structure”. Composites: Part A, 79, (2015), 192-202.

[32] Toscano C., et. al. “Lockin Thermography to Monitor Propagation of Delamination in CFRP Composites During Compression Testing”. Quantitative InfraRed Thermography 11th International Conference, 2012, http://dx.doi.org/10.21611/qirt.2012.335

[33] Gordon, G.A., et. Al. “Ultrasonic C-Scan Imaging for Material Characterization”. Ultrasonics, Volume 31, Issue 5, (1993), 373-380. https://doi.org/10.1016/0041-624X(93)90071-7

[34] Darmon M., et al. “Modelling of Scattering of Ultrasonic Flaws for NDT”. Springer Proceedings in Physics, Volume 128, (2009), 61-71, https://doi.org/10.1007/978-3-540-89105-5_6

[35] Hegemann J., Peiffer A., Broucke B. Van Den. “Modeling of Ultrasonic Testing of Woven Fabric Laminates: A Microstructure Approach”. AIP Conference Proceedings 1096, 1077, (2009). https://doi.org/10.1063/1.3114074

[36] Gros, X. E., K. Ogi, and K. Takahashi. "Eddy current, ultrasonic C-scan and scanning acoustic microscopy testing of delaminated quasi-isotropic CFRP materials: a case study." *Journal of reinforced plastics and composites* 17.5 (1998): 389-405.

[37] Rolfes R., Hammerschmidt U. “Transverse Thermal Conductivity of CFRP Laminates: A Numerical and Experimental Validation of Approximate Formulae”. Composite Science and Technology, Volume 54, Issue 1, (1995), 45-54. https://doi.org/10.1016/0266-3538(95)00036-4

[38] De Angelis, G., et al. "A new technique to detect defect size and depth in composite structures using digital shearography and unconstrained optimization." *Ndt & E International* 45.1 (2012): 91-96.

[39] Yang, L. X., and Y. Y. Hung. "Digital shearography for nondestructive evaluation and application in automotive and aerospace industries." *J. Hologr. Speckle* 1.248 (2004): 69-79.

[40] Chatterjee, Krishnendu, et al. "A comparison of the pulsed, lock-in and frequency modulated thermography nondestructive evaluation techniques." *Ndt & E International* 44.7 (2011): 655-667.

[41] Sharath, D., M. Menaka, and B. Venkatraman. "Defect characterization using pulsed thermography." *Journal of Nondestructive Evaluation* 32.2 (2013): 134-141.

[42] Tsao, C. C., and H. Hocheng. "Computerized tomography and C-Scan for measuring delamination in the drilling of composite materials using various drills." *International Journal of Machine Tools and Manufacture* 45.11 (2005): 1282-1287.

[43] Peeters, Jeroen, et al. "Robust quantitative depth estimation on CFRP samples using active thermography inspection and numerical simulation updating." *NDT & E International* 87 (2017): 119-123.

[44] Roach Dennis P., Rice Thomas M. "A QUANTITATIVE ASSESSMENT OF ADVANCED NONDESTRUCTIVE INSPECTION TECHNIQUES FOR DETECTING FLAWS IN COMPOSITE LAMINATE AIRCRAFT STRUCTURES" Sandia National Laboratory, Federal Aviation Administration, Mar. 2016, DOT/FAA/TC-15/4

[45] Roach Dennis P. "A QUANTITATIVE ASSESSMENT OF CONVENTIONAL AND ADVANCED NONDESTRUCTIVE INSPECTION TECHNIQUES FOR DETECTING FLAWS IN COMPOSITE HONEYCOMB AIRCRAFT STRUCTURES" Sandia National Laboratory, Federal Aviation Administration, Dec. 2016, DOT/FAA/TC-15/63

[46] Naghipour, Paria. "Simulation and Experimental Evaluation of Mixed Mode Delamination in Multidirectional CF/PEEK Laminates under Quasi-Static and Fatigue Loading". Ohio Aerospace Institute, (2011).

[47] Tomblin S. John, Ng C. Yeow, Raju Suresh K. "MATERIAL QUALIFICATION AND EQUIVALENCY FOR MATRIX COMPOSITE MATERIAL SYSTEMS: UPDATED PROCEEDURE". National Institute for Aviation Research, Federal Aviation Administration, Sept. 2003, DOT/FAA/AR-03/19

[48] Duong, Cong N., and Chun Hui Wang. "Composite repair: theory and design." Elsevier, 2010.

[49] Garg, Amar C. "Delamination—a damage mode in composite structures." Engineering Fracture Mechanics 29.5 (1988): 557-584.

[50] Sheedev Antony, Monssef Drissi-Habti, Venkadesh Raman, "Numerical Analysis to Enhance Delamination Strength around Bolt Holes of Unidirectional Pultruded Large Smart Composite Platform", Advances in Materials Science and Engineering, vol. 2018, Article ID 3154904, 12 pages, 2018. https://doi.org/10.1155/2018/3154904